Molecular Investigation of the Wood/pMDI Adhesive Bondline

by

Jianwen Ni

Dissertation submitted to the Faculty of the

Virginia Polytechnic Institute and State University

in partial fulfillment of the requirements for the degree of

DOCTOR OF PHILOSOPHY

IN

WOOD SCIENCE AND FOREST PRODUCTS

APPROVED:

C. E. Frazier, Chairman

W. G. Glasser

R. F. Helm

F. A. Kamke

J. P. Wightman

December 12, 1996

Blacksburg, Virginia

Keywords: polymeric diphenylmethane diisocyanate, solid-state NMR, IRCP, proton rotating frame T_1 relaxation, wood adhesive bondline

CHARACTERIZATION OF THE WOOD-ISOCYANATE WOOD ADHESIVE BONDLINE

by

Jianwen Ni

C. E. Frazier, Chairman

Wood Science and Forest Products

(ABSTRACT)

Polymeric diphenylmethane diisocyanate, pMDI, has become an important wood binder in recent years, due to its excellent performance in wood-based composites. However, much still remains unknown about the nature of their bonding mechanism. This research describes efforts to learn more molecular information about the pMDI-wood bondline, and to further improve the bonding performance.

In order to correlate molecular phenomena with macroscopic performance of wood-adhesive bondline, low frequency molecular motions in wood were probed using dynamic mechanical analysis (DMA) and ^{13}C cross-polarization, magic-angle spinning (CP/MAS) NMR. A correlation between the CP time constant $<T_{CH}>^*$ and the dynamic storage modulus E′ was established for dry wood, but was not valid for wet wood samples.

Two types of pMDI with properties similar to commercial resins, except for isomer ratio, was synthesized. The one with isomer ratio similar to commercial resins was analyzed with ^{15}N CP/MAS NMR. The results show that the pMDI-wood bondline is a heterogeneous complex of urethanes, polyureas, residual isocyanates and biurets. The

network structure is controlled by the curing variables such as temperature and time. Urethane formation was detected under relatively mild cure conditions. Thermal decomposition of urethanes (120^0C) and polyurets (185^0C) were detected. ^{15}N NMR was demonstrated as a powerful technique, but suffers from signal overlap which prevents a clear evaluation of the relative contributions of urethane and urea formation.

Another type of pMDI with higher 2,4′- isomer content was used to investigate the effects of isomer ratio on bonding mechanism. The chemical species found in the heterogeneous bondline are similar, except that urethane formation is less evident here. Relaxation studies show very different behaviors, in which the bondline with higher 2,4′-isomers may have a higher molecular mobility. A fracture toughness test method, contoured double cantilever beams (CDCB), was developed to evaluate the macroscopic performance. They both showed strong bonding, and there was no significant difference found.

To explain the strong bonding of pMDI and wood, an interpenetrating polymer network (IPN) theory was hypothesized. ^{13}C CP/MAS NMR and DMA were used to evaluate this hypothesis. The results were inconclusive due the limitations of the techniques.

ACKNOWLEDGEMENTS

I would like to express my grateful appreciation to my advisor and committee chair, Dr. Charles E. Frazier, for his guidance and personal support throughout this entire research project. Gratitude is extended to the other members of my research committee, Drs. Wolfgang G. Glasser, Richard F. Helm, Frederick A. Kamke, and James P. Wightman, for their valuable suggestions and input into this project.

I would also like to thank the supporting staff at the Brooks Forest Products Center for their support and assistance. I am especially indebted to Mr. Tom Glass for his skillful guidance and assistance in NMR experiments. I also wish to express my thanks to all of the colleagues and friends, especially to Dr. Ackah Toffey, Ms. Jody Jervis, and Dr. Gamini Samaranayake for their support.

Finally, I would like to thank my parents and my wife Grace, whose patience, support and encouragement made the completion of this dissertation possible. I dedicate this work to them.

TABLE OF CONTENTS

LIST OF TABLES

LIST OF FIGURES

CHAPTER 1

INTRODUCTION

Because of the declining availability of mature timber, the production of adhesively bonded wood composite materials has been strongly demanded. Wood adhesives are critical for the performance of these materials. A better understanding of the wood-adhesive interphase is therefore required to assist the evolution of wood composite technology.

This requires a molecular study of the components of the interphase of wood and the adhesive. Recently, a correlation between dynamic storage modulus and the mean cross-polarization time constant has been estabilished for a wide variety of synthetic polymers (1-4), with the time constant determined by an inversion recovery cross-polarization (IRCP) NMR pulse. Attempts have been made in this work to apply this correlation to the wood-adhesive bondlines. This correlation was first applied to solid wood, prior to studies of cured resins and cured resin-wood composites.

Polymeric diphenylmethane diisocyanate, pMDI, is the resin of interest in this research. pMDI has become an important wood binder in recent years, primarily for bonding oriented strand board (OSB) and similar particulate wood-based composites. It offers several unique features (5-9): cure in high moisture environments and at low press temperature; enhanced panel physical and mechanical performance, moisture resistance and durability; and no formaldehyde emission. pMDI also has a broad range of chemical reactivities, and this reactivity may prove to be quite useful in bonding a wide variety of surfaces.

. Research on pMDI in the past has been done mainly in the area of pMDI performance. While there is no doubt that pMDI performs well, it is still not very clear about how pMDI derives its superior adhesive properties. Isocyanates can react with wood hydroxyls to form urethane linkages. However, isocyanates are also highly reactive to moisture. The hydrophilic nature of wood always ensures a high moisture content. It can therefore be expected that there will be competition between these two reaction pathways. The exact bonding mechanism will also be affected by the cure conditions. As pMDI has a great propensity to wet and deeply penetrate wood, this distinguishing characteristic may have potential implications for improving wood bonding.

Commercial pMDI is composed of about 50% 4,4′-MDI and a small amount of 2,4′-MDI with a trace of the 2,2′- isomer, as well as 50% of higher order oligomeric polyisocyanates (10). It is likely that the performance of pMDI resin will depend on its composition, which is affected by molecular and structural isomerism, especially the 4,4′-/2,4′-isomer ratio. There has been no reported study of the effects of pMDI structural isomerism on wood bonding performance.

The ultimate goal of any study on wood adhesives is to understand and improve bonding performace. Therefore the techniques used for evalution of wood bonding performance are very important. However, many of the commonly used test methods are not very satisfactory, especially for quantitative analysis. The overall goal of this research project is to have a better understanding of the nature of the mechanism of pMDI-wood bonding. The specific objectives are:

1. To evaluate the validity of a correlation between dynamic storage modulus and cross-polarization time constant in solid wood.
2. To characterize the chemistry, morphology, and molecular dynamics of the pMDI-wood interphase under different cure conditions using primarily ^{15}N and ^{13}C CP/MAS NMR, and to a lesser extent dynamic mechanical analysis.
3. To investigate the effects of pMDI structural isomerism on the pMDI-wood bondline with ^{15}N NMR.
4. To evaluate the bonding performance of pMDI by using a fracture toughness test in cleavage with the contoured double cantilever beam specimen.

References

1. Parker, A. A., J. J. Marcinko, Y. T. Shieh, D. P. Hedrick and W. M. Ritchey. 1990. J. Appl.Polym. Sci. 40: 1717-1725.
2. Marcinko, J. J., A. A. Parker, Y. T. Shieh and W. M. Ritchey. 1992. J. Appl. Polym. Sci. 45: 391-398.
3. Parker, A. A., J. J. Marcinko, P. Rinaldi, D. P. Hedrick and W. M. Ritchey. 1993. J. Appl. Polym. Sci. 48: 677-681.
4. Marcinko, J. J., A. A. Parker, P. L. Rinaldi and W. M. Ritchey. 1994. J. Appl. Polym. Sci. 51: 1777-1780.
5. Frink, J. W. and H. I. Sachs. 1981. ACS Symp. Ser. Vol. 172: 285-309.
6. Frink, J. W. and H. D. Layton. 1985. Proc. of the 19th International Particleboard/Composite Materials Symp., T. M. Maloney Ed., Pullman, WA. pp. 323-347.
7. Chelak, W. and W. H. Newman. 1991. Proc. of the 25th International Particleboard/Composite Materials Symp., T. M. Maloney Ed., Pullman, WA. pp. 205-229.
8. McElrath, R. W. 1992. Proc. of the Southeastern Section of the Forest Products Research Society, T. D. Faust Ed., Atlanta, GA.
9. Galbraith, C. J. and W. H. Newman. 1992. Pacific Rim Bio-Based Composites Symp., Rotorua, New Zealand. pp.130-142.
10. Twichett, H. J. 1974. Chem. Soc. Rev. 3 (2): 209-230.

CHAPTER 2

LITERATURE REVIEW

2.1. Polymeric MDI as a Wood Binder

2.1.1. History

Polymeric MDI is well known for its industrial applications in polyurethane foams and binders. Since pMDI was first commercially produced in the early 1960s, it has been used mainly for the production of rigid and flexible foams, elastomers, coatings and adhesives. In 1991, approximately 2.6 billion pounds of pMDI were produced in the world (1) (about 1 billion pounds in North America (2)) for these types of applications.

As a wood binder, the value of pMDI has been known for some time. However, it is still a newcomer and plays a relatively minor role in the total amount of adhesives consumed in the wood industry. Pioneering work in the development of this new type of wood adhesive started in Europe in the late 1960s. In the early 1970s, Deppe and Ernst (3,4) first reported achieving V_{100} boards (West German exterior structural grade) by using pMDI as the binder. They found that pMDI bonded boards performed better or equivalent to phenolic bonded boards in terms of strength and moisture resistance. Shortly after that, the first pMDI-bonded particleboard was commercially produced by Deutsche Novopan of West Germany. They manufactured a product (Phenapan-V-100=Iso-Spanplatte) consisting of a pMDI-bonded core with phenolic-bonded face layer. This overcame the major problem of using pMDI, i.e., sticking to metal surfaces during

pressing. When compared to previous phenolic-bonded V-100 boards, pMDI-bonded boards are more hydrophobic and have better performance under permanent load in outdoor conditions (5,6).

In the United States, the Ellingson lumber company was among the first to utilize pMDI for making wood panel products. In the late 1970s, Ellingson (7) became the first commercial producer of pMDI-bonded particleboard in North America. They invented a process for bonding cellulosic materials with pMDI to produce a multiple-ply structural panel. This process can tolerate up to 22% precure moisture content of wood raw material and is able to include a large amount of bark and needles. By using this process, they made a product called Elcoboard which has a pMDI-bonded saw mill waste core and two surface veneers of varying grade. Elcoboard gained approval as an exterior grade plywood substitute in building applications.

With the large-scale introduction of waferboard/OSB, pMDI has gained huge momentum in the wood industry. Rubicon Chemicals Inc. first tested pMDI for producing waferboard in 1979 (8). In the early 1980s, the use of spinning disc atomizing applicators made it possible to take advantage of the low resin dosage levels required by pMDI, making this adhesive more economically competitive against conventional phenol formaldehyde (PF) resins. Subsequent advances in release agent technology allowed for 100% pMDI-bonded board. In the late 70s, Rubicon Chemicals (9-12) developed an emulsifiable MDI (EMDI) to solve the disadvantage of pMDI in some applications, that it is not "water borne". EMDI has a lower viscosity, spreading more efficiently on wood

chips. Clean up and disposal of the water emulsion is easier too. As a result of these developments, ICI converted the first waferboard plant to pMDI binders in 1985 (2). Since then, pMDI has been competing with PF resin effectively and it captured 15-20% of the OSB/waferboard resin market by 1990.

Efforts have also been made to combine pMDI with other adhesives, such as PF, urea formaldehyde (UF) and lignin. These mixes were believed to be able to lower cost and decrease toxicity of pMDI. As early as the 70s, Deppe and Earnst (3,4) sprayed particleboard chips with aminoplast resins followed by pMDI. This combination yielded considerable increases in internal bond strength even at low resin loading. At almost the same time, Hse (13,14) published papers on the development of both plywood and flakeboard adhesives combining isocyanate and phenolic resins. He claimed that plywood adhesives achieved adequate bonding with wetter veneers than conventional phenolic adhesives. For flake board, he also found a superior performance vs. phenolic resin at high flake moisture content, low binder content and low panel density. Later, Tinkelenberg et al. (15) reported a resin system with low formaldehyde-aminoplast glues and pMDI. They believed that their new system could meet the requirements of low formaldehyde emissions, good mechanical and physical properties, and low relative prices. In 1989, Dix and Marutzky (16) also developed formulations for particleboard and plywood adhesives based on combinations of diisocyanates and compounds from renewable resources. Others have also reported combinations of pMDI with lignins (17-20), tannins (21-23), and furfural (24,25). Glasser et al. (19) reported that

hydroxypropylated lignin derivatives are capable of contributing equal or even greater strength to relignified fiber composites than pMDI alone. In terms of the chemistry behind these types of coapplications, Pizzi et al. (26-28) have shown that pMDI can easily react by a novel mechanism with the methylol groups of PF resols, urea formaldehyde (UF) and melamine formaldehyde (MF) resins etc., even in the presence of excess water. The pMDI/PF resin has been applied industrially in Chile (26). It allowed bonding to marine-grade standards of veneer species, which were thought as difficult to bond. Aqueous vinyl polymer solution - isocyanate adhesives for wood have also been considered (29).

2.1.2. Benefits and Problems of Using pMDI

PF has dominated the resin market for exterior structural applications. The introduction of pMDI aimed to replace PF resins, and therefore, created direct competition between these two resins. During the last 20 years, extensive research has been performed to compare their bonding performances including mechanical and physical properties of their bonded wood composites.

It has been demonstrated that pMDI can be cured with higher precure moisture content chips under faster pressing rates, lower press temperature, and lower resin loading (1,2,8,30-35). Galbraith and Newman (1) studied the effects of wood precure moisture content on cure rate with PF and pMDI. They found that PF resin will not cure at all with MC's over 10%, at least not fully. MDI cures faster, even at lower temperatures and higher moisture contents, and this was attributed to the bonding mechanism. PF resins

cure by a condensation reaction which is inhibited by the presence of water. In contrast, pMDI actually consumes water and requires it for polymerization. Chelak and Newman (36) have performed reaction kinetics studies by using differential scanning calorimetry (DSC). They used wood fibers of varying moisture contents as model systems to compare pMDI with a liquid PF resin. Their results showed that PF resin needs high energy to cure in high moisture environments. pMDI cures at a lower temperatures at equal moisture levels, and at moisture content above 6%, the cure of PF is inhibited while the cure of pMDI is enhanced (36). High precure moisture content is advantageous for wood bonding, as it saves energy costs related to wood drying which in turn reduces VOC emissions. Lower temperature drying also reduces moisture related residual stresses, making the composite more stable. Moisture plasticizes wood and allows more intimate fiber to fiber contact which improves bonding. Literature (32,37) has shown that pMDI-bonded OSB/waferboards, hardboards, and medium density fiberboards (MDF) all performed well when cured at 10-12% moisture content. Johns et al. (37) even concluded that MDF does not achieve sufficient cure when bonded below 10% moisture. They further concluded that isocyanate resin requires water for optimum bond formation in composition board. The amount of moisture required is a function of the surface area of the particles of wood in the mat. The greater the surface area, the higher the amount of moisture required. It was also reported that the upper limit of good adhesion with pMDI is about 18% moisture content (30,38,39). Palardy et al. (40) even tried to make

flakeboard of reasonable quality at 210^{0}F and 25% moisture content. However, the pressing time required was well beyond the limits of commercial feasibility.

pMDI can start reacting at very low temperatures, even at room temperature. Even UF, which is known for its rapid cure, is slower than pMDI. Galbraith and Newman (1) pointed out that low temperature reaction is a key advantage of the use of pMDI. The glass transition temperature (Tg) of lignin is about 110^{0}C depending on moisture content, and there is little need for higher temperatures when pressing wood composites. However, PF resins need over 177^{0}C to be fully cured. Since pMDI can be pressed at lower press temperatures and shorter press times, it affords process efficiency that cannot be achieved by conventional resins. Again, low temperatures also bring environmental benefits, such as the elimination of "Blue Haze". Rubicon made some production trials using pMDI binder in the waferboard, oriented waferboard and OSB (8). pMDI binder demonstrated superior performance vs PF resin for waferboard and oriented waferboard. OSB has the highest performance requirements of the three composites. More recently, Fiore (41) concluded that using pMDI can reduce press cycle at least 20-30% compared to powdered PF resins. For 7/16 in. sheathing, the cook time for pMDI averages 14-16 seconds per sixteenth inch versus estimated averages of 23-32 seconds per sixteenth inch for PF in general.

Most of the above reports have discussed laboratory and pilot findings. Only Ellingson (7,42), Adams (43), and Ball (44) have reported actual production plant experiences. In 1985, Frink and Layton (45) presented an excellent overview of mill

experiences. A 3:1 blend of pMDI and furfural extender was used in the production of particleboard. Their results indicated an approximate total binder reduction of about 50% for the blend or about 60% if the isocyanate level alone was considered. By using 2.8-3.2% of pMDI on OSB, it was shown that by operating the press at a 50^0F lower temperature and increasing dryer capacity, there was a potential for reduction of 27-38% in binder usage while also saving energy. Dosages as low as 1.8% have been reported for production of American Plywood Association (APA) rated flooring and sheathing products (2). All this was done without sacrificing product quality.

pMDI also gives better mechanical and physical properties of wood composites compared to PF (2,30,36,46). Hawke et al. (47-50) found that 3% pMDI-bonded hardboard is superior in strength properties to those bonded with 3 % PF and superior or equal to panels bonded with 10% PF. There was no difference in modulus of elasticity (MOE) between the two adhesives. They also found marked improvement in 24-hour water-immersed water adsorption and thickness swell with use of pMDI as compared to 3 % and 10% PF. The 10% PF-bonded hardboard had less linear expansion than pMDI-bonded panels, while they were similar at the 3% adhesive level. Sun et al. (49, 50) also reported that pMDI-bonded panels were clearly better than PF-bonded panels in dry-modulus of rupture (MOR), accelerated-aging treatments (AAT)-MOR, and internal bond. The pMDI-AAT specimens had very high strength retentions, which means they were very durable.

Some concerns about pMDI-bonded board durability and creep have arisen recently. In the early 80s, Sekino and Suzuki (51) took note of this issue. They reported creep of pMDI-bonded oriented-particle board is the same in magnitude as that of PF bonded and UF bonded boards. Fiore (41) examined durability and creep testing of random 7/16 in. pMDI-bonded oriented waferboard as well as PF-bonded OSB, waferboard, and plywood. He demonstrated that pMDI-bonded panels performed very well for the ASTM and APA 6 cycle durability tests. The pMDI boards were comparable to PF-bonded boards for the ASTM D3434 automatic boil test and two hour boil test. In regards to creep behavior, the pMDI-bonded panels were comparable, if not better than the PF-bonded.

Another advantage offered by pMDI is that it contains no free formaldehyde (52). The methylene bridge in the cured pMDI/wood composites will not break down and form formaldehyde under high temperature and humidity conditions.

While enjoying all of the above advantages, pMDI also has some problems associated with its application. Pound for pound, pMDI has higher cost than PF and UF resins. However, this can be balanced by savings elsewhere in the production process. As mentioned before, lower dose is permitted with pMDI. Lower board density results in savings in raw material and shipping costs. Lower wax levels and no catalysts or hardeners are needed. pMDI also can tolerate higher moisture chips, which leads to energy savings on drying. Also the superior performance of pMDI-bonded boards will command a price premium. In addition to the above intrinsic savings offered by pMDI, a

great amount of research has been initiated to co-apply pMDI with other types of adhesives. This will further reduce the cost of pMDI.

A major initial problem is that pMDI causes the wood to stick to the metal press platens and caul plates (9,53). It was attributed to the reaction of the isocyanate groups with the molecular film of adsorbed water and with the oxyhydrate layer on metal surfaces. There have been several methods to solve this problem. The earliest method was to use PF or UF face layers over pMDI core (3). This method has proven to be successful in commercial production, but it does not produce a 100% pMDI-bonded board. Such a product is desirable in the case of interior-grade particleboard where the major justification for the use of isocyanate binder has been its lack of formaldehyde emissions. A self-release isocyanate has been invented by Rubicon to address this problem. Higher dosages of pMDI are required to overcome the internal release effect. Permanent release coatings on cauls and press have also been considered. However, it is expensive, and the durability of coatings has not been proven (8). Gallagher (54) also did some exploratory work on solving this problem. He prepared a series of urethane adhesives by mixing isocyanates and polyol. The isocyanate-polyol reaction occurs in the press. Sticking problems were avoided by using a nearly stoichiometric quantity of isocyanate and polyol. Milota and Wilson (55) also showed that isocyanate-polyol resin can offer satisfactory performance if the right formulation is used. But research stopped at the laboratory level. Currently, the most popular method is to use external spray release agents (45,56). A variety of well known lubricants or surface-active materials such as

soaps, detergents, fatty esters, waxes, and the like could be used. Also, catalysts were used that promoted formation of a brittle polymer at the wood-metal interface (57). It has been effectively and economically used for full production of MDI-bonded composite boards.

Another problem lies in the areas of health and hygiene. The main hazard associated with pMDI is inhalation of MDI vapor or aerosol which can give rise to respiratory problems. However, MDI has a vapor pressure of approximately 10^{-5} torr. Even though the threshold limit is only 0.02 ppm, the low vapor pressure makes this value relatively easy to maintain (58,59). Two major producers of pMDI have published several papers on this issue (9). They conclude that the MDI levels in manufacturing plants were generally below the Occupational Safety and Health Administration's (OSHA) maximum permissible exposure limit (PEL). There was also a concern about hydrogen cyanide gas generation upon combustion of isocyanate-bonded wood products. There was evidence that isocyanates impose a greater cyanide hazard than UF resins. Frink and Layton (45) have pointed out that no data support this implication. They referenced two previous reports to contradict this statement. Those two papers assert that isocyanate bonded boards generate slightly more HCN than their PF bonded conterparts, but considerably less than the UF bonded boards.

2.1.3. Cure Chemistry for Wood/pMDI Adhesion

While extensive studies have been done on the performance of pMDI bonding, less effort has been spent on elucidating mechanisms of wood/pMDI bonding. That pMDI bonds wood is without doubt, however little is known on how it works and why it performs so differently from other conventional resins. pMDI is a highly reactive chemical compound which contains the R-N=C=O group. This group has the ability to react with a variety of compounds possessing an active hydrogen such as water, amines, alcohols, and acids. A short review of the nature of isocyanate chemistry is presented to aid in understanding the pMDI/wood reaction mechanism.

Reactions of isocyanates with hydroxyl groups

Reactions of isocyanates with polyols or wood hydroxyls occur according to reactivities of these hydroxyl groups. Although reactivity of the hydroxyl group varies, its general reaction with isocyanate is

$$\text{R-NCO} + \text{R'OH} \longrightarrow \underset{\text{Urethane}}{\text{R-N(H)-C(=O)-O-R'}} \qquad (2.1)$$

R = aliphatic or aromatic groups, etc.

R′ = aliphatic or aromatic groups, etc.

Wood consists of three different polymers which contain primary and secondary aliphatic hydroxyls, and aromatic hydroxyls. Thus, different types of urethanes could be formed.

Reactions of isocyanates with water

Isocyanates are highly reactive to moisture. The reaction of isocyanate with water is illustrated in equation (2.2). Carbamic acid is not stable and decomposes to form a primary amine and carbon dioxide.

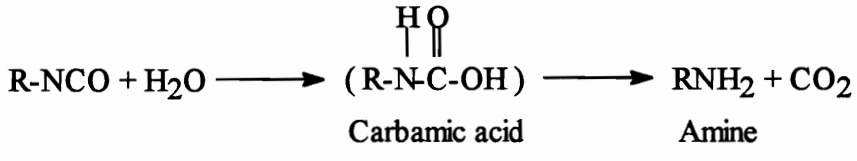

(2.2)

Reaction of isocyanates with amine

Reaction of isocyanate with amine is by far the fastest reaction compared to other active hydrogen-containing compounds (60). The hydrophilic nature of wood always ensures a high degree of wood hydration. This reaction must be considered. Reaction of isocyanate with amine is shown in equation (2.3). A following chain of reactions between isocyanates and its derivative is also presented.

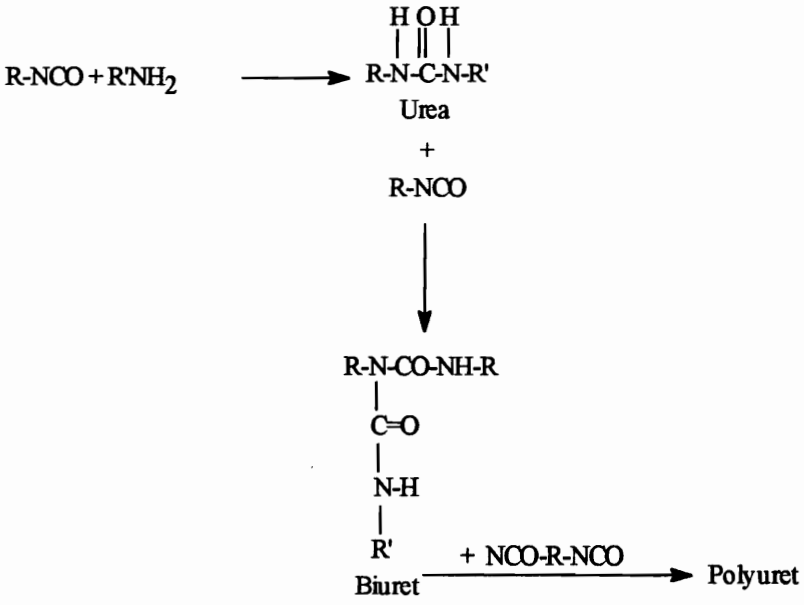

(2.3)

Reaction of isocyanates with urethane

In the presence of an excess of isocyanate, the hydrogen atoms of the urethane will react with isocyanate to form an allophanate (2.4).

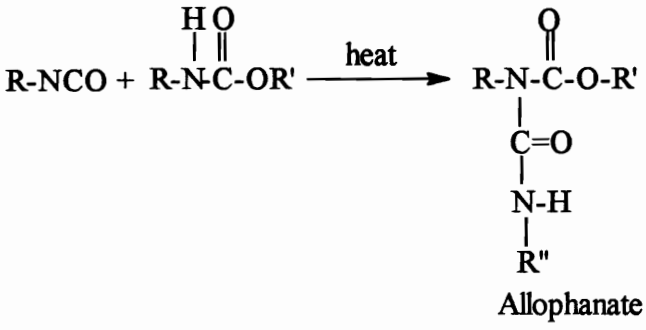

(2.4)

Dimerization of isocyanates

Aromatic isocyanates such as MDI and TDI, have a tendency to dimerize. The rate of self-polymerization (dimerization) depends upon the electronic or steric influences of the ring substitutes. MDI dimerizes slowly on standing at room temperature (61). The dimerization of isocyanates is illustrated in equation (2.5).

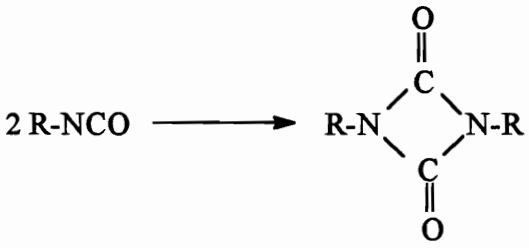

(2.5)

Upon heating to a certain high temperature, the dimer formed will decompose back to isocyanate.

Trimerization of isocyanates

Trimerization of isocyanates is shown in equation (2.6).

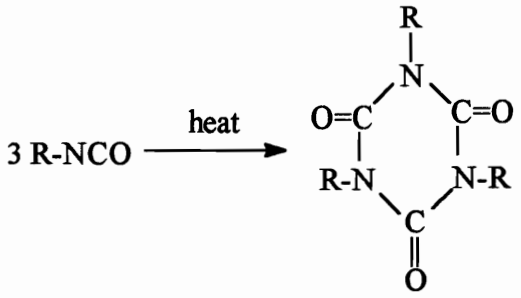

(2.6)

It was also noticed by Reegen and Frisch (61) that substitution and steric effects on phenyl nuclei of the aromatic isocyanates greatly affect the reactivity of the isocyanates. Regarding effects of the p-methyl substitution, the tendency for pMDI to trimerize is low in wood bonding process.

Reaction mechanism for wood/pMDI bonding

A review of the work done on the chemical reactions of isocyanates has been compiled by Frisch et al. (62). Earlier research led people to believe that pMDI derives its strong bonding to wood from the formation of covalent bonds with the lignocellulosic substrate (3,31,63-65,66-68). However, two papers have questioned this theory (69,70). This bonding mechanism is just an assumption as there is no direct experimental evidence to support its validity in industrial processes of pMDI-bonded composites. Although opinions differ, it is generally accepted that there are multiple, competing pathways for the pMDI/wood reaction (30). The hydroxyl groups of wood components (cellulose, hemicellulose, and lignin etc.) offer ample opportunity for covalent bonding with pMDI. On the other hand, the hydrophilic nature of wood always ensures a high degree of wood hydration. The pMDI-water reaction will lead to urea formation. Urethanes and ureas

may further react with isocyanates to form allophenates and biurets, respectively. pMDI also has a tendency to dimerize to form uretidione. It can be expected that there will be competitions among these different reaction pathways.

In the early seventies, Morak and coworkers (63-65) performed some of the earliest work on the wood/isocyanate reaction. The work was to improve the properties of paper and liner board made with isocyanate treatment. It was claimed that diisocyanates are capable of cross-linking with cellulose hydroxyls thus increasing structural and flexural rigidity at high relative humidity, and improving dimensional stability. The reactivity could be improved by using swelling agents such as dimethylformamide (DMF) or catalysts, especially di-n-butyltin diacetate. In fact, most of studies were in the presence of either swelling solvents or catalyst, which is not common in the manufacturing process of wood composites. Water was always present in the samples and its effects were not discussed. No direct evidence was given about the cross-linking between hydroxyl groups with isocyanates other than the improvement of paper performance.

Rowell et al. (66-68) extended this area by examining the reactions between mono- and di-isocyanates with woody material. Their work aimed at better understanding the role of wood hydroxyl groups in the weathering and biodegrability of wood and cellulose. They treated oven-dry southern pine with vapor phase methyl isocyanate at 120^0C, 150 psi. Fourier Transform Infrared (FTIR) spectroscopy was employed to show the evidence of urethane formation. They assigned the peak at 1730 cm^{-1} to the carbonyl band from urethane. As the weight percent gain (WPG) of treated wood increases, this band gets

stronger (68). There is also an increase in the absorption bands, such as 1550 cm^{-1}, 1270 cm^{-1} and 770 to 780 cm^{-1}, which are all associated with nitrogen from urethane. Studies showed that both carbohydrate and lignin components of wood react with isocyanates (68). Additional evidence of cross-linking was obtained from the finding that the calculated volume of methyl isocyanates added to the wood is approximately equal to the volume expansion of the wood. However it was not the case with higher molecular weight isocyanates (68). Nitrogen analysis after extraction also showed that a real increase in unextractable nitrogen, and the increase in nitrogen content paralleled the reaction time. No unreacted isocyanates remain in the samples after extractions (68). This was proven in that the isocyanate absorption at 2275-2240 cm^{-1} was absent in the IR spectra. The nitrogen content was converted to the degree of substitution (DS) of the hydroxyl groups in each component of wood. It was found that the DS is higher in the lignin than in the holocellulose. Finally, they concluded that the dimensional stability of wood and its resistance to biological deterioration was due to the removal of active hydroxyl groups by reaction with the isocyanate group to yield a urethane linkage (68).

In the late 80s, Owen and coworkers (71) also utilized FTIR to gain insight into what happens to functional groups in the wood structure when scots pine (*Pinus sylvestris*) was treated with n-butyl isocyanate. They followed the change in the absorbance value of the carbonyl absorption at 1710 cm^{-1}, which was taken from a "difference" spectrum between the treated and untreated wood. After excess isocyanate was used, they found that the very strong O-H stretching absorption band from wood had

been replaced by a much weaker and sharper absorption at 3360 cm^{-1}, and the carbonyl absorption region showed a clear doublet (1726 and 1692 cm^{-1}). They attributed these changes to the fact that all the hydroxyl groups had been replaced with excess isocyanate. They assigned the new 3360 cm^{-1} absorption to the carbamate N-H bonds. Additionally they found that the excess isocyanate reacted with some of the carbamate groups to form allophanate. The doublet at the carbonyl absorption was quoted for the twin C=O vibrations of an allophante. They also concluded that the initial reaction is faster for lignin, but later the holocellulose reaction dominates as the majority of hydroxyl groups are contained in the cellulosic part of wood (71).

The above works have focused on using isocyanates to chemically modify wood (63-65,72,73). These studies did not intend to use isocyanates as a wood adhesive; therefore they used small monofunctional isocyanates, vapor phase isocyanates (72,73), catalysts promoting the isocyanate/hydroxyl reaction (63-65), and solvents swelling the wood microstructure (63-65,72,73). They proved that low molecular weight isocyanates can chemically react with wood under certain conditions. Galbraith and Newman did use commercial pMDI to study the cure chemistry (1). They employed DSC and FTIR, and found that wood reacts with isocyanate to form urethane. However, they used ground wood in their experiments. Very little evidence shows that urethane bonds exist in a typical wood-isocyanate bondline. Instead, McLaughlin (46) has found copious amounts of polyureas in wood treated with 4,4'-MDI and pressed at 5% moisture content. He used subtractive difference analysis with FTIR spectroscopy of untreated wood and cured

pMDI/wood composites, and showed no presence of any urethane formation. Only when excess amounts of catalysts were used to enhance the probability of urethane reactions was a small amount of the urethane linkage detected. In another experiment, Whitman (74) showed the presence of large amounts of carbon dioxide during the hot pressing of a wood-isocyanate mat. This further proves that the isocyanate-to-polyurea reaction dominates the cure chemistry, since carbon dioxide is a byproduct of that reaction.

Steiner et al. (75) provided a better understanding of the sequence of reactions that take place during the curing of pMDI wood composite products. Unlike most of the previous studies, they investigated the reaction in the presence of moisture and without the use of solvent or catalyst. First they used DSC to study the water-MDI reaction. Endothermic and exothermic peaks were observed between 110^0C and 150^0C and were associated with reactions between pMDI and water. There was evidence of reactions between water and pMDI at moderate temperatures. Then they investigated the pMDI reaction in the presence of wood. Wood with 5% MC shows an exothermal peak in the range of 40^0C-50^0C when treated with more than 9% pMDI. The size of the peak increases with the increasing amount of resin loading. Since the peak was not shown in the pure water-pMDI mixture, the authors attributed it to the rapid reaction between pMDI and wood. At higher MC (28%), the exothermal peak at about 40^0C decreases while a much larger endothermic peak appears from about 80^0C at 0% pMDI to 95^0C at 28% pMDI addition. This endothermic region was considered similar to that of the pMDI-water reaction (75). The authors further examined the reactions by IR analysis.

The N=C=O absorbance region at about 2250 cm^{-1} is the most characteristic band for pMDI. By following this band, they found the absorbance band shape changed as the reaction proceeds. They could not establish a precise interpretation of these intensity changes, however these changes indicated the pMDI-wood reaction involves at least two distinct stages during curing. Spectral changes in the 1800 to 1500 cm^{-1} region were also examined. Cure at 25^0C or 60^0C for 17 hours showed an increase in the 1670 cm^{-1} absorbance intensity which is assigned to amide C=O stretching. At 160^0C, this band decreased and a new band appeared at about 1670 cm^{-1}. This spectral change was attributed to different stages of urethane formation or initial formation of polyurea from moisture present in the wood. This would be followed by further reaction with pMDI to give urethane products. The authors have also employed thermal softening to support their conclusion that the pMDI/wood curing reaction involves at least two distinct phases. They claimed that the initial rapid stage involves isocyanate with primary, secondary, or phenolic hydroxyl groups in wood, creating linear bridges between wood components with some minor cross-linking. The second stage reaction involves primarily cross-linking reactions.

More recently, Weaver and Owen et al. (71,76,77) have used infrared spectroscopy to investigate wood-isocyanate bonding chemistry. Their studies of the reaction of n-butyl isocyanate with wood under high pressure showed that the formation of urethanes and allophanates is feasible under certain conditions (71). Then they continued to study the reaction of phenyl isocyanate at ambient conditions with β-D-glucose, cellulose, dioxane

lignin and wood flour with FTIR. They monitored how the intensity of urethane carbonyl band varies with the ratio of wood/isocyanate for the different values of moisture content. The results suggested that lignin reacts much more quickly with phenyl isocyanate than does cellulose. The reaction of wood with phenyl isocyanate depends on the moisture content of the wood. For wood at 30% MC down to 19% MC, the isocyanate reaction appeared to be almost exclusively with the water present in the wood. Only at the wood/isocyanate ratio of 1:4 for the 19% MC samples was there evidence that the isocyanate is reacting with the wood. The 1:1 ratio mixture for wood with 7% MC also showed little evidence for chemical bonding to the wood , but at 1:2 and 1:4 ratios, the spectral evidence suggests that urethane bond is also present. They attributed this to the fact that the excess isocyanate had ensured that all water present has already reacted.

Pizzi and Owens (78) have also investigated the bonding mechanism of pMDI. By using DSC, they confirmed that MDI reacts with water in a series of reactions in the temperature range 87-117^{0}C. These reactions are catalytically activated by the presence of a lignocellulosic substrate. In the temperature range of 128-180^{0}C, MDI appears to bond covantly to cellulose and to wood.

Wendler has pointed out that the complexity of the FTIR spectrum for wood/isocyanate systems makes interpretation of the spectra difficult (79). This contributes to the continuing controversy over the exact mechanism of adhesion for pMDI-bonded wood composites. He utilized ^{15}N cross-polarization/magic angle spinning (CP/MAS) solid state NMR to study the pMDI bonding mechanism (80-82). He

investigated the effects of precure moisture content, cure temperature, and cure time. The first direct evidence of urethane formation was provided. However, it was under high temperature (185^0C) and long cure time (60 minutes), which is not a normal industrial manufacturing condition. The pMDI-water reaction dominated the cure chemistry under all the conditions. Biuret linkage was found to be thermally unstable and decompose to polyurea and isocyanate (82). The bondline was found to be a complex of polyureas, biurets, polyurets, and possibly urethanes. The chemistry and performance of the pMDI-wood bondline is highly dependent upon the position of that bondline within the composite panel. However, the pMDI used in those studies has an extremely high molecular weight (82) which may make its bonding significantly different from the commercial resin.

2.1.4. Effects of Isomer Ratio

Commercial pMDI is composed of diisocyanates and higher order oligomeric polyisocyanates. The diisocyanate fraction is composed of about 95% 4,4'-MDI and a small amount of 2,4'- with a trace of 2,2'-isomers (83). This composition of pMDI is determined during synthesis which will be discussed later. The structures of these different isomers and polyisocyanate are shown in Figure 2.1. It is likely that the performance pMDI resins will depend on its composition, especially the 4,4'-/2,4'- isomer ratio. However, no study of the effects of pMDI structural isomerism on wood bonding performance has been reported.

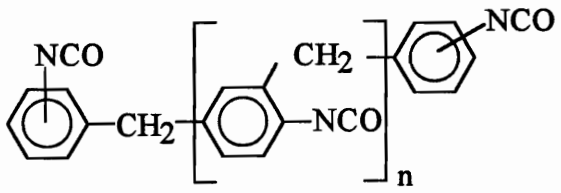

General Structure of pMDI

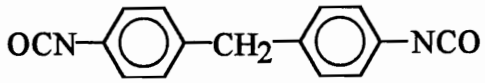

4,4'-MDI

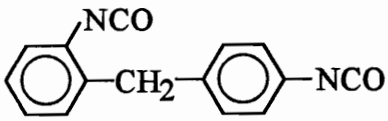

2,4'-MDI

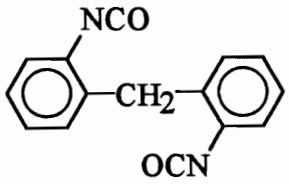

2,2'-MDI

Figure 2.1: Structures of pMDI and different MDI isomers.

While the effects of structural isomerism on pMDI-wood bonding are unknown, this topic has been actively investigated for other MDI based products. It has been reported that structural isomerism has a considerable effect on the chemistry and physical properties of MDI based flexible foams (84-89). These flexible foams consist of hard segment polyureas formed by the reaction of MDI and water and soft segment polyurethanes formed by the reaction of MDI with polyol. Steric bulk near the ortho isocyanate reduces the reactivity of 2,4'- and 2,2'- MDI as compared to 4,4'- MDI (87). The lower reactivity of 2,4'- MDI curtails the formation of polyurea and directs more isocyanate into the formation of urethane (88). The level of 2,4'- MDI content also affects the chain morphology of the foams (86, 87). Higher 2,4'- MDI content polyurea has a much lower level of crystallinity than the higher 4,4'- MDI. The higher level of ortho-NCO groups interrupts the molecular symmetry so that fewer of the polyurea oligmers can crystallize. It subsequently affects the macroscopic properties of these foams. High levels of the 2,4'- MDI serve to enhance elongation and tear strength. However, it also adversely affects other foam properties such as hardness, tensile strength, and humid aging (86, 87).

2.2. Synthesis of pMDI

2.2.1. Introduction

Many methods for the preparation of isocyanates are reported in the literature (90). The commercial process is a two-step reaction (Figure 2.2). The first step is the synthesis

STEP 1

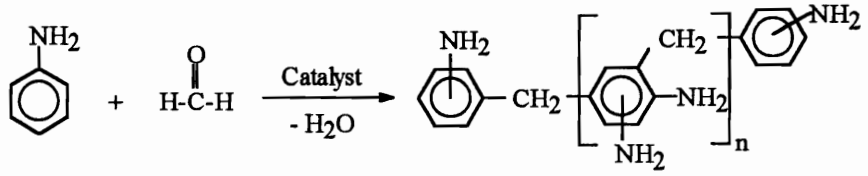

Aniline Formaldehyde Polyamine

STEP 2

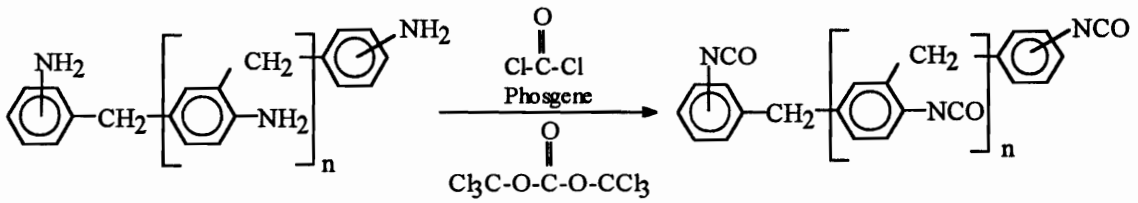

Polyamine Triphosgene pMDI

Figure 2.2: The overall reaction process for the synthesis of pMDI.

of polyamine from the catalyzed condensation of aniline with paraformaldehyde. The second step involves the phosgenation of the polyamine.

The commercial product is a mixture containing about 45-50% 4,4′-MDI and a small amount of 2,4′- with a trace of the 2,2′- isomers. The remainders (50%) are higher order oligomeric polyisocyanates (83). The degree of polymerization, n, can reach as large as 8 (30), while the average n value is only about 0.8 (83). It has an isocyanate content of about 30%.

2.2.2. Condensation

Numerous literature (91-100) are available regarding the condensation reaction. However, most of them are lacking detail. Only Twichett (83) discussed the reaction mechanism in detail. As shown below, the process begins with the addition of formaldehyde (or paraformaldehyde) with aniline in the presence of an acidic catalyst.

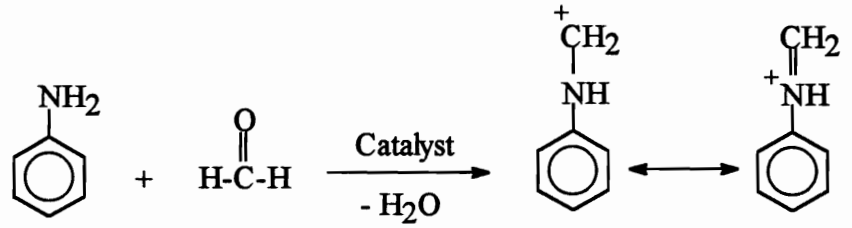

Aniline Formaldehyde Iminium Ion (2.7)

A strongly electrophilic imminium ion is formed with the elimination of water. The imminium ion is susceptible to attack by another aniline molecule to give para- and ortho-substituted aminobenzylaniline (2.8).

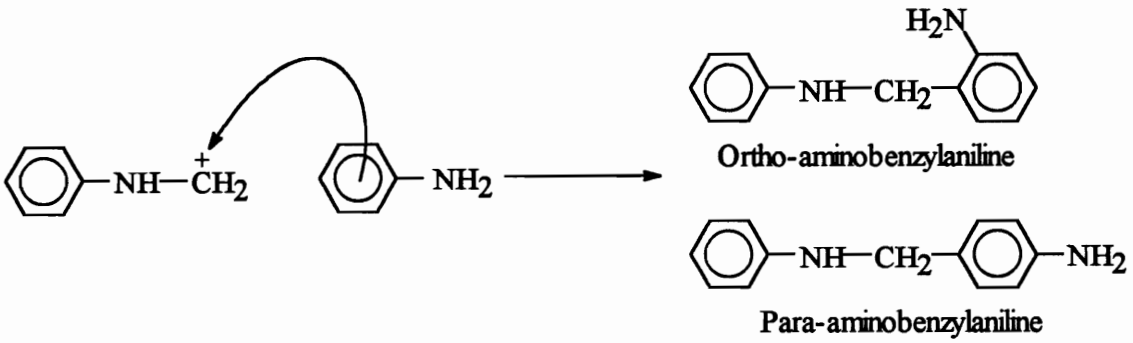

(2.8)

Next, the resulting secondary amines (aminobenzylanilines) are protonated by HCl and subsequently attacked at the benzyl carbon by another mole of aniline (2.9).

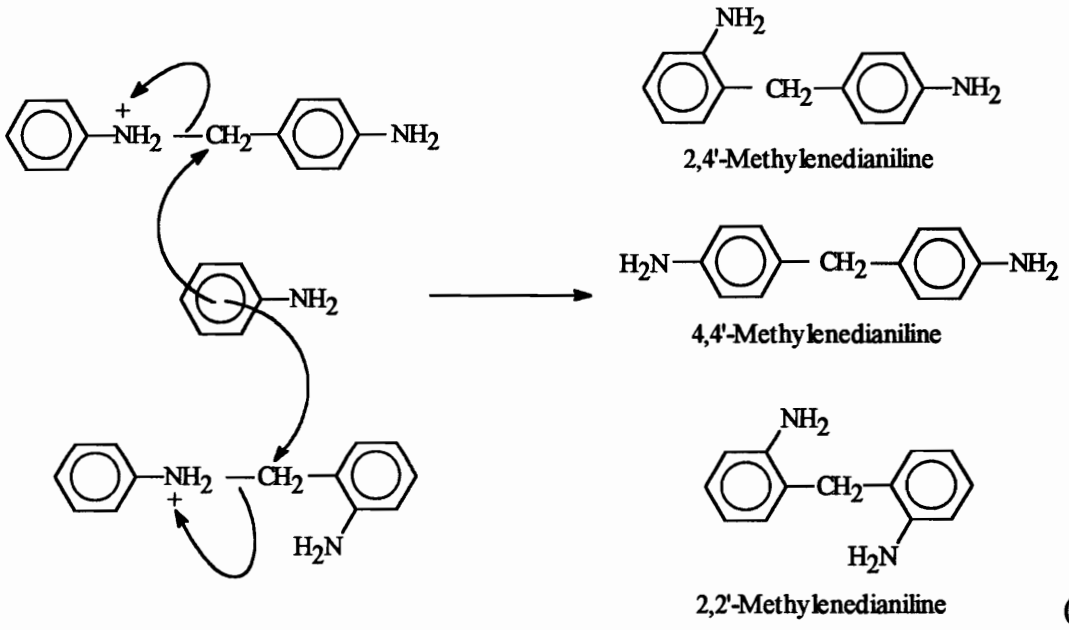

(2.9)

Reactions (2.8) and (2.9) both involve competition between ortho and para substitution. Therefore, three structural isomerisms of methylenedianiline are formed. Steric effects favor 4,4′- isomer formation, followed by 2,4′- and 2,2′- isomers. In reaction (2.9), if the

attacking nucleophile is the aromatic electrons of methylenedianiline, triamine will be formed.

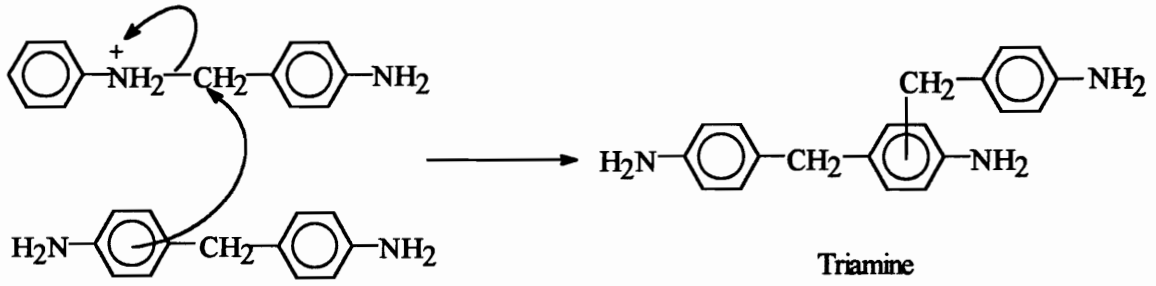

Triamine

(2.10)

By the same mechanism, higher methylene-bridged polyamines are also formed.

The composition of the polyamine can be varied widely according to the reaction conditions. The major factors include the molar ratio of aniline/formaldehyde, the molar ratio of aniline/HCl, and the reaction temperature and time (83). Large excess of aniline favors the production of 4,4′-diamine, while small amount of HCl increases the 2,4′-diamine and polyamine content.

To obtain a higher 2,4′- diamine, a catalysed high-temperature process needs to be employed. The high reaction temperature reduces stereoselectivity. Bentley (101) claimed that the 2,4′- isomer content of the diamine portion can be varied from about 15 wt.% to about 95 wt.%. He utilized a solid acidic siliceous clay catalyst with the temperature ranging from about 120^0C to about 200^0C. Heterogeneous catalysis reduces dimensionality, and therefore reduces the activation energy (102) to reduce stereoselectivity. Pressure is not critical with respect to the process as long as it is

sufficient to provide for liquid phase reaction conditions. Depending on the catalyst selected, the 2,4′- isomer content is determined by the initial or final reaction temperature.

2.2.3. Phosgenation

Phosgenation of polyamine is usually carried out by first dissolving it in an inert solvent such as chloro- or dichloro-benzene, and then treating with excess phosgene (83). The solvent chosen must have high boiling point to allow suitably high reaction temperatures to be attained. Triphosgene has been reported to be used as a phosgene substitute to avoid using the highly toxic, gaseous phosgene as the reagent (103). Triphosgene is a crystalline, stable solid, which is easy to handle in laboratory. The product is a complex mixture (79). Primary amines first react with phosgene to form carbamoyl chlorides which are unstable and decompose to isocyanate and HCl (2.11).

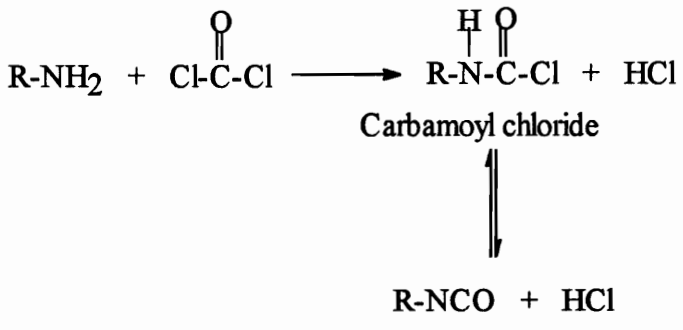

(2.11)

Several important side reactions also occur. Linear ureas appear to be formed by the reaction of isocyanate with residual amine or the amine generated from isocyanate-water reaction. Urea can further react with isocyanate to form biuret or polyuret. At the same time, urea can react with phosgene to form N-carbonyl chlorides (2.12).

(2.12)

Any residual secondary amine from condensation reaction can react with phosgene to give a secondary carbamoyl chloride. Unlike primary carbamoyl chloride, secondary carbamoyl chlorides do not dissociate (2.13). Instead they remain as chlorine-containing impurities. Therefore it is important to make sure that the secondary amines completely convert to primary amines during the condensation reaction. This can be achieved by using sufficiently high temperatures and long reaction times.

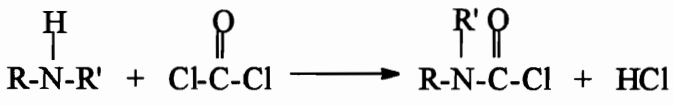

(2.13)

Another important side reaction is the dimerization of isocyanates. Isocyantes can be dimerized to substituted uretediones through a reversible reaction. The dimer is insoluble and more thermodynamically stable at room temperature. However, the uretedione can be dissociated completely at 200^0C. Therefore, heat treatment at 200^0C followed by quench cooling can prevent dimerization. Control of these side reactions is of great importance as pMDI is often used without distillation and impurities remain as contaminants. These contaminants can considerably affect the resin bonding performance.

2.3. Techniques for Characterizing Thermoset Resins

Most research concerning adhesives is aimed toward improving their bonding properties. To do this systematically requires an understanding of molecular-level influences on macroscopic behavior. Chemical structure, morphology, and chain dynamics have important effects on bulk material properties. These have been characterized by various forms of spectroscopy.

A wide range of analytical techniques are used to charaterize adhesives. The primary characterization must be chemical, which include the chemical components of adhesives and the cured bondline. Ultraviolet/visible spectroscopy and mass spectroscopy (MS) of fragments broken from the polymer chain are often used. Even more common are infrared (IR) absorption and nuclear magnetic resonance (NMR). IR can follow reactions from liquids into the solid state, but the spectral bands for various chemical groups often overlap in the important "fingerprint" region, leading to difficulties in making quantitative determinations (104). NMR also gives local information, on a very fine scale, about the environment of the atoms investigated. Solid state NMR can also determine the mobility of atoms in various regions and the orientation of molecules.

The molecular weight distribution is also an important characteristic of adhesives. The methods used include viscometry, osmometry, light scattering and gel permeation chromatography (GPC). Known alternatively by its more descriptive name "size exclusion chromatography", GPC is a rapid, efficient and reliable method (105).

To optimize the bonding performance, it is also important to understand the curing process. The cure of thermosetting resins is a complex process that is associated with

significant chemical and physical changes. Thermoset resins are very difficult to study due to their insolubility and infusibility (106). The widely used DSC technique provides considerable insight into the reaction mechanism. It measures the cure of resins by sensing the exothermic heat output of small resin samples during controlled heating (104, 107). However, the data do not directly inform about mechanical property build up. Events like gelation and vitrification are not observable by this method. Gillham (108-110) used torsional braid analysis to introduce the time-temperature-transformation (TTT) diagram for thermosetting resins. Dynamic mechanical thermal analysis (DMTA) has also been used for this task (106,111). More recently, dielectric thermal analysis (DETA) has been used successefully to study the chemistry and rheology of thermosets during cure. Not only being able to monitor the cure process, DMTA and DETA can also be used to investigate mechanical properties at the molecular level. Some main techniques used in this dissertation will be briefly reviewed in the following section.

2.3.1. Solid State NMR

In 1946, Bloch and Purcell, working independently, observed the absorption of electromagnetic radiation as a consequence of energy-level transitions of nuclei in a strong magnetic field (112). In the first five years following the discovery of nuclear magnetic resonance, chemists became aware that the molecular environment influences the absorption by a nucleus in a magnetic field and that this effect can be correlated with molecular structure. Since then the growth of NMR spectroscopy has been explosive, and

the technique has had profound effects on providing details of molecular structure and dynamics of chemical substances. For years, high resolution NMR has been limited to the liquid state (113). In spite of the success of solution NMR, many interesting properties of bulk polymers disappear if the samples are put into solution. Cured thermoset resin cannot be dissolved under conditions such that the structural integrity of the sample is retained. Therefore, if high resolution solid state NMR data could be obtained, new details concerning the nature of the solid state of polymers might be uncovered. Recent advances in the techniques have now made this goal possible (114).

There are two main problems associated with high resolution solid state NMR. One is the severe line-broadening effects which would cause sensitivity problems in spreading a given signal intensity over a broad line. Another is the inherent sensitivity problem associated with the related low measuring frequencies employed in NMR. The latter difficulty has been alleviated by improvements in NMR instrumentation (higher magnetic fields). The line-broadening problems have also been addressed successfully by the continuing development of line-narrowing techniques such as cross-polarization (CP) (115), magic angle spinning (MAS) (116), and high power proton decoupling (117). Since the combination of these techniques by Schaefer and Stejaskal (116), high-resolution solid state NMR has become one of the most powerful and versatile tools available for the study of polymer structure, morphology, and dynamics (117,118).

Solid state NMR, specially ^{13}C CP/MAS NMR, has proven very effective in the characterization of thermoset resins. It has been used in various wood adhesive systems

such as PF (119-123), UF (124,125), and MF (126) etc. However, the ^{13}C spectrum of a pMDI-bonded wood composite is complicated due to signals from the wood substrate. Numerous additional resonances from carbons of the wood components overlap with signals from the pMDI structure, as well as those from the cured chemical species. This makes interpretation of the spectrum extremely difficult. Therefore, a ^{15}N NMR is often employed to investigate the MDI based system (79-82, 127-131). A more detailed review of ^{15}N will be given in a later chapter.

2.3.2. Dynamic Mechanical Analysis

Dynamic mechanical analysis (DMA) measures the stored and dissipated energies of a viscoelastic specimen put under oscillation at varying temperatures. The stored energy depends on the polymer type, temperature, and frequency of oscillation and is represented as the storage modulus (E′). The dissipated energy represented by the loss modulus (E″) is due to the molecular frictions occurring in the viscous flow. The loss tangent, or tan δ, is given by E″/E′ and represents the ratio of energy dissipated to energy stored per cycle. The measurements of these properties are capable of detecting motional transitions such as glass and secondary transitions, and of quantitatively determining the polymer mechanical properties on the molecular level.

DMA has been used to study the response of individual wood components *in situ* to an applied perturbation (132-135). DMA allowed for a great understanding of the contributions made by individual wood polymers, as well as their interaction, to

composites properties. DMA has also been extensively used to monitor the cure process of resins (136-142). Cure parameters such as gelation time and vitrification time can be obtained through the DMA method. The method is useful in optimizing the cure conditions for resins.

2.3.3. Dielectric Spectroscopy

While the DMA method measures the ability of the system to resist movement, dielectric thermal analysis (DETA) measures the ability of the system to move. Dielectric analysis measures the two fundamental characteristics of a material: 1) capacitance, or its ability to store electric charge, and 2) conductance, its ability to transfer electric charge-as functions of time, temperature, and frequency. These electrical properties are correlated to molecular mobility. Such correlations probe the chemistry, rheology, and molecular mobility of polymeric materials (143-146).

The two fundamental dielectric properties are the permittivity (ε') and the loss factor (ε''), which are the result of dipole motion and ionic conduction. The permittivity measures the degree of alignment of dipoles, and the loss factor is a measure of the energy expended to align dipoles and move ions. During the isothermal curing of a thermosetting resin, dipoles tend to align along the electric field and the ions move toward the electrode. At the early stage of curing, movement of the dipoles and ions are quite free in the liquid resin. However, as the curing progresses, molecules grows larger and a network starts to form. This growth will restrict the movement of dipoles and ions. Eventually, the dipoles

will remain randomly oriented and ions will become immobilized. These molecular level changes can be detected by the DEA. Ionic conductivity (σ) is more commonly measured to monitor the curing process. It can be derived from loss factor, which results from a dipole term (D) and an ionic conductivity contribution:

$$\varepsilon'' = (\sigma/\varepsilon_0\omega) + D$$

where ε_0 is permittivity of free space and ω is the applied field frequency.

At sufficient low frequencies, the dipole term D can be ignored. Therefore, ionic conductivity can be easily determined through the measurement of loss factor. As the resin cures, the ionic conductivity decreases and its inversion, ionic viscosity, increases. This can be used to monitor the onset of gelation and vitrification.

Recently, microdielectric analysis has been intoduced that makes possible *in situ* production monitoring and cure control of thermosetting resins (147). It has been used for a variety of thermosetting polymers (144,148,149), including PF resins (150, 151) and pMDI (152).

References

1. Galbraith, C. J. and W. H. Newman. 1992. Pacific Rim Bio-Based Composites Symp., Rotorua, New Zealand. pp. 130-142.
2. McElrath, R. W. 1992. Proc. of the Southeastern Section of the Forest Products Research Society, T. D. Faust Ed., Atlanta, GA.
3. Deppe, H. J. 1977. Proc., 11th International Particleboard/Composite Materials Symp., T. M. Maloney Ed., Pullman, WA. pp. 13-31.
4. Deppe, H. J. and K. Ernst. 1971. Holz als Roh-und Werkstoff 29 (2): 45-50.
5. Ernst, K. 1975. Holz-Zentralblatt. 122.
6. Loew, G. and H. I. Sachs. 1977. Proc., 11th International Particleboard/Composite Materials Symp., T. M. Maloney Ed., Pullman, WA. pp. 473-492.
7. Ellingson, G. P. 1977. Proc., 11th International Particleboard/Composite Materials Symp., T. M. Maloney Ed., Pullman, WA. pp. 369-382.
8. Galbraith, C. J., Jr. 1986.. Proc., 20th International Particleboard/Composite Materials Symp., T. M. Maloney Ed., Pullman, WA. pp. 55-81.
9. Adams, A. D. 1980. . Proc., 14th International Particleboard/Composite Materials Symp., T. M. Maloney Ed., Pullman, WA. pp. 195-205.
10. McLaughlin, A., H. E. Reymore, Jr. and R. H. Richter. 1979. U. S. Patent 4,143,014.

11. Galbraith, C. J., Jr., S. C. Cohen and P. R. Sutula. 1985. Proc., 19th International Particleboard/Composite Materials Symp., T. M. Maloney Ed., Pullman, WA. pp. 301-322.

12. Galbraith, C. J., Jr., S. C. Cohen and G. W. Ball. 1983. .Proc., 17th International Particleboard/Composite Materials Symp., T. M. Maloney Ed., Pullman, WA. pp. 263-282.

13. Hse, C. Y. 1978. Proc. of Complete Tree Util. South. Pine symp., C. W. McMillin Ed. pp. 411-415.

14. Hse, C. Y. 1980. U. S. Patent 4,209,433.

15. Tinkelenberg, A., H. W. Vaessen and K. W. Suen. 1982. J. Adhesion 14: 219-231.

16. Dix, B. and R. Marutzky. 1989. ACS Symp. Ser. 385: 229-241.

17. Stephanou, A. and A. Pizzi. 1993. Holzforschung 47: 439-445.

18. Stephanou, A. and A. Pizzi. 1993. Holzforschung 47: 501-506.

19. Glasser, W. G., V. P. Saraf and W. H. Newman. 1982. J. Adhesion 14: 233-255.

20. Newman, W. H. and W. G. Glasser. 1985. Holzforschung 39: 345-353.

21. Pizzi, A. 1981. J. Macromol. Sci.-Chem. A16 (7): 1243-1250.

22. Pizzi, A. 1982. Holz als Roh- und Werkstoff 40: 293-301.

23. Pizzi, A., E. P. von Leyser, J. Valenzuela and J. G. Clark. 1993. Holzforschung 47: 168-174.

24. Leitheiser, R. H. and W. E. Johns. 1983. Proc., 17th International Particleboard/Composite Materials Symp., T. M. Maloney Ed., Pullman, WA. pp. 249-258.

25. Sellers, T., Jr. 1989. Forest Prod. J. 39 (11/12): 53-56.

26. Pizzi, A. and T. Walton. 1992. Holaforschung 46: 541-547.

27. Pizzi, A., J. Valenzuela and C. Westermeyer. 1993. Holzforschung 47: 68-71.

28. Batubenga, D. B., A. Pizzi, A. Stephanou, R. Krause and P. Cheesman. 1995. Holzforschung 49: 84-86.

29. Taki, K. 1985. Mokuzai Gakkaishi 31 (7): 573-578.

30. Frink, J. W. and H. I. Sachs. 1981. ACS Symp. Ser. 172: 285-309.

31. Johns, W. E., T. M. Maloney, E. M. Huffaker, J. B. Saunders and M. T. Lentz. 1981.. Proc., 15th International Particleboard/Composite Materials Symp., T. M. Maloney Ed., Pullman, WA. pp. 213-239.

32. McLaughlin, A., W. J. Farrissey, Jr., L. M. Alberino, D. P. Waszeciak. 1981. Proc., 15th International Particleboard/Composite Materials Symp., T. M. Maloney Ed., Pullman, WA. pp. 255-264.

33. Subiyanto, B., S. Kawai, H. Sasaki, N. Kahar and S. Ishihara. 1988. Mokuzai Gakkaishi 34: 333-336.

34. Palardy, R. D., F. H. Story and S. M. Shaler. 1989. Proc., 23rd International Particleboard/Composite Materials Symp., T. M. Maloney Ed., Pullman, WA. pp. 235-245.

35. Palardy, R. D., B. A. Haataja, S. M. Shaler, A. D. Williams, T. L. Laufenberg. 1989. Forest Prod. J. 39 (4): 27-32.

36. Chelak, W. and W. H. Newman. 1991. Proc., 25th International Particleboard/Composite Materials Symp., T. M. Maloney Ed., Pullman, WA. pp. 205-229.

37. Johns, W. E., G. C. Myers, M. T. Lentz, E. M. Huffaker, J. B. Saunders. 1984. Proc., 18th International Particleboard/Composite Materials Symp., T. M. Maloney Ed., Pullman, WA. pp. 101-116.

38. Palardy, R. D., B. R. Grenley, F. H. Story, W. A. Yrjana. 1990. Wood Adhesives 1990. pp.124-128.

39. Clark, R. J., J. J. Karchesy, R. L. Krahmer. 1988. Forest Prod. J. 38 (7/8): 71-75.

40. Palardy, R. D., B. A. Haataja, S. M. Shaler, A. D. Williams, T. L. Laufenberg. 1989. Forest Prod. J. 39 (4):27-32.

41. Fiore, J., III. 1988. Proc., 22d International Particleboard/Composite Materials Symp., T. M. Maloney Ed., Pullman, WA. pp. 183-202.

42. Ellingson, G. P. and F. W. Braun. 1979. Proc., 13th International Particleboard/Composite Materials Symp., T. M. Maloney Ed., Pullman, WA. pp. 83-95.

43. Adams, A. D. 1981. Proc., 15th International Particleboard/Composite Materials Symp., T. M. Maloney Ed., Pullman, WA. pp. 241-254.

44. Ball, G. W. 1981. Proc., 15th International Particleboard/Composite Materials Symp., T. M. Maloney Ed., Pullman, WA. pp. 265-285.

45. Frink, J. W. and H. D. Layton. 1985. Proc., 19th International Particleboard/Composite Materials Symp., T. M. Maloney Ed., Pullman, WA. pp. 323-347.

46. McLaughlin, A. 1980.. Proc., 14th International Particleboard/Composite Materials Symp., T. M. Maloney Ed., Pullman, WA. pp. 207-211.

47. Hawke, R. N., B. C. H. Sun and M. R. Gale. 1992. Forest Prod. J. 42 (11/12): 61-68.

48. Hawke, R. N., B. C. H. Sun and M. R. Gale. 1993. Forest Prod. J. 43 (1): 15-20.

49. Sun, B. C. H., R. N. Hawke and M. R. Gale. 1994. Forest Prod. J. 44 (3): 34-40.

50. Sun, B. C. H., R. N. Hawke and M. R. Gale. 1994. Forest Prod. J. 44 (4): 53-58.

51. Sekino, N. and M. Suzuki. 1984. Mokuzai Gakkaishi 30 (1): 17-22.

52. Ball, G. W., A. P. Redman and A. D. Adams. 1979. Forest Industries 106 (4): 76-79, 117.

53. Schollenberger, C. S. 1977. Handbook of Adhesives, 2nd Edition, Skeist, I. Ed. Van Nostrand Reinhold, New York.

54. Gallagher, J. A. 1982. Forest Prod. J. 32 (4): 26-33.

55. Milota, M. and J. B. Wilson. 1985. Forest Prod. J. 35 (7/8): 44-48.

56. Leitheiser, R. H. and F. C. Grant-Acquah. 1983. Proc., 17th International Particleboard/Composite Materials Symp., T. M. Maloney Ed., Pullman, WA. pp. 259-261.

57. Diehr, H. J., K. J. Kraft and H. I. Sachs. 1975. U. S. Patent 3,870,665.

58. Johns, W. E. 1980. Proc., 14th International Particleboard/Composite Materials Symp., T. M. Maloney Ed., Pullman, WA. pp. 177-193.

59. Ball, G. W. 1978. Proc. of FESYP Symp.

60. Doyle, E. N. Ed. 1971. The Development and Use of Polyurethane Products. McGraw-Hill Book Company. New York. Chapt. 3.

61. Reegen, S. L. and K. C. Frisch. 1971. Advances in Urethane Sci. and Tech., Vol. 1., K. C. Frisch and S. L. Reegen Ed. Technomic Publishing Co. Chapt. 1.

62. Frisch, K. C., L. P. Rumao and A. Pizzi. 1989. Wood Adhesives Chemistry and Technology, Vol. 1, A. Pizzi Ed. Marcel Dekker, New York. pp. 289-317.

63. Morak, A. J. and K. Ward, Jr. 1970. Tappi 53 (4): 652-656.

64. Morak, A. J. and K. Ward, Jr. 1970. Tappi 53 (6): 1055-1058.

65. Morak, A. J., K. Ward, Jr. and D. C. Johnson. Tappi 53 (12): 2278-2283.

66. Rowell, R. M. and W. D. Ellis. 1979. Wood Sci. 12 (1): 52-58.

67. Rowell, R. M., W. C. Feist and W. D. Ellis. 1981. Wood Sci. 13 (4): 202-208.

68. Rowell, R. M. and W. D. Ellis. 1981. Urethane Chemistry and Application, K. N. Edwards Ed., ACS Symp. Ser. 172: 264-284.

69. Johns, W. E. 1989. Wood Adhesives Chemistry and Technology, Vol. 2, A. Pizzi Ed., Marcel Dekker, New York. pp. 75-96.

70. Udvardy, O. G. 1979. Proc., 13th International Particleboard/Composite Materials Symp., T. M. Maloney Ed., Pullman, WA. pp. 159-177.

71. Owen., N. L., W. B. Banks and H. West. 1988. J. Molecular Structure 175: 389-394.

72. Clermont, L. P. and F. Bender. 1957. Forest Prod. J. May: 167-170.

73. Baird, B. R. 1969. Wood and Fiber 1 (1): 54-63.

74. Whitman, O. 1976. Holz Rohst. Werkst. 34: 427-431.

75. Steiner, P. R., S. Chow and S. Vadja. 1980. Forest Prod. J. 30 (7): 21-27.

76. Weaver, F. W. and N. L. Owen. 1992. Pacific Bio-Based Composites Symp., Rotorua, New Zealand. pp. 143-153.

77. Weaver, F. W. and N. L. Owen. 1995. Applied Spectroscopy 49 (2): 171-176.

78. Pizzi, A. and N. A. Owens. 1995. Holzforschung 49 (3): 269-272.

79. Wendler, S. L. 1994. Master Thesis. Characterization of the Wood/Isocyanate Bondline. Virginia Tech.

80. Wendler, S. L. and C. E. Frazier. 1995. J. Adhesion 50: 135-153.

81. Wendler, S. L. and C. E. Frazier. 1996. J. Appl. Polym. Sci. 61: 775-782.

82. Wendler, S. L. and C. E. Frazier. 1996. Int. J. Adhesion and Adhesives 16 (3): 179-186.

83. Twichett, H. J. 1974. Chem. Soc. Rev. 3 (2): 209-230.

84. Cuscurida, M., T. Howard. 1976. U. S. Patent 3,960,788.

85. Dominguez, R. J. G. 1984. U. S. Patent 4,448,904.

86. Berkowski, L., C. Reichel and J. Taylor. 1987. Advances in Urethane Science and Technology, Vol. 10, K. C. Frisch and D. Klempner Ed., Technomic Publish., Lancaster, PA. pp. 1-15.

87. Thoen, J., R. Elwell, R. Sewell, R. Broos, L. Pellacani, L. Pedroni and G. Bergianti. 1992. J. Cellular Plastics 28: 48-65.

88. Buethe, I., C. J. Reichel and J. D. Taylor. 1983. Polyurethane: New Paths Prog., Mark., Technol., Proc. SPI Int. Tech/Mark. Conf., 6th, Soc. Plast. Ind., Polyurethane Div., New York, NY. pp. 156-160.

89. Lockwood, R. J., T. R. McClellan, L. M. Alberino and P. D. Harkins. 1982. Proc. SPI Annu. Tech./Mark. Conf.

90. Frisch, K. C. and H. C. Vogt. 1964. Chemical Reactions of Polymers, E. M. Fettes Ed., Interscience Publishers. pp. 927-1008.

91. Braun, J. V. 1908. J. Ber. 41: 2145.

92. Rivier H. and A. Farine. 1929. Helv. Chim. Acta 12: 865.

93. Wagner, E. C. 1934. J. Am. Chem. Soc. 56: 1944.

94. Hall, J. A. and P. C. Johnson. 1966. British Patent 1 038 266.

95. Bircher, B. J. and J. H. Wild. 1967. British Patent 1 080 717.

96. Kerrigan, V. 1971. British Patent 1 229 695.

97. Knofel, H. and G. Ellendt. 1978. U. S. Patent 4,087,459.

98. Knofel, H. and G. Ellendt. 1979. U. S. Patent 4,147,724.

99. Knofel, H. et al. 1990. U. S. Patent 4,924,028.

100. Knofel, H. et al. 1994. U. S. Patent 5,359,141.

101. Bentley, F. E. 1978. U. S. Patent 4,071,558.

102. Laszlo, P. 1991. Surfactant Sci. Ser. 38: 437-459.

103. Eckner, H. and B. Forster. 1987. Angew. Chem. Int. Ed. Engl. 26 (9): 894-895.

104. Myers, G. E. et al. J. Appl. Polym. Sci.

105. Cowie, J. W. G. 1991. Polymers: Chemistry and Physics, 2nd edition. Chapman and Hall, New York, NY.

106. Hofmann, K. and W. G. Glasser. 1990. Thermochimica Acta 166: 169-184.

107. Kay, R. and A. R. Westwood. 1975. Eur. Polym. J. 11: 25.

108. Enns, J. B. and J. K. Gillham. 1983. J. Appl. Polym. Sci. 28: 2567.

109. Peng, X. and J. K. Gillham. 1985. J. Appl. Polym. Sci. 30: 4685.

110. Aronhime, M. T. and J. K. Gillham. 1986. Advances in Polymer Sciences, Vol. 18, K. Dusek Ed., Springer-Verlag, Berlin. pp. 83.

111. Wingard, D., W. Williams, K. Wolking and C. L. Beatty. 1988. ACS Symp. Ser. 367: 200.

112. Friebolin, H. 1991. Basic One- and Two- Dimensional NMR Spectroscopy. VCH Publishers, New York, NY.

113. Maciel, G. E. 1984. Science 226: 282-288.

114. Havens J. R. and J. L. Koenig. 1983. Appl. Spectrosc. 37 (3): 226-249.

115. Pines, A., M. G. Gibby and J. S. Waugh. 1973. J. Chem. Phys. 59 (2): 569-590.

116. Schaefer, J. and E. O. Stejskal. 1975. J. Amer. Chem. Soc. 98 (4): 1031-1032.

117. Fyfe, C. A. Solid State NMR for Chemists.

118. Komoroski, R. A. Ed. 1986. High Resolution NMR Spectroscopy of Synthetic Polymers in Bulk. VCH Publishers, Inc., Deerfield Beach, FL.

119. Fyfe, C. A., A. Rudin and W. Tchir. 1980. Macromoleculs 13: 1322-1324.

120. Fyfe, C. A. and M. S. McKinnon. 1983. Macromolecules 16: 1216-1219.

121. Bryson, R. G. R. Hatfield, T. A. Early, A. R. Palmer and G. E. Maciel. 1983. Macromolecules 16: 1669-1672.

122. Maciel, G. E. and I-S Chuang. 1984. Macromolecules 17: 1081-1087.

123. Hatfield G., R. and G. E. Maciel. 1987. Macromolecules 20: 608-615.

124. Maciel, G. E., N. M. Szeverenyi, T. A. Early and G. E. Myers. 1983. Macromolecules 16: 598-604.

125. Chuang, I. and G. E. Maciel. 1992. Macromolecules 25:3204.

126. Andreis, M., J. L. Koenig, M. Gupta and S. Ramesh. 1995. J. Polym. Sci. B 33: 1461-1479.

127. Kricheldorf, H. R. and W. E. Hull. 1981. Makromol. Chem. 182: 1177-1196.

128. Duff, D. W. and G. E. Maciel. 1990. Macromolecules 23: 3069-3079.

129. Duff, D. W. and G. E. Maciel. 1991. Macromolecules 24 (2):387-397.

130. Duff, D. W. and G. E. Maciel. 1991. Macromolecules 24: 651-658.

131. Fyfe, C. A. et al. 1992. Macromolecules 25: 6289-6301.

132. Salmen, N. L. 1984. J. Mater. Sci. 19: 3090.

133. Back, E. L. and N. L. Salmen. 1982. Tappi 65 (7): 107.

134. Salmen, N. L., E. Back and Y. Alwarsdotter. 1984. J. Wood Chem. Tech. 4 (3): 347.

135. Kelley, S. S. 1987. J. Mater. Sci. 22: 617.

136. Follensbee, R. A., J. A. Koutsky, A. W. Christiansen, G. E. Myers and R. L. Geimer. 1993. J. Appl. Polym. Sci. 47: 1481-1496.

137. Strauss, C. R. 1980. North American Thermal Analysis Soc. Proc. 10: 311.

138. Provder, T., C. M. Neag, G. Carlson, C. Kuo and R. M. Holsworth. 1984. In: Analytical Calorimetry, Vol. 5, J. F. Johnson and P. S. Gill Eds., Plenum, New York. pp. 377.

139. Provder, T. 1989. J. Coat. Technol. 61 (770): 33.

140. Landi, V. R., J. M. Mersereau and S. E. Doeman. 1986. Polym. Compos. 7(3): 152.

141. Steiner, P. R. and S. R. Warren. 1981. Holzforschung 35: 273.

142. Young, R. H. 1986. In: Wood Adhesives in 1985: Status and Needs. pp. 267-276.

143. Danial, V. 1971. Dielectric Relaxation. Academic Press, New York. pp. 241.

144. Day, D. R. 1989. Dielectric Properties of Polymeric Materials. Micromet Instruments, Inc., Cambridge, Mass. pp. 51.

145. Grentzer, T. and J. Leckenby. 1989. American Laboratory (Jan): 82-89.

146. Bromberg, M. L., D. R. Day and K. R. Snable. 1986. IEEE Electrical Insulation Magazine 2 (3): 18-23.

147. Bromberg, M. L., D. R. Day, H. L. Lee and K. A. Russell.

148. Holmes, B. S. and C. A. Trask. 1988. J. of Appl. Polym. Sci. 35: 1399-1408.

149. Connolly, M. and B. Tobias. 1992. American Laboratory 41: 38-42.

150. Rials, T. 1990. In: Wood Adhesives 1990. pp. 91-96.

151. Rials, T. G. 1992. ACS Symp. Ser. 489: 282-294.

152. Wolcott, M. P. and T. G. Rials. Forest Prod. J. 45 (2): 72-77.

CHAPTER 3

MOLECULAR CORRELATION TO MACROSCOPIC WOOD PERFORMANCE USING CP/MAS NMR

3.1. Introduction

Extensive studies have shown that various relaxation measurements have utility for elucidating polymer dynamics in the solid state (1-3). Attempts have been made to correlate many of these relaxation phenomena with the macroscopic performance of polymeric solids. For example, Schaefer et al. (4) successfully correlated the impact strength of several glassy polymers with the ratio of the cross-polarization (T_{CH}) and carbon rotating-frame relaxation ($T_{1\rho C}$) time constants. More recently it has been shown that cross-polarization measurements can be used to study the motional and morphological heterogeneities in solid polymers (5,6). With this technique, Parker et al. (7,8) and Marcinko et al. (9,10) have established a correlation between dynamic storage modulus (E') and the mean cross-polarization time constant, $\langle T_{CH} \rangle$, for a wide variety of synthetic polymers.

This more recent correlation employs an inversion recovery cross-polarization, IRCP, pulse. It is a standard cross-polarization (CP) process, in which the spin-locked protons are brought into contact with the carbons for a period t_1, whereupon the spin temperature of the protons is inverted, Figure 3.1. In time period t_2, the carbons realign

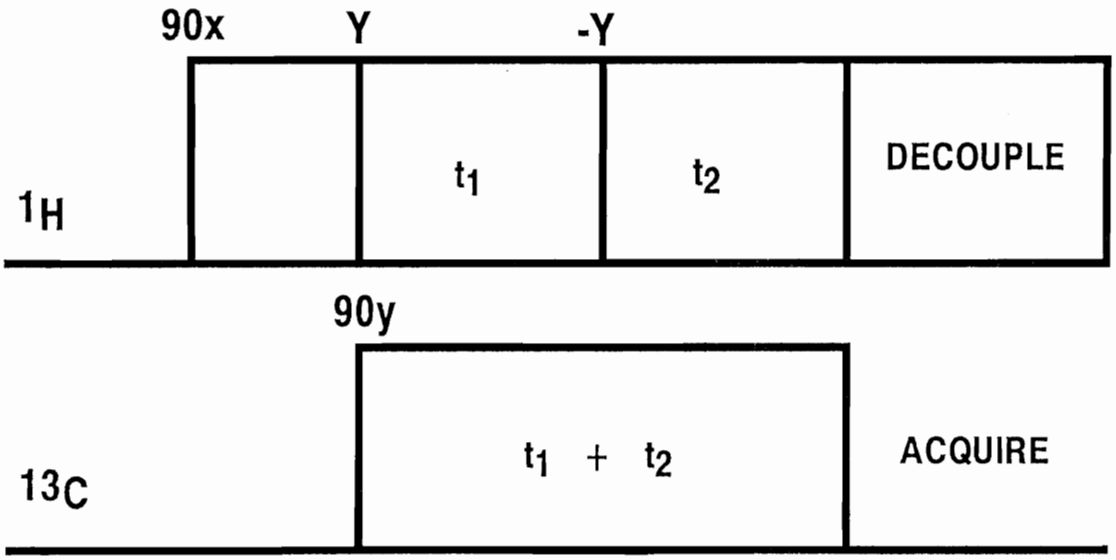

Figure 3.1: CP/MAS pulse sequence for Inversion Recovery Cross-Polarization.

with the protons with the CP rate $1/T_{CH}$. The general CP process (with carbon signal inversion) can be described by the following single exponential equation (3),

$$M(t_2) = M_0 \exp(-t_2 / T_{1\rho_H})[2\exp(-t_2 / T_{CH}) - 1] \qquad (3.1)$$

where M_0 is the magnetization at $t_2 = 0$, and $T_{1\rho H}$ is the proton rotating frame relaxation constant. Wu et al. (11) have noted that the CP process displays biexponential behavior for carbons having directly attached protons. The initial fast component arises from the strong dipolar effect within isolated $^{13}C^1H_n$ subsystems. The slow component is from long range CP between $^{13}C^1H_n$ subsystems and the rest of the proton reservoir. For example, Figure 3.2 demonstrates the biexponential and monoexponential CP behavior of protonated and nonprotonated carbons in yellow poplar (*Liriodendren tulipifera*) wood using the IRCP pulse. Note in Figure 3.2 that the protonated cellulose carbon displays clearly biexponential behavior, while the nonprotonated lignin carbon cross-relaxes with a smooth monoexponential. Wu et al. (11) point out that the "turning point" or discontinuity of the biexponential can be qualitatively predicted as a value of $(N + 1)^{-1}$ times the initial magnetization, when t_2=0, and where N is the number of attached protons. This relation considers the short range spatial effects of CP, that is the ^{13}C-^1H internuclear distance, and not the motional effects. Assuming that the Hartmann-Hahn condition is optimized, the rate of the fast and slow processes as well as the fine positioning of the discontinuity are regulated by the low frequency motions of the ^{13}C-^1H internuclear vector with respect to the orientation of the external magnetic field (2,3,5). It is this motional

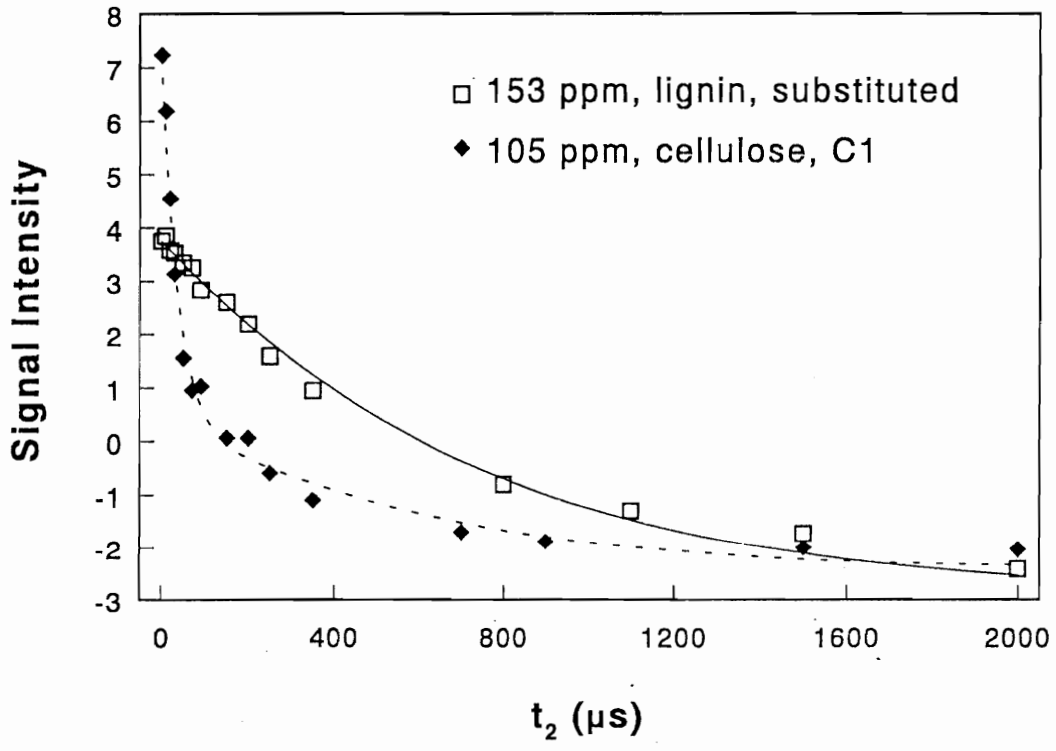

Figure 3.2: Inversion Recovery Cross-Polarization data for protonated cellulose carbon C1 (105 ppm) and non-protonated lignin carbons (153 ppm) showing biexponential and monoexponential cross-polarization behavior, respectively.

effect that provides the correlation between $<T_{CH}>$ and the dynamic modulus in polymeric materials (7).

The biexponential behavior of protonated carbons can be described by the following equation (6):

$$M(t_2) = X\{M_0 \exp(-t_2 / T_{1\rho_H})[2\exp(-t_2 / T_{CH1}) - 1]\} + (1 - X)\{M_0 \exp(-t_2 / T_{1\rho_H})[2\exp(-t_2 / T_{CH2}) - 1]\} \quad (3.2)$$

where M_0 is the magnetization at $t_2 = 0$. The variables X and 1-X represent the fractional contributions of the fast and slow processes to the total signal buildup (11,12). Cory and Ritchey (5); and Parker et al. (6) assign morphological meaning to X as that fractional component of a material which cross-polarizes very rapidly and is therefore motionally rigid. Conversely, 1-X is presumed as that component of a solid which cross-polarizes slowly and is therefore mobile. The fast and slow CP rates are then used to calculate an overall average CP rate, $<T_{CH}>$, which is weighted by the fractional contributions, X and 1-X. Therefore, the parameter $<T_{CH}>$ represents a material property characteristic of the average of all low frequency motions that modulate CP. The physical significance of $<T_{CH}>$ will depend upon the structural nature of the carbon atom used to measure $<T_{CH}>$. For example, $<T_{CH}>$ for a polymer backbone carbon should be more representative of a material's mechanical response, whereas that for a sidegroup carbon may have a more complex relationship to mechanical response, if any at all.

The long range goal of this research is to correlate molecular phenomena with the macroscopic performance of the wood-adhesive bondline. As a first step attention was

directed to solid wood, prior to studies of cured resins and cured resin-wood composites. Consequently, the objective of this chapter is to probe low frequency molecular motions in wood using dynamic mechanical analysis and CP studies, and to determine if a substantial correlation exists between the two.

3.2. Materials and Methods

Materials

Yellow Poplar (*Liriodendron tulipifera*) and Hard Maple (*Acer spp.*) samples were used in this study. Dimethyacetamide (DMAc) and inorganic salts such as LiCl, KBr, etc. were obtained from commercial sources, and used as received.

Dynamic Mechanical Analysis

A Polymer Laboratories' Dynamic Mechanical Thermal Analyzer, DMTA, was used to determine dynamic modulus, E'. The experiments were performed at 25^0C, a frequency of 1 Hz, and a strain level of 4% under dual cantilever bending with 8 mm free length. Samples were prepared as 35 mm x 6 mm rectangular beams of 1-2 mm thickness. Prior to each set of measurements, a standard copper sample was tested to calibrate the DMTA.

CP/MAS NMR

After DMA measurements, wood samples were ground to pass 40 mesh in a Wiley mill. NMR spectra were obtained with a Bruker MSL-300 operating at 75.47 MHz for ^{13}C nuclei. The proton spin-lock field strength was approximately 56 KHz. Samples were loaded into a zirconium oxide rotor with a Kel-F cap which was sealed with a flexible

silicone sealant to prevent moisture change. The magic angle was set using the KBr method, and the sealed rotor was spun at 5.5 KHz. The Hartmann-Hahn match was established with adamantane. Standard phase cycling was employed during acquisition (13). Room temperature experiments utilized in-house compressed air for the drive and bearing pressures. Subambient experiments employed high-pressure dry nitrogen running through a heat exchanger submerged in a liquid nitrogen bath.

The IRCP experiments were run using the pulse sequence (5) shown in Figure 3.1. CP variable contact time experiments demonstrated that maximum CP occurred at or near 1.5 ms for all samples, consequently a contact time (t_1 in Figure 3.1) of 1.5 ms was selected for all IRCP experiments. The variable time t_2 was varied from 1ms to 2 ms. Representaitve variable delay times (t_2) are shown in Figures 3.2 and 3.4. A delay time of 3.75 s was used between successive pulses, and 1000 scans were accumulated for each experiment. $T_{1\rho H}$ time constants were obtained from a standard variable spin lock (prior to a fixed contact) CP pulse with spin-lock times from 400 ms to 14 ms and a contact time of 1.5 ms.

Wood Treatments

Wood samples were subjected to one of three treatments as follows:

(1) Moisture Content Control

Sealed containers with different saturated inorganic salt solutions were used to control relative humidity. The samples were equilibrated in these containers for one week. In all cases sample weights became constant in less than 5 days.

(2) Densification

Samples were cut to dimensions measuring 7.5 cm by 10 cm, and conditioned to a moisture content of approximately 25 percent (wt of H_2O/wt of dry wood + wt of H_2O). The edges of the samples were sealed with a flexible silicone sealant to prevent moisture loss. A thin strip of silicone sealant was also applied along a 10 mm wide outer edge of both faces of the samples. The samples were then pressed on a 0.6 m by 0.6 m hot press at 135^{0}C and 12.4 MPa for 28 minutes. Then the heat was turned off, and the samples were cooled slowly at full pressure for 23 minutes. The samples were removed from the press and allowed to cool to ambient temperature. This process reduced the sample thickness by approximately 50 percent. Densified samples were stored with a desiccant.

A group of densified wood samples was rewetted by immersion into water for about ten hours. Then they were dried under 3 mm Hg vacuum at 50^{0}C and stored over desiccant. The rewetting of the densified wood returned the samples to their original thickness which existed prior to densification.

(3) DMAc/LiCl Impregnation

Samples were immersed into DMAc, containing 9% LiCl, under a vacuum of 3 mm Hg for 2 hours. Samples were initially floating on the solution, but by the end of the 2 hour period they were completely immersed. Then the vacuum was released, and the temperature was raised to 70^{0}C. Samples were kept in the solution for an additional 36 hours, then washed thoroughly with running tap water for 24 hours.

After washing, the samples were dried under a 3 mm Hg vacuum at 50°C for 24 hours and then stored over a desiccant.

3.3. Results and Discussion

Figure 3.3 illustrates the IRCP spectra for yellow poplar as a function of the time, t_2. Peak assignments have been reported in the literature (14-16). The peak at 105 ppm corresponds to C_1 of cellulose. For both cellulose and hemicellulose, C_2, C_3 and C_5 carbons appear around 72 ppm. The peak at 20 ppm is the acetyl methyl carbon of hemicellulose. The methoxyl and hydroxyl substituted C_3 and C_4 carbons of lignin appear at 153 ppm (not shown in Figure 3.3), and the lignin methoxyl carbon appears at 56 ppm. As expected, Figure 3.3 shows that different wood components have distinct CP rates. For example in the middle of the series of Figure 3.3, the slow cross-polarizing acetyl and methoxyl carbon signals are still positive while carbohydrate signals are absent or inverted.

For the purpose of testing the correlation between $\langle T_{CH} \rangle$ and dynamic modulus, we have performed a number of treatments on yellow poplar (*Liriodendron tulipifera*) that are expected to change the dynamic modulus with little or no change to the chemical structure. The treatments involved equilibrating the specimens to various moisture contents, impregnation with dimethylacetamide, DMAc, and LiCl, and densification using moisture, heat and pressure. An additional treatment involved immersion of densified samples into water, followed by drying. The rewetting of the densified samples plasticizes wood thereby allowing the samples to relax back to a lower density. An untreated hard

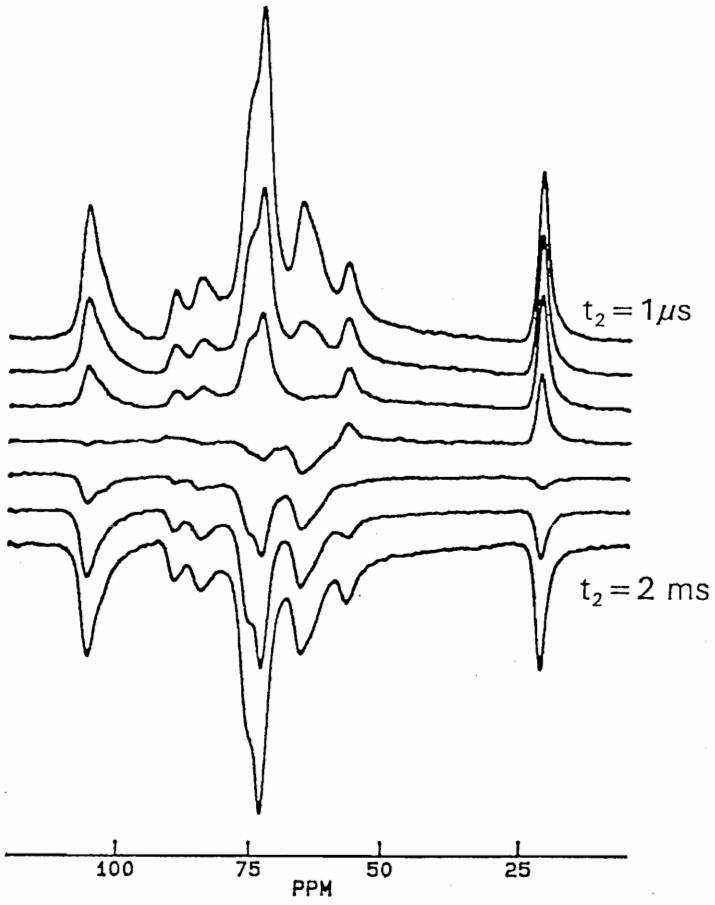

Figure 3.3: Inversion Recovery Cross-Polarization spectra of yellow poplar; t_1 = 1.5 ms and t_2 was varied from 1 μs to 2000 μs.

maple (*Acer spp.*) sample was also included as a comparison to untreated yellow poplar. All of these samples were subjected to DMA, and then to CP/MAS analysis for determination of $T_{1\rho H}$ and $\langle T_{CH} \rangle$. The correlation with dynamic modulus will be discussed later, after a brief examination of the CP behavior of the components of yellow poplar wood.

As previously mentioned, the CP character of the separate wood components is observed by plotting the signal intensity against the delay time t_2, Figure 3.2. Such data may be fit to either a single exponential (Equation 3.1) or a double exponential (Equation 3.2) depending on the number of attached protons or on the motional heterogeneity inherent to a particular carbon atom. Tables 3.1 and 3.2 list the results of the curve fitting for the variously treated wood specimens. In Table 3.1, note the results for carbon 1 of cellulose, 105 ppm, of the two dry samples. A cursory interpretation of this data implies that about 65% of the cellulose in these dry yellow poplar samples is rigid, cross-polarizing with a time constant of about 44 ms. The remaining 35% percent is mobile cross-polarizing more slowly with a T_{CH2} of about 820 ms. The C1 carbon of cellulose has one attached proton. Purely spatial effects from the attached proton should place the CP discontinuity (or X) at a factor of $(N+1)^{-1}$ times the initial signal intensity (at $t_2 = 0$) (11). In other words, exclusively spatial contributions to CP should produce a fast and slow component that equally contribute to the total magnetization for the cellulose C1 carbon. Note again however, that the CP discontinuity for the C1 carbon occurs at X = 65% of the total magnetization. The disparity between the N+1 prediction and the observed behavior

Table 3.1. IRCP relaxation constants (ms) of yellow poplar samples with different moisture contents. Numbers in parentheses are standard errors.

M.C. (%)	153ppm				105ppm				20ppm				$\langle T_{CH}\rangle^*$ (ms)
	X	T_{CH1}	T_{CH2}	$\langle T_{CH}\rangle$	X	T_{CH1}	T_{CH2}	$\langle T_{CH}\rangle$	X	T_{CH1}	T_{CH2}	$\langle T_{CH}\rangle$	
0	0.10	41	1078	974(26)	0.65	47	800	311(69)	0.42	39	1025	611(119)	581(44)
0	0.08	24	1048	966(63)	0.66	40	839	312(74)	0.39	41	941	590(119)	574(49)
3.6	0.19	24	1578	1283(61)	0.64	35	1039	396(86)	0.46	48	1692	936(149)	794(58)
5.4	0.28	203	1292	987(291)	0.60	34	646	279(52)	0.58	76	2278	1001(181)	672(99)
6.2	0.36	205	1020	727(163)	0.62	33	1145	456(70)	0.70	95	2771	898(225)	650(82)
13		-[a]		548(16)	0.61	39	876	365(56)	0.75	94	2687	742(156)	516(48)
15.8	0.17	95	1449	1219(154)	0.65	37	825	313(63)	0.52	69	2122	1054(193)	768(73)
20		-[a]		875(39)	0.64	38	870	338(96)	0.43	60	1486	8739110)	633(53)

[a] Monoexponential behavior

Table 3.2. IRCP relaxation constants (ms) of oven-dry wood samples under different treatments. Numbers in parentheses are standard errors.

Wood Species	153ppm				105ppm				20ppm				$\langle T_{CH} \rangle$* (ms)
	X	T_{CH1}	T_{CH2}	$\langle T_{CH} \rangle$	X	T_{CH1}	T_{CH2}	$\langle T_{CH} \rangle$	X	T_{CH1}	T_{CH2}	$\langle T_{CH} \rangle$	
Yellow Poplar untreated	0.10	41	1078	974(26)	0.65	47	800	311(69)	0.42	39	1025	611(119)	581(44)
Yellow Poplar untreated	0.08	24	1048	966(63)	0.66	40	839	312(74)	0.39	41	941	590(119)	574(49)
Yellow Poplar densified		-[a]		760(45)	0.67	41	688	255(73)	0.64	81	1445	572(237)	484(71)
Yellow Poplar densified-rewetted		-[a]		897(32)	0.62	36	662	274(58)	0.47	44	1474	802(164)	592(51)
Yellow Poplar DMAc/LiCl impregnated	0.14	129	1049	920(64)	0.64	38	738	338(64)	0.52	82	1392	711(145)	604(51)
Hard Maple untreated	0.15	51	1191	1020(58)	0.61	48	681	295(67)	0.63	103	1035	448(148)	545(52)

[a] Monoexponential behavior

for cellulose may be atrributed to two things. The first is that the 105 ppm peak is a composite signal with overlap from other wood components (17). Secondly, high cellulose crystallinity and the relative rigidity of amorphous cellulose favor efficient and therefore rapid CP. The overall rigidity of cellulose provides a motional contribution to the fast component of CP, in addition to the spatial effect. It could be tempting to assign the fast component (X=65%) to the percentage crystallinity of cellulose, however this may be an erroneous assumption. In this case, 65% cellulose crystallinity in a hardwood species is in poor agreement with the average value of 54% found by Newman and Hemmingson (17) using a selective detection pulse (18). Consequently, the motional heterogeneity detected in wood cellulose must be a function of cellulose crystallinity, but it is also likely to be affected by contributions from other wood components.

Fortunately, the lignin signal at 153 ppm is not a composite resonance. It has been well established that carbon peaks in the range of 150-155 ppm arise from oxygen substituted aromatic carbons (16,19,20). These nonprotonated carbons cross-polarize more slowly and are expected to exhibit single exponential behavior because they must rely on long range effects for CP (11). The expected behavior for the 153 ppm lignin peak is shown in Figure 3.2. Interestingly, it was found that single exponential behavior was exceptional, and that for most samples the 153 ppm peak displayed biexponential CP. Figure 3.4 compares the single and double exponential behavior for the 153 ppm peak in two different yellow poplar samples. It was normaly clear when any particular sample exhibited biexponential CP for the 153 ppm signal, but not in all cases. When it was

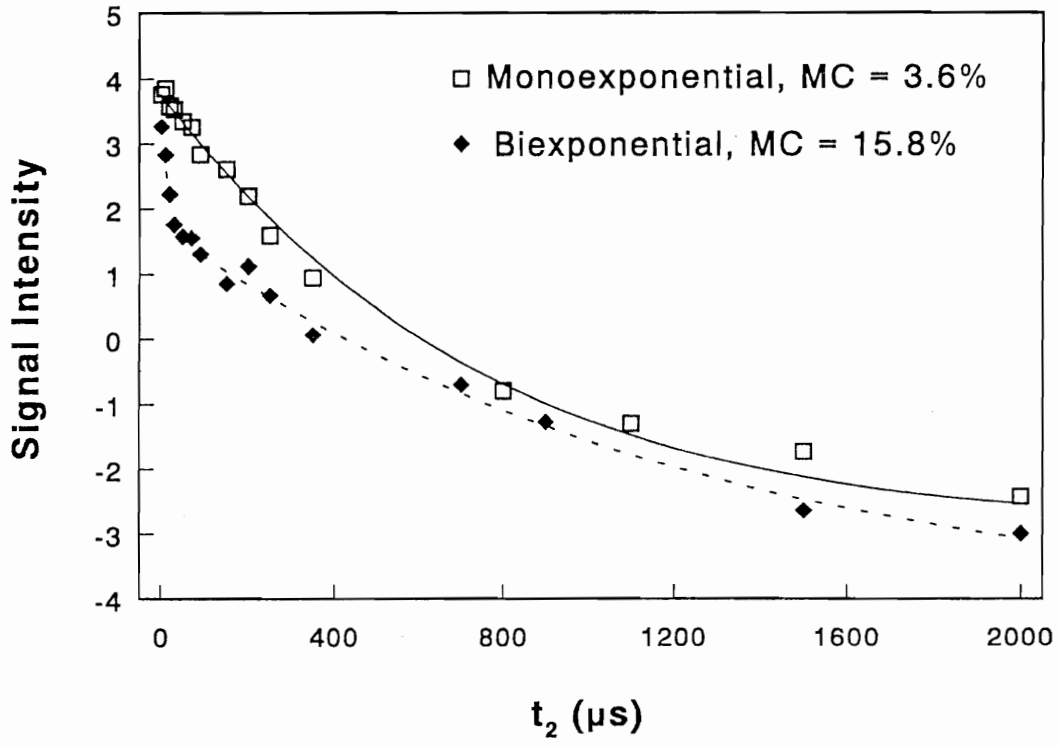

Figure 3.4: Yellow poplar samples, with moisture contents of 3.6% and 15.8%, showing monoexponential and biexponential cross-polarization behavior for non-protonated lignin carbons (153 ppm).

unclear and the data were equally well fit by equations 1 and 2, the single exponential was assigned to that peak, as is shown in Tables 3.1 and 3.2. This finding of two component CP indicates that low frequency motional heterogeneity is present in lignin's native state. There is little doubt about this conclusion because the spatial effects of attached protons are not present. The two component cross-relaxation must therefore arise from motional effects. For example, in the case of dry or low moisture yellow poplar, the data indicate that a small portion of lignin, on the order of 10-20%, is quite rigid with a CP rate of 25 to 50 ms^{-1}. This is comparable to the rigidity shown by cellulose. One could postulate that motional heterogeneity in lignin might be a manifestation of the supramolecular arrangement of the woody structure. A relatively rigid lignin component may be associated with a transitional or interfacial zone at lignin phase boundaries. It is not clear why a few yellow poplar samples gave single exponential CP. CP dynamics are sensitive to the quality of the Hartmann-Hahn match; this is especially true for nonprotonated carbons (5,12). It is conceivable that the exactness of the Hartmann-Hahn match was occasionally compromised during spectrometer setup and tuning. A Hartmann-Hahn mismatch could obscure observation of biexponential CP of nonprotonated carbons in lignin. Otherwise, this may be an effect of natural wood variability. One should also note that this biexponential CP is not an artifact from spinning sidebands from the main cellulose peak at 73 ppm. The spinning rate used in this study would indeed place a low frequency first order spinning sideband in the area of the 153 ppm peak. If a cellulose sideband were to overlap with the 153 ppm lignin signal, one could expect to observe

biexponential CP for that composite signal as a result of the overlap. This possibility was investigated by searching for the high frequency sideband that would appear near zero ppm. No such spinning sideband was detected in the zero ppm region. Consequently, spinning sidebands have not affected this analysis.

In the case of hemicellulose, 20 ppm, it is difficult to discuss motional heterogeneity with any confidence. The 20 ppm signal is the acetyl methyl carbon which has three attached hydrogens. Spatial contributions to CP predict that the discontinuity (X) should occur at $(3+1)^{-1}$ times the initial magnetization, or X=0.75. In this study X was always less than 0.75 which implies that the great mobility of the acetyl sidegroup attenuates CP. This demonstrates the difficulty associated with attempting to deconvolute spatial effects (attached protons) from motional effects. Generally, motional effects are more clearly observed by noting the changes in X, T_{CH1}, and T_{CH2} for the individual wood components between samples, and as a function of the various treatments listed in Tables 3.1 and 3.2. We will attempt to do so in the upcoming discussion.

As shown above, the detailed interpretation of CP dynamics in polymeric solids is not always straightforward. Nevertheless, the IRCP technique is valuable because it is sensitive to a distribution of motional regimes within the solid. This makes possible the assignment of an average relaxation rate which is representative of the entire material. This is conceptually similar to a DMA experiment which senses all material components and their organization within one sample. For example, one must consider the CP behavior of each wood component in order to assign an average value for the composite

material. Each wood component has its own $<T_{CH}>$ calculated from the fast and slow contributions to CP.

$$< T_{CH} >= \sum N_i T_{CHi} / \sum N_i \qquad (3.3)$$

Here N_i corresponds to X or 1-X and T_{CHi} is the CP time constant of either the rigid (X, T_{CH1}) or of the mobile (1-X, T_{CH2}) motional regime within cellulose, hemicellulose, or lignin. The overall average CP time constant of wood, $<T_{CH}>^*$, is obtained by taking the weighted average of $<T_{CH}>$ over the three wood components. In this study, the composition of all wood samples was taken as 45% cellulose, 26% hemicellulose, and 29% lignin. These percentages were used to weigh the average CP rates of the three NMR signals shown in Tables 3.1 and 3.2 which gives the overall CP response for the wood sample, $<T_{CH}>^*$. As mentioned, $<T_{CH}>^*$ should represent an average of all low frequency motions in wood, and may be related to wood's mechanical behavior. The mechanical response of polymeric solids largely arises from the transmission of stress through the backbone carbons of the chains comprising the solid. Therefore NMR correlations to mechanical response should be based upon the observation of backbone carbons. In this work, $<T_{CH}>^*$ was calculated using the C1 carbon of cellulose (backbone 105 ppm), the nonprotonated carbons of lignin (backbone, 153 ppm) and the acetyl methyl carbon of hemicellulose (sidegroup, 20 ppm). Signal overlap makes it impossible to observe a well resolved backbone carbon for hemicellulose. Consequently I am forced to use the acetyl methyl carbon, a side group, as an approximation of backbone motion in

hemicellulose. While this is conceptually unsatisfactory, it will be shown that this appears to be a reasonable approach.

In order to establish the correlation between $<T_{CH}>^*$ and E', a series of yellow poplar samples with different moisture contents were tested with NMR and DMA. In Figure 3.5, $<T_{CH}>^*$ and E' are compared as a function of wood moisture content. There is no apparent correlation between $<T_{CH}>^*$ and E' for these samples. As expected, the dynamic modulus of wood decreases as moisture content increases. But there is no clear trend in $<T_{CH}>^*$, which changes randomly. It is well known that water plasticizes wood components (21). Plasticization increases the mobility of wood polymer molecules and may reduce the CP efficiency at room temperature. CP attenuation due to water plasticization may invalidate the correlation between $<T_{CH}>^*$ and E' in wet samples. To verify this hypothesis, a subambient (-40^0C) IRCP experiment was run on the 20% M.C. sample and then compared to room temperature results of the same 20% MC sample. The signal intensities of each wood component were compared at the same CP time, $t_1 + t_2$. All carbon signal intensities from the subambient experiment increased 20-30% over the same signals in the same sample run at room temperature. (Note that this is separate from the effects reported by Willis and Herring (16) where moisture is known to enhance signal to noise as well as resolution in comparison to dry samples.) This indicates that cooling the wet sample to -40°C freezes molecular motions that result from water plasticization. The result is an increase in signal intensity as CP efficiency is enhanced. Therefore, as wood moisture content increases the additional chain mobility from plasticization causes

the IRCP experiment to sample less and less wood material. The reader must therefore keep this in mind when attempting to interpret the IRCP data in Table 3.1. The DMA experiment on the other hand samples all wood macromolecules, wet or dry. Therefore the correlation between E' and $<T_{CH}>^*$ is not apropriate for wet samples, as is demonstrated in Figure 3.5.

Another series of samples were investigated in the oven-dry condition. They were treated as previously mentioned, e.g., densification, DMAc/LiCl impregnation, etc.. Values of $T_{1r}H$ for this second set of samples are shown in Table 3.3. It is evident that these treatments cause significant changes in $T_{1r}H$ of the wood components. Proton rotating frame relaxation can complicate CP measurements if $T_{1\rho H}$ is very short (see equation 3.1). Fortunately this is not the case here because $T_{1\rho H}$ values are well above the longest CP rates exhibited by these samples. IRCP data for these samples is shown in Table 3.2. In the case of the densified sample, note that the $<T_{CH}>$ value of lignin is reduced significantly from that of the untreated sample. Such a reduction in T_{CH} indicates a reduction in molecular mobility. Table 3.2 indicates that densification does not significantly affect the average mobility of cellulose. Densification produces drastic changes in the CP character of hemicellulose. The rigid fraction X rises from about 40% in untreated wood to 64% in densified wood. Both the rigid and mobile components in hemicellulose become more mobile as a result of densification. This unexpected result may arise from chain scission occurring in hemicellulose during densification. It is not ed that, among the three wood components, lignin shows the most significant reduction in overall

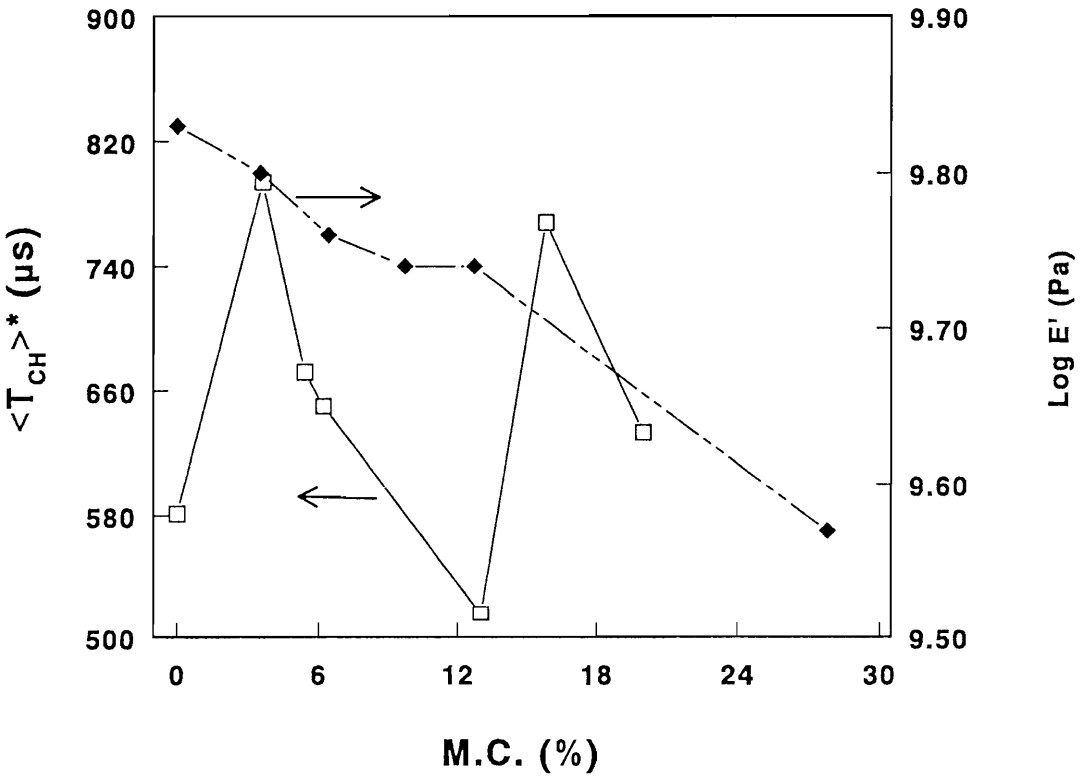

Figure 3.5: The relationship between yellow poplar wood moisture contents, $<T_{CH}>^*$ and E′.

Table 3.3. $T_{1\rho}H$ (ms) relaxation constants for wood samples under different treatments and moisture contents. All experiments were performed at 25°C unless otherwise indicated.

Wood Species	M.C. (%)	153 ppm	105ppm	20ppm
Yellow Poplar untreated	0	10.1	10.5	10.4
Yellow Poplar untreated	0	10.2	10.9	10.1
Yellow Poplar densified	0	7.6	9.3	8.7
Yellow Poplar densified-rewetted	0	10.3	10.3	10.2
Yellow Poplar untreated	20	11.8	15.2	12.5
Yellow Poplar untreated (-40°C)	20	8.9	7.9	8.0
Yellow Poplar DMAc/LiCl impregnated	0	7.5	9.1	8.5
Hard Maple untreated	0	8.5	8.9	9.4

molecular mobility. Also note that $<T_{CH}>^*$ for the densified sample is less than that for the untreated samples. This implies that the dynamic modulus of the dry densified sample should be higher than for dry untreated yellow poplar wood. I will return to this point later.

The analysis of densified samples which were rewetted with water and then dried again indicate that some of the effects of densification are reversible while others are not, Table 3.2. For example, lignin mobility in the rewetted sample is greater than in the densified sample, but it does not recover to the level seen in untreated wood. Similarly, the mobile component of cellulose does not recover any mobility after rewetting. Curiously, the rigid component of cellulose becomes slightly more rigid after rewetting. Hemicellulose in the rewetted sample displays recovery in the rigid component and apparently irreversible damage in the mobile fraction. Impregnation with DMAc/LiCl causes significant changes in lignin and hemicellulose mobility while the effects in cellulose are less dramatic. Lastly, the reader is encouraged to compare the CP behavior of the dry untreated maple sample to the dry untreated yellow poplar samples.

The last column in Table 3.2 shows the overall CP behavior for each sample, $<T_{CH}>^*$. As previously mentioned, this overall CP rate should correlate with the dynamic modulus of the samples. The parameters $<T_{CH}>^*$ and E' are plotted in Figure 3.6 in a function that Parker et al. have developed previously (7). Assuming a perfect Hartmann-Hahn match, a relation can be given as

$$E' \propto \{[\omega^2 (1/ < T_{CH} > ^*)^2]/[1+\omega^2 (1/ < T_{CH} > ^*)^2]\} \qquad (3.4)$$

where w is the frequency of the mechanical perturbation. In this study, w = 1 Hz, and $<T_{CH}>^*$ is on the order of 10^{-4} second. Therefore, the relation (4) can be simplified to:

$$E' \propto (1 - < T_{CH} >^{*2}) \tag{3.5}$$

A linear relationship, with a negative slope, between E' and $<T_{CH}>^{*2}$ is shown in Figure 3.6. The squared correlation coefficient, r^2, for this linear relationship is 0.91, indicating a strong relationship between $<T_{CH}>^*$ and dynamic modulus in dry wood. Figure 3.6 shows that the changes in CP dynamics for densified wood correlate with a large increase in dynamic modulus. Rewetting of the densified samples reduces the dynamic modulus to a point lower than untreated yellow poplar wood. This suggests that densification produces irreversible damage as was suspected from analysis of CP behavior. However, note that the $<T_{CH}>^*$ of the rewetted sample is very similar to untreated wood suggesting that DMA is more sensitive to the damage caused by densification. Impregnation with DMAc/LiCl did not have a significant effect on dynamic modulus while CP dynamics were obviously changed. Interestingly, the maple sample which has a density intermediate between densified and untreated yellow poplar has an overall CP rate which is also intermediate. Overall, there appears to be a reasonably good correlation between the molecular NMR information and the macroscopic performance of these samples in dynamic bending. One must be cautious in the explanation of this correlation. For example, the interpretation of changes in T_{CH1}, T_{CH2}, and X as a function of the various wood treatments is at times confusing. Fortunately, the overall CP behavior of the samples, as represented by $<T_{CH}>^*$, does appear to describe a discrete material

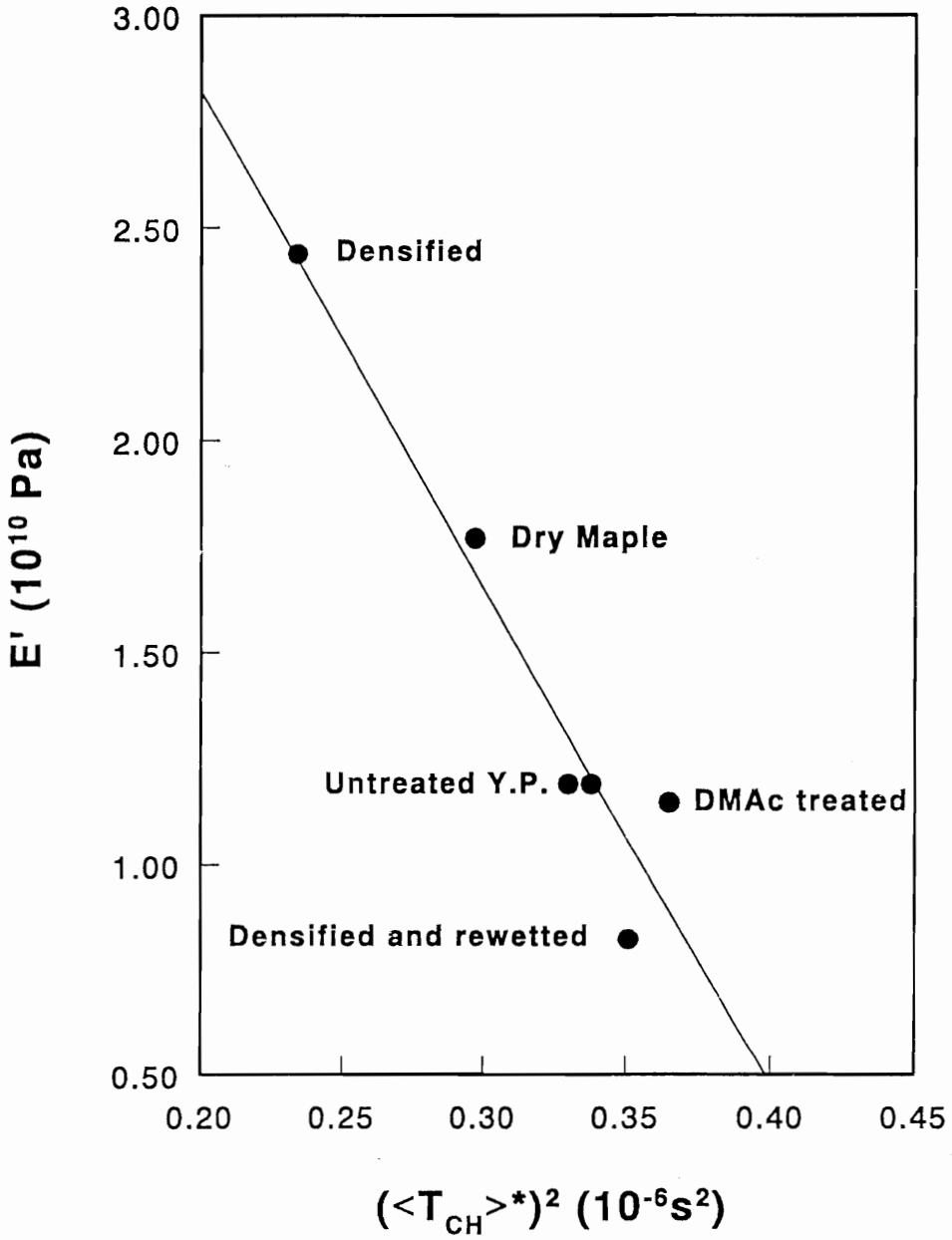

Figure 3.6: Correlation between $\langle T_{CH} \rangle^*$ and E′ for oven-dry wood samples under different treatments. The solid line is a linear fit to eq. 3.4.

characteristic of individual samples. While the value of this correlation is presently unclear, it is at least minimally gratifying to see that wood behaves similarly to the numerous synthetic polymers that also exhibit this correlation. In both cases, it is apparent that DMA and CP experiments both probe low frequency motions that overlap to a large degree.

3.4. Conclusions

1. IRCP can be used to study the motional and morphological heterogeneities in solid wood.
2. The native lignin in yellow poplar (*Liriodendron tulipifera*) and hard maple (*Acer spp.*) samples analyzed herein display a clearly detectable motional heterogeneity, which may result from the supramolecular organization of the woody material.
3. A good correlation exists between $<T_{CH}>^*$ and E' of the dry wood samples, indicating that near-static motion dominates both $<T_{CH}>^*$ and E'.
4. The correlation between $<T_{CH}>^*$ and E' is not suitable for wet wood samples. Moisture plasticizes wood which reduces cross-polarization efficiency.
5. The IRCP technique represents a step forward in our goal of relating molecular phenomena with macroscopic performance of wood and wood composites.

References

1. Fyfe, C. A.. 1983. Solid state NMR for chemists. C. F. C. Press, Ontario, Canada.
2. Komoroski, R. A.. 1986. High resolution NMR spectroscopy of synthetic polymers in bulk. VCH Publishers: Deerfield Beach.
3. Mehring, M.. 1983. Principles of high resolution NMR in solids, 2nd ed.. Springer-Verlag, New York.
4. Schaefer, J., E. O., Stejskal and R. Buchdahl. 1977. Macromolecules 10 (2): 384-405.
5. Cory, D.G. and W.M. Ritchey. 1989. Macromolecules 22 (4): 1611-1615.
6. Parker, A. A., J. J. Marcinko, Y. T. Shieh, C. Shields, D. P. Hedrick and W. M. Ritchey. 1989. Polymer Bulletin 21: 229-234.
7. Parker, A. A., J. J. Marcinko, Y. T. Shieh, D. P. Hedrick and W. M. Ritchey. 1990. J. Appl. Polym. Sci. 40: 1717-1725.
8. Parker, A. A., J. J. Marcinko, P. Rinaldi, D. P. Hedrick and W. M. Ritchey. 1993. J. Appl. Polym. Sci. 48: 677-681.
9. Marcinko, J. J., A. A. Parker, Y. T. Shieh and W. M. Ritchey. 1992. J. Appl. Polym. Sci. 45: 391-398.
10. Marcinko, J. J., A. A. Parker, P. L. Rinaldi and W. M. Ritchey. 1994. J. Appl. Polym. Sci. 51: 1777-1780.
11. Wu, X., S. Zhang and X. Wu. 1988. Phys. Rev. B 37 (16): 9827-9829.
12. Wu, X. and K. W. Zilm. 1991. J. Magn. Resonance 93: 265-278.

13. Stejskal, E. O. and J. Schaefer. 1975. J. Magn. Resonance 18: 560-563.

14. Atalla, R. H., J. C. Gast, D. W. Sindorf, V. J. Bartuska and G. E. Maciel. 1980. J. Am. Chem. Soc. 102 (9): 3249-3251.

15. Earl, W. L. and D. L. VanderHart. 1980. J. Am. Chem. Soc. 102 (9): 3251-3252.

16. Willis, J. M. and F. G. Herring. 1987. Macromolecules 20 (7): 1554-1556.

17. Newman, R.H., and J.A. Hemmingson. 1990. Holzforschung 44; 351-355.

18. Zumbulyadis, N. 1983. J. Magn. Resonance 53: 486-494.

19. Gerasimowicz, W.V., K.B. Hicks, and P.E. Pfeffer. 1984. Macromolecules. 17: 2597-2603.

20. Manders, W. F. 1987. Holzforschung 41: 13-18.

21. Kelly, S. S., T. G. Rials and W. G. Glasser. 1987. J. Mater. Sci. 22: 617-624.

CHAPTER 4

EFFECTS OF CURE TEMPERATURE AND TIME ON THE PMDI/WOOD BONDLINE

4.1. Introduction

In the previous chapter, it was shown that the IRCP technique can be used to study the motional and morphological heterogeneities in solid wood. However, it also has its limitation on wet wood. In the following chapters, other techniques of solid state NMR will be used to reveal the molecular information of wood-adhesive bondline.

While extensive studies have been done on the performance of pMDI (1-5), less effort has been spent on revealing the mechanism of wood/pMDI bonding. This chapter represents a continuation of recent work aimed at determining the wood/pMDI bonding mechanism under conditions similar to industrial panel manufacture. Commercial pMDI, used as a wood binder, is roughly composed of about 45-50% of 4,4′-MDI and a small amount of 2,4′- MDI with a trace of the 2,2′- isomer. The remainder (~ 50%) is comprised of higher order oligomeric polyisocyanates (6). It is likely that the performance of pMDI resin will depend upon its composition, which is affected by molecular weight and structural isomerism, especially the 4,4′-/2,4′- isomer ratio. There has been no reported study of the effects of pMDI structural isomerism. This study begins to address these effects, specifically the 4,4′-/2,4′- isomer ratio.

The focus of this work is on the cure chemistry of a pMDI resin with a high 4,4′-MDI content The analytical tool employed is ^{15}N cross-polarization/magic angle spinning (CP/MAS) NMR. ^{15}N CP/MAS NMR is particularly suitable for the study of the pMDI/wood bondline (7,8). Unlike ^{13}C, ^{15}N NMR excludes overlapping wood signals so that resin chemistry can be directly observed. This is a continuation of previous studies (7-9). However the resin used here is more similar to industrial resins used in the forest products industry. Specifically, the molecular weight is lower and the isocyanate content is higher than in earlier studies.

In this chapter, the effects of cure temperature and time were studied by using the ^{15}N CP/MAS NMR, and were compared to previous results. Chapter 5 will be directed at a pMDI resin with a much higher 2,4′- MDI content as a comparison to this discussion.

4.2. Materials and Methods

Materials

99% ^{15}N-labeled aniline was purchased from Cambridge Isotope Laboratories and used as received. It had a deep yellow color indicating some impurities, however, further purification was not attempted to prevent loss of the reagent. 95% paraformaldehyde, 37% aqueous hydrochloric acid, 10 N aqueous sodium hydroxide, as well as 98% triphosgene and anhydrous 1,2- dichlorobenzene (ODCB) were purchased from Aldrich Chemical and were used as received. Chloroform was distilled under dry nitrogen using anhydrous calcium chloride as desiccant.

Methods

1. Synthesis of pMDI

The synthesis of pMDI is a two-step process. The first step is the synthesis of polyamine from the HCl catalyzed condensation of aniline with paraformaldehyde. The second step involves the phosgenation of the polyamine.

Step 1: Aniline was degassed by N_2 bubbling for 3 minutes before use. The aniline:HCl molar ratio was chosen as 1:1.5, and the aniline:formaldehyde molar ratio was 4:1. 6N HCl (39.6 ml, 0.238 mole) was first added into a 100 ml triple neck round-bottom flask, which was submerged in a cold water bath . Aniline (14.4 ml, 0.158 mole) was added slowly with stirring followed by 95% paraformaldehyde (1.25 g, 0.040 mole). Heat was then applied to reflux the mixture at 105^0C for 8 hours. The mixture was allowed to cool to room temperature, and added to a 250 ml separatory funnel containing freshly distilled chloroform (25 ml). The aqueous phase was neutralized with 10N NaOH, and then extracted with chloroform (3 x 25 ml). The chloroform fractions were combined and washed with double distilled water (3 x 25 ml), dried over excess Na_2SO_4, and concentrated on a rotational evaporator. Residual aniline was removed with vacuum distillation at 4 mmHg and 120^0C, and the polyamine product was stored under dry N_2.

Step 2: All reagents were degassed by N_2 bubbling, and all glassware was flamed under a slow N_2 purge before use. Polyamine was vacuum dried overnight at 10 mmHg and 50^0C immediately before use. The polyamine (6.783 g) was dissolved in 11 times its weight of dry ODCB (74.6 g). The amine content was calculated assuming a complete

conversion of paraformaldehyde to methylenedianiline (0.0676 mole). Triphosgene (7.62 g, 0.026 mole) was dissolved in dry ODCB (76.2 g,). The triphosgene solution was added to the flask, followed by addition of polyamine solution. When adding polyamine to the triphosgene, vigorous stirring is critical to prevent particle agglomeration. After addition of the polyamine solution, the reaction mixture was heated to 175^0C for 30 minutes, then cooled to 150^0C and degassed with N_2 bubbling for 15 minutes. The resulting mixture was vacuum distilled (10 mmHg and 90^0C) to remove ODCB. The flask containing polyisocyanates was immersed into a oil bath, which was heated to 205^0C for 10 minutes under N_2 purge. Immediately after heating, the flask was quench cooled by spraying with acetone and submerging the flask into a cold water bath. This heat treatment was performed to remove chlorine-containing impurities and to break down isocyanate dimers

The isocyanate content was measured according to ASTM Standard D 5155-91, Test Method C, however the procedure was scaled down to one tenth of the ASTM standard size. The sample was tested twice yielding isocyanate contents of 27.8% and 27.9% (mean = 27.9%).

Molecular weight was determined by using gel permeation chromatography (GPC) at 40^0C. Solvent was HPLC grade tetrahydrofuran. Columns were Waters Ultrasyragel with pore diameters of 10^3A, 10^2A, and 10 A. Other GPC equipment included Waters Model 510 HPLC pump, Waters Model 410 Differential Refractometer, and Viscotek Model 100 Differential Viscometer. A urea derivative of pMDI was made for GPC analysis as follows. pMDI (0.1 g) was dissolved in freshly distilled chloroform (1 ml), and

then slowly added into diethylamine (0.8 ml). After a 30 minutes reaction time, the chloroform and residual diethylamine were removed on a rotational evaporator. The resulting urea derivative was used for GPC testing. Number average molecular weight (M_n) of the pMDI was determined as 340 g/mole, and weight average molecular weight (M_w) was 514 g/mole (corrected for urea derivatization).

The diisocyanate isomer ratio was measured using gas chromatography. A Hewlett Packard HP6890 GC System was used with capillary column (Hewlett Packard, HP-5), and solvent for pMDI was chloroform. Gas chromatography analysis showed that the diisocyanate fraction was composed of 94.8% 4,4′- isomer, 5.2% 2,4′- isomer, and a trace of 2,2′- isomer.

2. Preparation of Wood Composites

A block of yellow poplar (*Liriodendron tulipifera*), clear of visible defects with cross sectional dimensions of 1.95 in. by 1.95 in., was immersed in tap water for three days. The block was then sliced with a CAE disk flaker. All flakes were cut from the radial face of the block to a thickness of 0.012-0.015 in. The flakes were vacuum dried at 10 mmHg and room temperature for 24 hours to obtain their dry weight. They were then conditioned in a sealed container over saturated $CaCl_2$ solution for three days. The equilibrium precure moisture content of the flakes was 4.5-5.0% based on the dry weight of wood. To minimize the effects of wood surface deactivation, flakes were stored in the dark and used within 1-3 days after conditioning.

The ^{15}N-pMDI resin was sprayed onto two pieces of wood flake in the open atmosphere using an airbrush at a loading of 12% of the total composite weight. The resin was uniformly distributed over the entire surface area of one side of both flakes. The two wood flakes were pressed between thin teflon sheets using a Carver Laboratory Press at different cure conditions (temperature and time) and 500 psi. The post cure resin content was approximately 10% based on the dry weight of the wood. Samples were stored in individual sealed containers under N_2 and over desiccant in a freezer to prevent postcure reactions.

3. NMR measurements

^{15}N CP/MAS spectra were obtained at 30.4 MHz on a Bruker MSL-300 MHz spectrometer using a 7 mm Probenkopf MAS.07.D8 probe. Small disks were punched out of the composites using a paper hole puncher, randomly inserted into a zirconium oxide rotor, and filled in and around with powered aluminum oxide to facilitate rapid spinning. The ^{1}H channel was tuned using adamantine while ^{15}N-glycine was used to set the Hartmann-Hahn Condition. Standard phase cycling was used during acquisition. $T_{1\rho H}$ measurements were made using a standard CP acquisition with a variable spin-lock delay (0.5 ms to 12 ms) prior to a fixed contact time (5 ms). The proton 90^0 pulse was 8 μs in duration. 800 scans were collected for each contact time with a repetition time of 6 s. Samples were spun at 6 KHz and the magic angle was set using the KBr method. Spectra were referenced externally to ^{15}N-glycine at 31 ppm. In addition, a series of CP/MAS

interrupted-decoupling experiments were performed with interrupt times of 10 μs to 70 μs.

4.3. Results and Discussions

It is generally accepted that there are multiple, competing pathways for pMDI/wood reactions (1-4, 10-12). The isocyanate group reacts readily with hydroxyl groups to form urethane linkages. Therefore, wood components (cellulose, hemicellulose and lignin etc.) will offer ample opportunity for covalent bonding with pMDI. However, the hydrophilic nature of wood always ensures a high degree of wood hydration. Isocyanates react readily with water, which leads to urea formation. Urethanes and ureas may further react with isocyanates to form allophenates and biurets, respectively. In addition to the above reactions, pMDI also has a tendency to dimerize to form uretidione. We can expect that there will be competition among these different reaction pathways.

Two series of wood/^{15}N-pMDI composites were cured as a function of time using 4.5-5.0% wood precure moisture content, 10 wt.% resin, and 500 psi pressure. Two different cure temperatures, 120^{0}C and 185^{0}C, were chosen as respective approximations of mat core and platen temperatures, which occur during industrial OSB manufacturing processes.

Figure 4.1 illustrates the ^{15}N CP/MAS spectra for the samples cured at 120^{0}C as a function of cure time. Chemical shifts are referenced to glycine at 31 ppm and are similar to literature reports (13). The peak at 44 ppm corresponds to residual isocyanate, urea

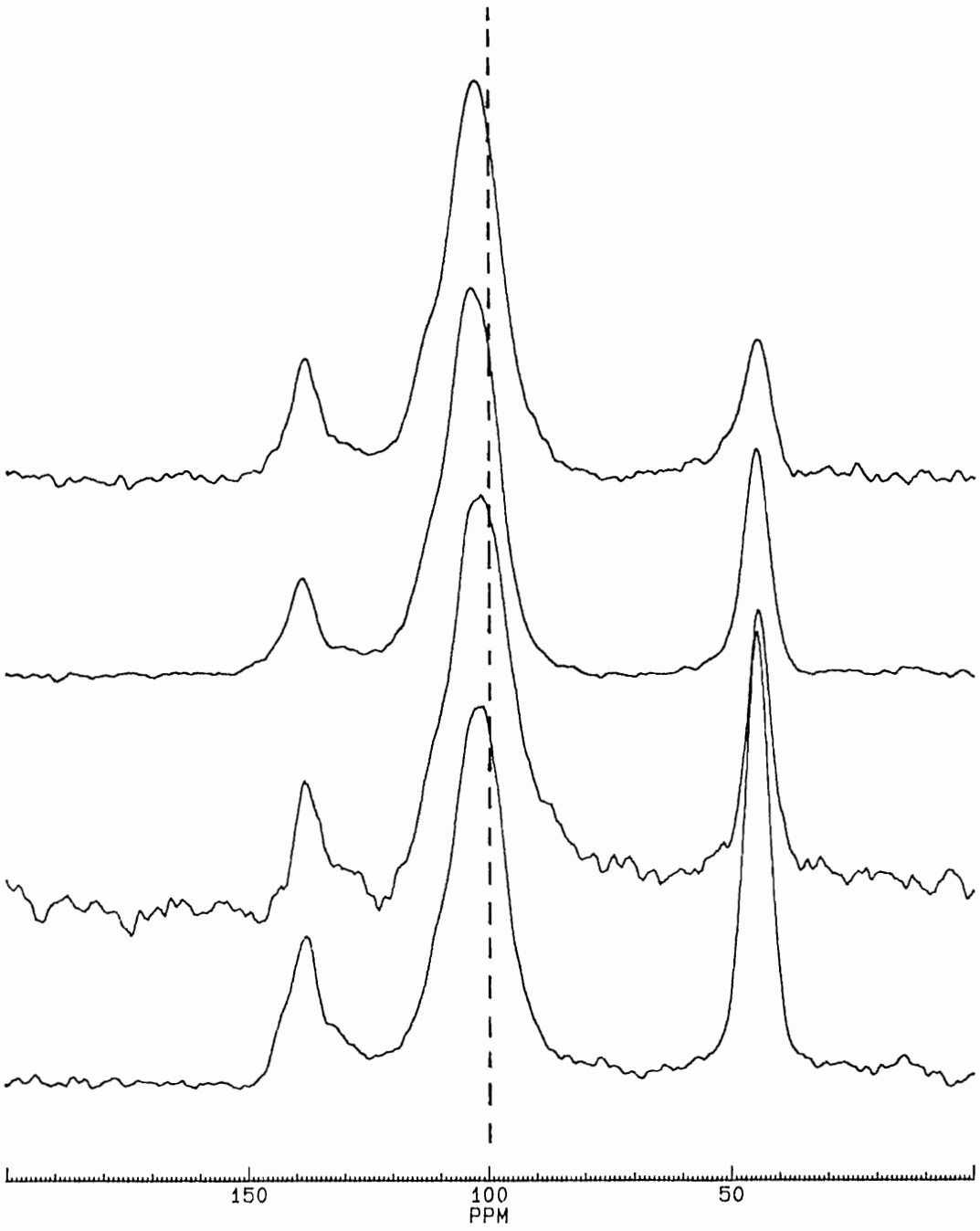

Figure 4.1: ^{15}N CP/MAS NMR spectra of wood/^{15}N-pMDI composites as a function of cure time. They were cured with precure moisture content of 4.5-5%, 10 wt.% resin, 500 psi, at 120^0C.

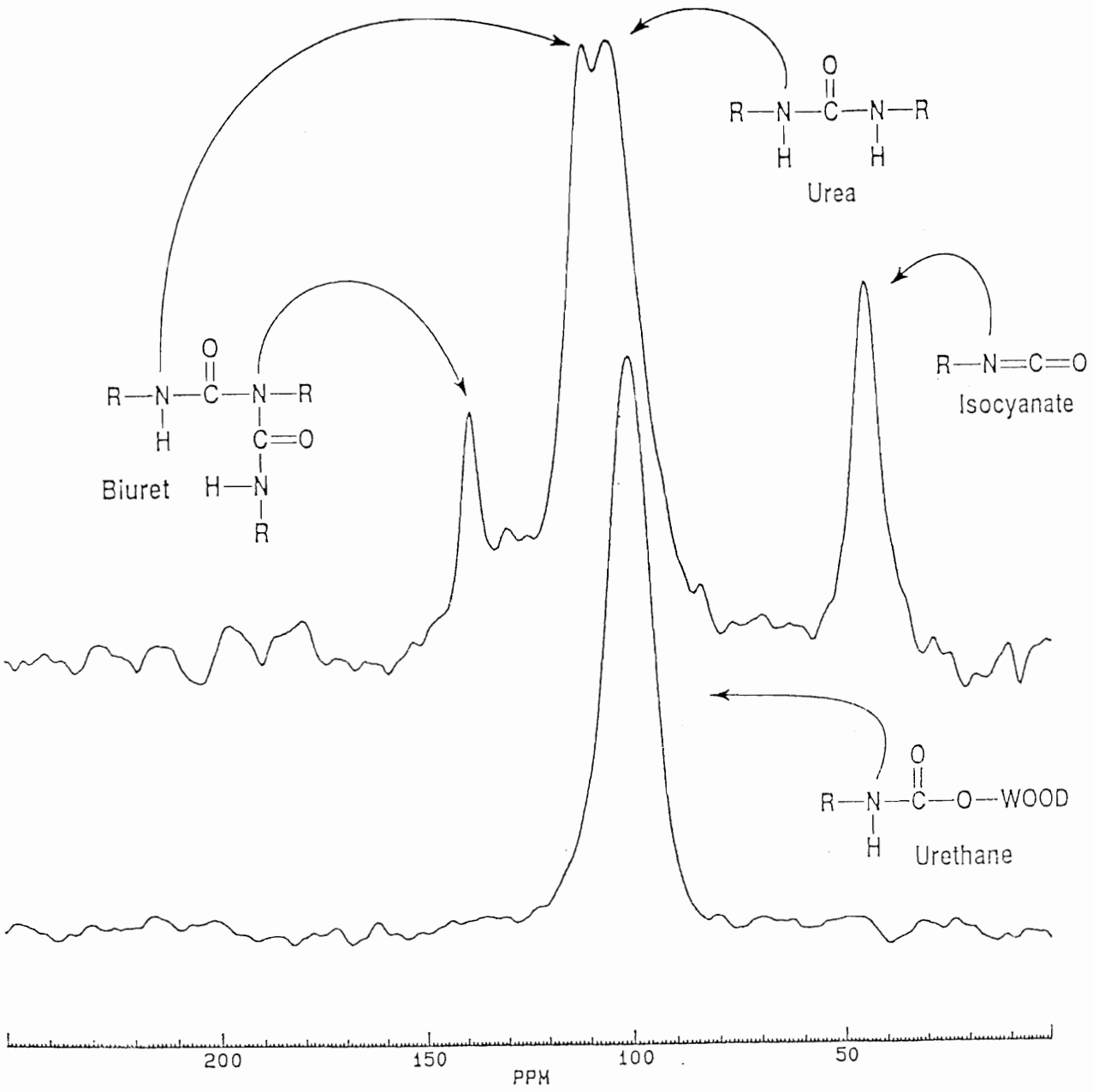

Figure 4.2: Top: ^{15}N CP/MAS NMR spectrum of wood/^{15}N-pMDI composites. Bottom: spectrum for model urethane. Reproduced with permission from Charles E. Frazier (8).

appears at 104 ppm. Biuret amide nitrogen occurs at 111 ppm, and biuret imide nitrogen is located at 138 ppm. Previous studies (9) showed that the wood/isocyanate urethane signal overlaps the urea signal, appearing at 101 ppm (Figure 4.2).

At 140 sec., there are three distinct resonances in the spectrum. One is at 44 ppm (residual isocyanate). Another is a broad peak centered at about 103 ppm and with maxima at 101 ppm. The third peak is at 138 ppm (biuret imide). A small shoulder appears on the right side of the biuret imide peak at 130 ppm. This shoulder was also noticed previously, however, the identity of this peak is still unknown (9). On the left side of the biuret imide peak, there is a clear shoulder at about 143 ppm, which according to the literature corresponds to the uretidione nitrogen, which is the isocyanate dimer (13). The broad central peak appears to contain possibly three signals at 101 ppm, 104 ppm, and 111 ppm. A line has been arbitrarily drawn at 100 ppm in order to accent signal intensity in that region. The maxima at 101 ppm suggests the presence of urethane. The breadth of the central peak also indicates that a significant amount of urea is present. Biuret amide is seen as a shoulder on the left side of the central peak at 111 ppm.

The overlap of the urea and urethane signal complicates the clear identification of urethane. Nevertheless, careful inspection of the 140 s spectrum reveals a central peak with low field (biuret amide) shoulder. While this is not plainly clear, the signal intensity in the 101 ppm region appears to be the first indication of urethane formation under conditions similar to industrial panel manufacture. In previous work using a higher molecular weight and lower isocyanate content resin, urethane (signal maxima at 101

ppm) was detected only under high temperatures and long cure times (8). The resin used here has a much lower molecular weight (M_w = 514 g/mole vs. 4500 g/mole) and higher isocyanate content (27.9% vs. 25.6%), which is more similar to industrial resins used in the wood products industry. When compared to previous findings, it can be seen that bondline chemistry has a clear resin dependence, i.e. molecular weight and/or isocyanate content dependence. While the effects of isocyanate content are not yet clear, molecular weight probably plays an important role. Previously, Wendler et al. showed that the pMDI-water reaction dominated cure chemistry while urethane formation was not often detected (7,8). It is reasonable to conclude that a lower molecular weight pMDI will be more mobile and more reactive than a higher molecular mass resin. Consequently, urethane formation might occur more readily as seems to be the case here. However, because of the signal overlap, we cannot conclude which reaction dominates the cure chemistry of the bondline. Nevertheless, it is likely true that there is urethane formation in the bondline besides polyurea, biurets and residual isocyanate. Resins of lower molecular weight may be favorable for covalent bonding.

At 4 min. of cure time, the spectrum is very similar to the one at 140 sec. cure time (Figure 4.1). However, as cure time further increases to 10 min. and 60 min., the central peak maxima shifts from urethane at 101 ppm to urea at 103-104 ppm. This conclusion is stated cautiously because of the minor changes in peak maxima. Furthermore, ^{15}N chemical shifts are quite sensitive to secondary interactions occurring in the local environment (14,15). Consequently, a complimentary technique is required before

definitive conclusions are stated. Nevertheless, previous work indicates that the urea and wood urethane maxima occur at 104 and 101 ppm respectively(9). The conclusions herein are based upon these previous findings.

The possible change from urethane to polyurea dominance is an interesting phenomenon which seems to suggest that urethane thermally decomposes, reverting back to isocyanate. It has been reported that the thermal dissociation of urethane occurs in the following order (16):

Aryl-NHCOO-Alkyl (Alkyl urethane) 200^0C

Aryl-NHCOO-Aryl (Aryl urethane) 120^0C

Weaver and Owen found that isocyanate reacts with lignin more readily than with wood polysaccharides (11,17). There are about 15 phenolic hydroxyl groups per 100 C_6C_3 units in hardwood lignin (22). Extractives in wood also contain some phenolic hydroxyl groups. Isocyanates penetrate deeply into wood, and have a high possibility to react with these phenolic hydroxyl groups. Therefore the urethane formed during wood/pMDI curing may likely be in the form of Aryl-NHCOO-Aryl, which has a limited stability. As the cure time is increased to 10 min. and longer, the central peak shifts from 101 ppm to 103-104 ppm possibly because of the thermal decomposition of aryl urethane. This suggests that any remaining urethane is in the form of alkyl urethane, resulting from reaction with cellulose and hemicellulose. The thermally stable alkyl urethanes could be hidden under the urea signal for samples cured for 10 and 60 minutes.

Although quantitative analysis of peak intensities was not attempted, we still can qualitatively analyze the effects of cure time on the cure chemistry. As the cure time progresses, the amount of residual isocyanate steadily drops. The intensity and shape of the 138 ppm peak changes slightly, and the biuret amide shoulder becomes more pronounced at 60 min. These changes may indicate the thermal decomposition of biurets and polyurets which was noted previously (8).

Figure 4.3 shows the ^{15}N spectra for the series of composites cured at 185^0C. The major and minor peaks are similar to those noted in Figure 4.1. Unlike the series cured at 120^0C, there is no distinctive urethane peak detected. As mentioned before, aryl urethane is unstable above 120^0C. As before, an undetected alkyl urethane may be covered by the broad urea signal.

Wendler et al. found that when curing at 185^0C, biurets were favored at short times, and polyureas were favored at longer times (8). In this study biurets are less common, and the biuret amide shows only as a shoulder at 111 ppm throughout the different cure times. The central band always has its maxima at 104 ppm. The upfield, or righthand, side of the 104 ppm peak broadens with increasing cure time at 185^0C. This phenomenon was also reported in the previous work (8). This upfield broadening could be the indication of urethane formation. The biuret imide and the amide shoulder appear to decline slightly. If this is true, and not an artifact of variable signal relaxation, then it could appear that biurets are thermally decomposing. This is consistent with previous quantitative studies (8)

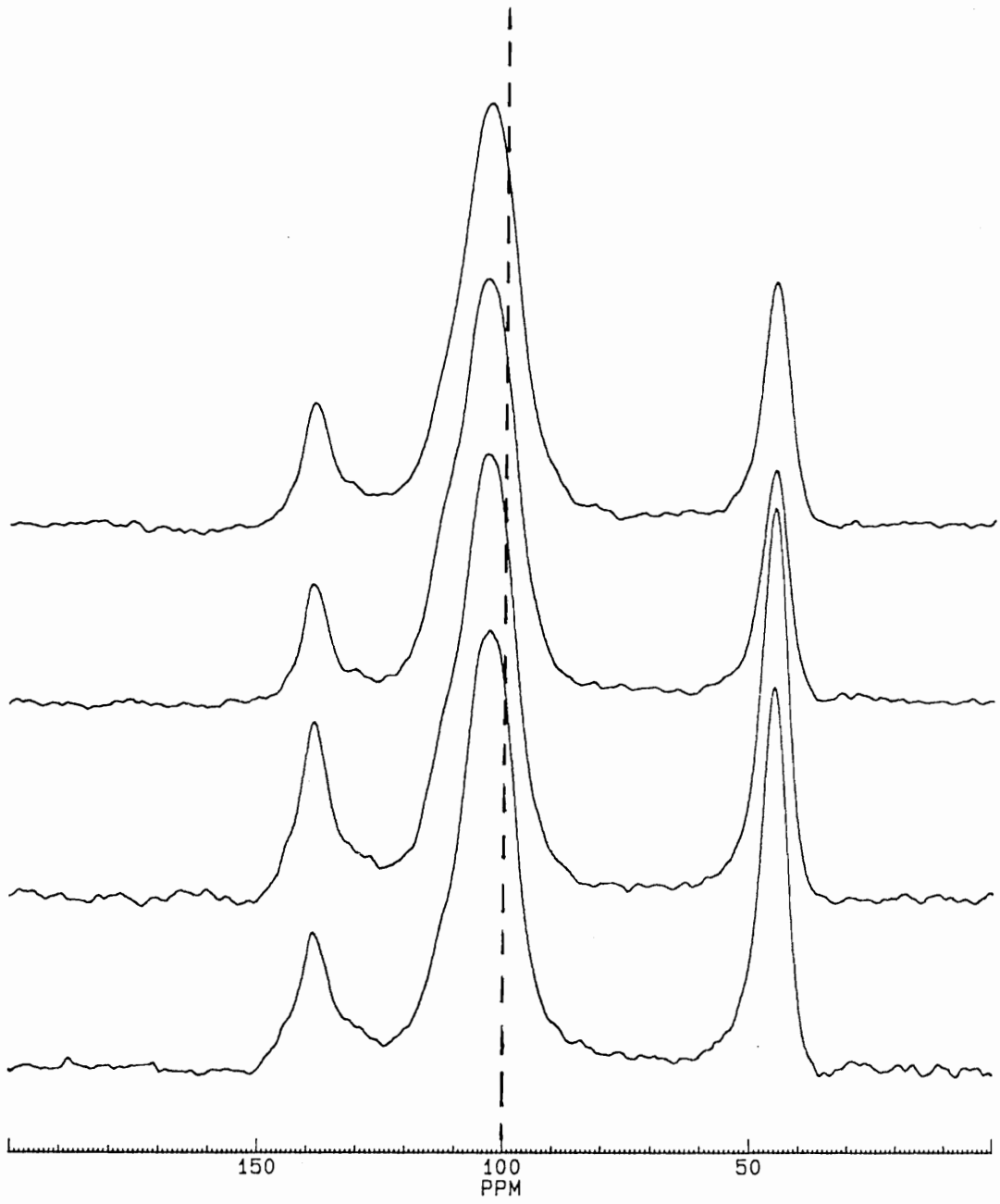

Figure 4.3: ^{15}N CP/MAS NMR spectra of wood/^{15}N-pMDI composites as a function of cure time. They were cured with precure moisture content of 4.5-5%, 10 wt.% resin, 500 psi, at 185^{0}C.

It is possible that thermal decomposition of biuret liberates isocyanate which then forms alkyl urethane.

The above discussions are all qualitative rather than quantitative. The ^{1}H-^{15}N cross-polarization and rotating-frame proton spin-lattice relaxations are competing effects which determine signal intensity (18,19). Their rates (T_{NH} and $T_{1\rho H}$ respectively) are not the same for all types of nitrogen. Direct comparisons of intensities at a given contact time are inaccurate. There is no quantitative treatment on the signal intensities. Furthermore, the signal overlap complicates any attempt to quantitatively analyze the signal intensities.

Molecular motions in these samples were probed with measurement of proton longitudinal relaxation in the rotating frame, $T_{1\rho H}$. $T_{1\rho H}$ relaxation times are presented in Tables 4.1 and 4.2. Each value was reproduced two or three times by preparing separate sample composites. At $120^{0}C$, $T_{1\rho H}$ of residual isocyanate increases with cure time. The biuret imide $T_{1\rho H}$ slightly increases. Relaxations for the central peak are more complicated. $T_{1\rho H}$ increases from 4.4 ms to 4.9 ms, as cure time increases from 140 sec. to 4 min. At 10 min., the $T_{1\rho H}$ drops to 4.0 ms and remains unchanged at 60 min. It is interesting to note that this discontinuity in relaxation behavior coincides with the transition of the peak maxima from 101 ppm to 103-104 ppm. This may be another indication of a transition from urethane to urea, because it is feasible for these groups to display different mobilities.

It may be possible to resolve the two signals if the mobilities of urea and urethane are sufficiently different. An interrupted decoupling experiment was employed to test this

Table 4.1. Effects of cure time on $T_{1\rho H}$[a] of pMDI-wood composites cured at 120°C.[b]

Cure Time	Peak (ppm)			
(min:s)	138	104	101	44
2:20	4.3 (0.1)[c]	-	4.4 (0.1)	4.2 (0.1)
4:00	4.5 (0.1)	-	4.9 (0.1)	4.1 (0.3)
10:00	4.8 (0.1)	4.1 (0.1)	-	5.1 (0.2)
60:00	4.9 (0.1)	4.0 (0.1)	-	5.0 (0.1)

a. $T_{1\rho H}$ values are averages of two or three separate experiments using separate samples.

b. Cured at 12 wt.% resin, 500 psi.

c. Values in parenthesis are standard errors.

Table 4.2. Effects of cure time on $T_{1\rho H}$[a] of pMDI-wood composites cured at 185°C.[b]

Cure Time	Peak (ppm)		
(min:s)	138	104	44
2:20	4.4 (0.1)[c]	4.2 (0.1)	4.6 (0.1)
4:00	4.3 (0.1)	4.3 (0.1)	4.7 (0.2)
10:00	4.8 (0.1)	4.2 (0.1)	5.2 (0.1)
60:00	4.8 (0.1)	4.2 (0.1)	5.1 (0.1)

a. $T_{1\rho H}$ values are averages of two or three separate experiments using separate samples.

b. Cured at 12 wt.% resin, 500 psi.

c. Values in parenthesis are standard errors of the $T_{1\rho H}$.

hypothesis. In this experiment, delay periods of 10, 30, 50, and 70 μs were inserted between the CP contact period and the beginning of data acquisition. During that delay period, the ^{1}H decoupler is turned off and ^{15}N magnetization is attenuated by dephasing associated with the ^{15}N-^{1}H dipolar interaction. ^{15}N nuclei with different relaxation rates will have different degrees of attenuation which may allow resolution of overlapping signals.

Figure 4.4 shows the results of the interrupted-decoupling experiment. The spectrum at 10 μs is very similar to the one in Figure 4.1, except that shoulders appear more clearly on the left side of the central band. There may be two shoulders at 104 ppm and 111 ppm. As the interrupt time increases, the signal intensities for protonated nitrogen drop quickly while the ones for non-protonated nitrogen drop slowly. At the interrupt time of 50 μs, the central band has its maxima at 101 ppm, and the shoulders on the left side of the central band become more clear. They are located at 104 ppm and 111 ppm. This may further prove the co-existance of urea, biuret, and urethane in the bondline. The bondline is a complex of different chemical species with different mobilities.

To associate $T_{1\rho H}$ values in Table 4.1 to molecular mobility of the bondline, a variable temperature experiment was carried out. An increase in $T_{1\rho H}$ can indicate that the sample gets either more rigid or more mobile depending on the motional characteristics of the sample (20). $T_{1\rho H}$ was measured for one sample at two temperatures, 25°C and 40°C. The results are shown in Table 4.3. As temperature was raised from 25°C to 40°C, the $T_{1\rho H}$ values of all signals drop slightly. This data indicate that increases in $T_{1\rho H}$ correlate

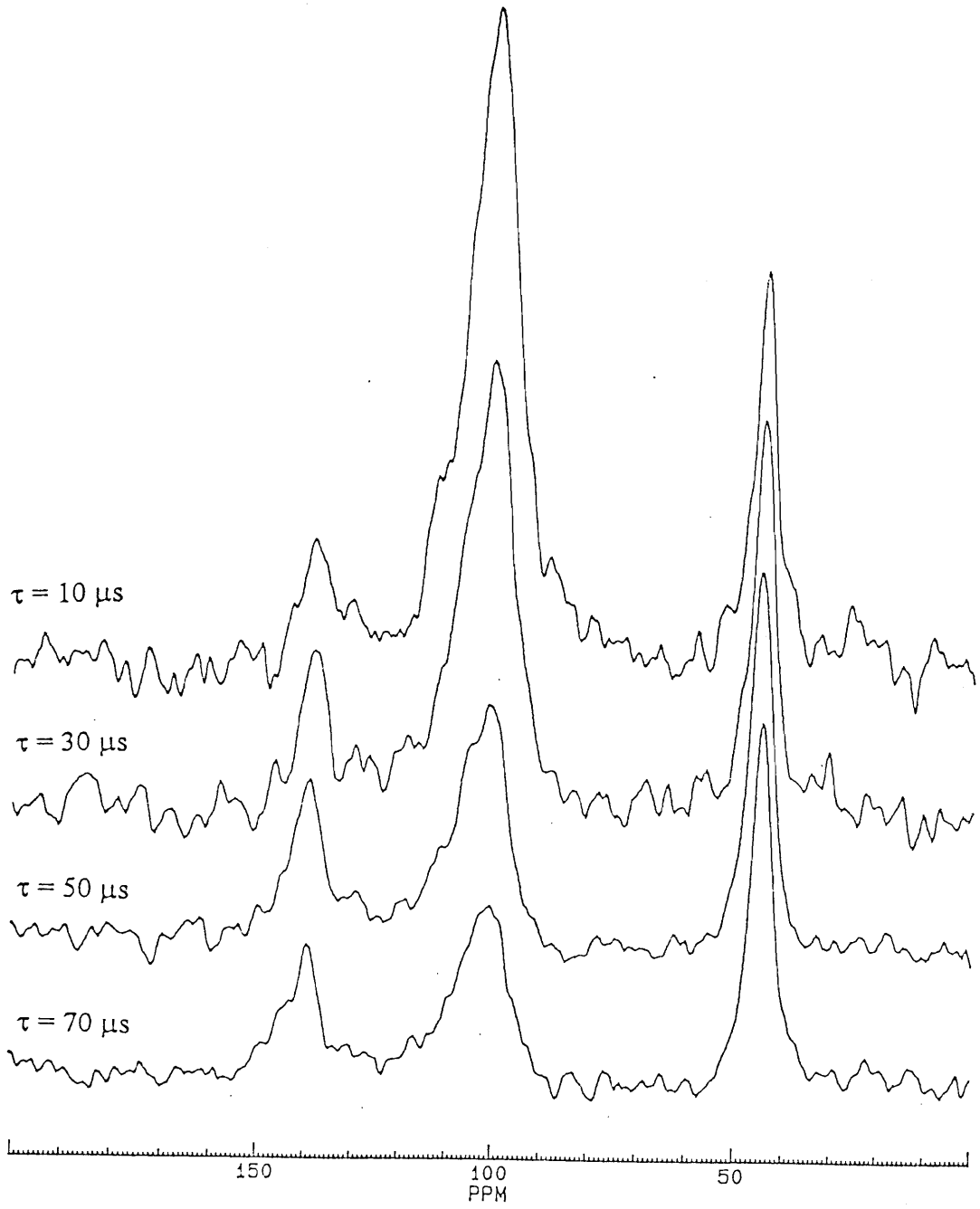

Figure 4.4: ^{15}N CP/MAS NMR spectra of wood/^{15}N-pMDI composite in an interrupted-decoupling experiment. The sample was cured at 120^{0}C for 4 min.

Table 4.3. $T_{1\rho H}$ Values of a pMDI-Wood Composite[a] in a Variable Temperature Experiment.

Temperature	Peak (ppm)		
(^{0}C)	138	104	44
25	4.3 (0.2)[b]	3.7 (0.1)	4.6 (0.1)
40	3.9 (0.2)	3.5 (0.1)	4.1 (0.1)

a. Cured at 12 wt.% resin, 500 psi, and 120^{0}C for 60 minutes.

b. Values in parenthesis are standard errors of the $T_{1\rho H}$.

with reduced molecular mobility. So the increase of $T_{1\rho H}$ with cure time probably indicates that the bondline gets more rigid as the cure time progresses.

The $T_{1\rho H}$ is generally influenced by molecular mobility and spin diffusion. Due to spin diffusion, protons in a homogeneous system will efficiently communicate and exhibit the same $T_{1\rho H}$ for all chemical moieties present (21). In a heterogeneous system, phase boundaries inhibit energy transfer between two phases. Distinct phases have their own distinctive relaxation rates. Table 4.1 shows that the three chemical species have similar $T_{1\rho H}$ at 120^{0}C and 140 sec. It suggests that the cured sample is a homogeneous system. However, as cure time increases, their $T_{1\rho H}$ become different from each other. Residual isocyanate and biuret imide have similar $T_{1\rho H}$, which is different from those of polyurea or urethane. It appears that a heterogeneous system develops in the pMDI-wood bondline as cure progresses.

In Table 4.2, the $T_{1\rho H}$ values for the series at 185^{0}C are listed. For residual isocyanate and biuret imide, their $T_{1\rho H}$ values all increase with cure time. Again this probably is associated with reduced mobility. However, polyurea $T_{1\rho H}$ values remain unchanged. This shows that these three species do have different mobilities. Polyurea's $T_{1\rho H}$ is less sensitive to the mobility change than the other two. Also from the $T_{1\rho H}$ values, we can find a heterogeneous bondline existing. The heterogeneity becomes stronger as cure time increases. Residual isocyanates and biurets have similar $T_{1\rho H}$, which is different from the one of polyurea. Polyurea has a smaller $T_{1\rho H}$ which indicates a higher mobility. That is also consistent with the assumption that polyurea is closer to the bottom of the curve than the other two species.

Comparing the results of samples cured under 120^{0}C and 185^{0}C, the chemical information is very similar. They involve biurets, polyurea and residue isocyanates in the bondline. When the sample is cured at 120^{0}C for 140 sec. and 4 min., urethane formation was detected. This phenomena was not found at 185^{0}C. Urethane can usually be formed under mild conditions, with high temperature such as 185^{0}C, they will not be stable. At short cure times (140 sec and 4 min.), $T_{1\rho H}$ at 185^{0}C is longer than those at 120^{0}C. As the cure time gets longer, the difference is reduced. At 120^{0}C, the sample cures slower, and 4 min. may not be enough to fully cure the sample. The samples are more mobile than the ones cured at 185^{0}C. As cure time reaches 10 minutes or longer, even at 120^{0}C, the sample is very close to fully cured. Therefore, there is less difference between a fully cured sample whether at 120^{0}C or 185^{0}C.

4.4. Conclusions

Two series of wood/^{15}N-pMDI composites were cured as a function of cure time at 120^{0}C and 185^{0}C. ^{15}N CP/MAS NMR has been used to probe cure chemistry, morphology, and molecular dynamics of the wood/adhesive interphase. Network formation occurs via the isocyanate/water reaction which produces urea and biuret linkages. Urethane linkages were also detected under relatively mild conditions. Residual isocyanate exists in the bondline even after being cured at 185^{0}C for 60 minutes. Aryl urethane linkage is not be thermally stable, and starts to decompose at 120^{0}C. The thermal instability of biuret linkage may also be detected at 185^{0}C. A summary of the cure chemistry is shown in Figure 4.5. Relaxation studies show that the bondline is a heterogeneous interphase. ^{15}N CP/MAS has been proven a powerful technique for studying the pMDI-wood interphase. However, it also suffers from the signal overlap of the urea and urethane signals, which limits any quantitative analysis of their relative contributions. A complimentary technique must be developed to add further insight into the chemical nature of this bondline.

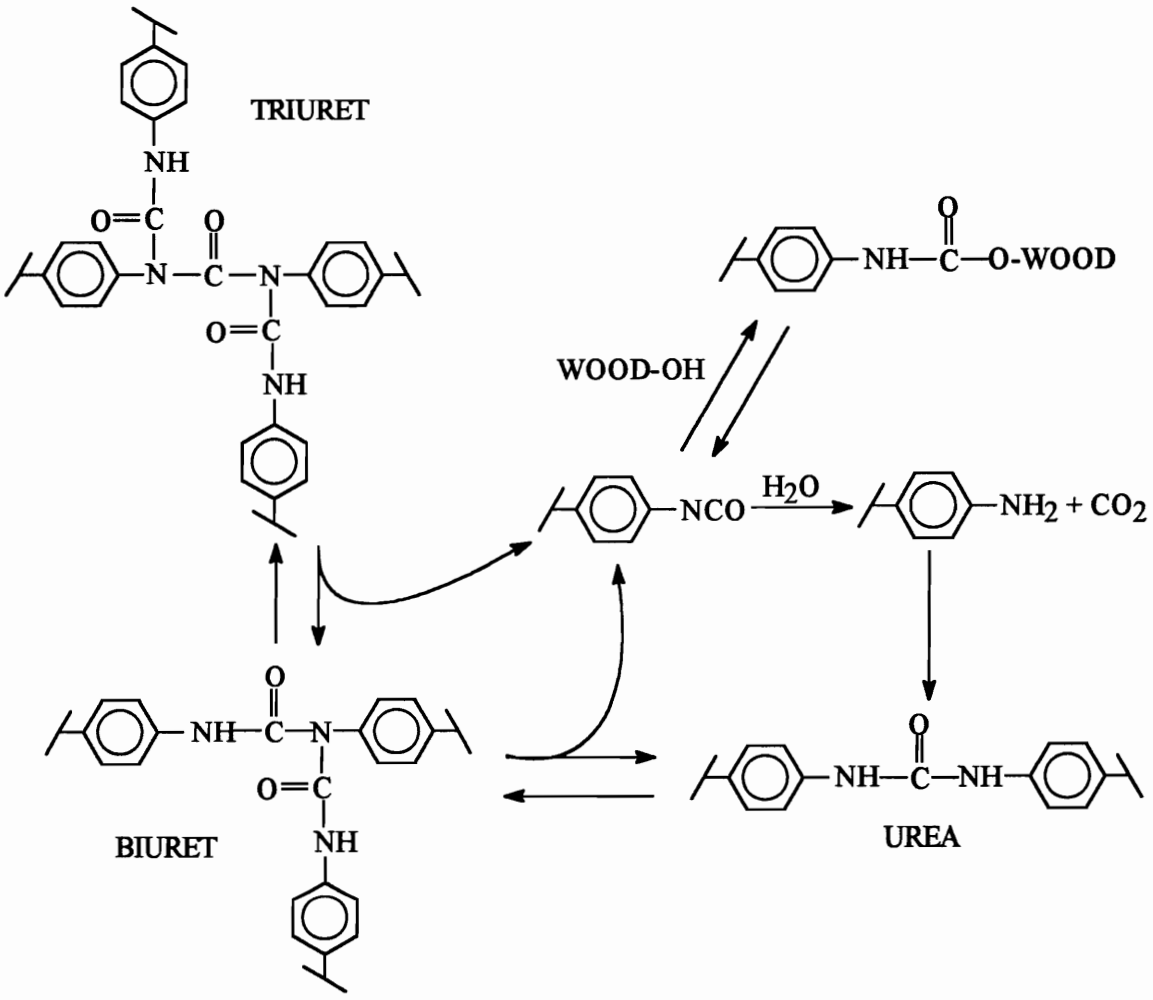

Figure 4.5: Generalized reaction scheme showing the possible reactions which may occur in the curing pMDI-wood bondline.

References

1. Frink, J. W. and H. I. Sachs. 1981. Urethane Chemistry and Applications, ACS Symp. Series No. 172, Washington D.C., Am. Chem. Soc. pp. 285.
2. Frink, J. W. and H. D. Layton. 1985. Proc. of the 19th International Particleboard/composite Materials Symp., T. M. Maloney, Ed., Pullman, WA. pp. 323.
3. Chelak, W. and W. H. Newman. 1991. Proc. of the 25th International Particleboard/composite Materials Symp., T. M. Maloney, Ed., Pullman, WA. pp. 205.
4. Galbraith, C. J. and W. H. Newman. 1992. Pacific Rim Bio-Based Composites Symp., Rotorua, New Zealand, FRI Bulletin No. 177. pp. 130.
5. McElrath, R. W. 1992. Proc. of the Southeastern Section of the Forest Products Research Society, T. D. Faust editor, Atlanta, GA, Session I. pp. 1.
6. Twitchett, H. J. 1974. Chem. Soc. Rev. 3 (2): 209.
7. Wendler, S. L. and C. E. Frazier. 1996. J. Appl. Poly. Sci. 61: 775-782.
8. Wendler, S. L. and C. E. Frazier. 1996. Int. J. Adhesion and Adhesives 16 (3): 179-186.
9. Wendler, S. L. and C. E. Frazier. 1995. J. Adhesion 50: 135-153.
10. Johns, W. E. 1989. Wood Adhesives Chemistry and Technology, Vol. 2, A. Pizzi, Ed. Marcel Dekker, New York, Chap. 3. pp. 75.
11. Weaver, F. W. and N. L. Owen. 1995. Appl. Spectroscopy 49: 171.

12. Johns, W. E., G. C. Myers, M. T. Lentz, E. M. Huffaker and J. B. Saunders. 1984. Proc. of the 18th International Particleboard/composite Materials Symp., T. M. Maloney, Ed., Pullman, WA. pp. 101-116.

13. Duff, D. W. and G. E. Maciel. 1991. Macromolecules 24 (2): 387.

14. Witanowski, M., L. Stefaniak, and H. Januszewski. 1973. Nitrogen NMR, M. Witanowski and G. A. Webb, ED. Plenum Publishing Company Ltd, London and New York, Chap. 4, pp. 245-254.

15. Hatfield, G. R., J. H. Glans, and W. B. Hammond. 1990. Macromolecules 23: 1654.

16. Wicks, Z. W., Jr. 1975. Progress in Organic Coatings 3: 73.

17. Owen, N. L., W. B. Banks, and H. West. 1988. J. Mol. Structure 175: 389.

18. Duff, D. W. and G. E. Maciel. 1990. Macromolecules 23: 3069.

19. Mehring, M. 1983. High Resolution NMR Spectroscopy in Solids, 2nd. ed. Springer-Verlag, Berlin. pp. 153.

20. Jones, A. A. 1986. High Resolution NMR Spectroscopy of Synthetic Polymers in Bulk, R. A. Komoroski, Ed., VCH Publishers, Inc. Deerfield Beach, Florida. Chap. 7. pp. 258.

21. Schaefer, J., E. O. Stejskal and R. Buchdahl. 1977. Macromolecules 10: 384.

22. Sjostrom, E. 1981. Wood Chemistry: Fundamentals and Applications. Academic Press, Inc., San Diego, CA. pp. 77-78.

CHAPTER 5

EFFECTS OF STRUCTURAL ISOMERISM ON THE PMDI/WOOD BONDLINE

5.1. Introduction

The objective of this chapter is to evaluate the effects of pMDI structural isomerism on the chemistry, morphology and molecular motions of the wood-pMDI bondline. Structural isomerism refers to the positioning of the isocyanate group on the benzene ring (see Figure 2.1). It is determined by the ratio of ortho/para substitution. The primary source of the structural isomerism lies in the chemistry of pMDI synthesis. During the first step (condensation) reaction, production of the 4,4′- isomer is highly favored, followed by 2,4′- and 2,2′- isomer. Commercial pMDI is composed of about 45-50% of 4,4′-MDI and a small amount of 2,4′- with a trace of 2,2′- isomers. The remainder (about 50%) are higher order oligomeric polyisocyanates (2).

Although the effects of structural isomerism on pMDI-wood bonding were unknown, it has been found to have considerable effects on the chemistry and physical properties of MDI based flexible foams, which are made by reacting pMDI with a polyol and water (3-6). The chemistry and chain morphologies, as well as macroscopic performance, were affected by the structural isomerism. As an analog to the polyurethane-urea foams, pMDI-wood bonding may be expected to be affected by the structural isomerism.

This is a continuation of a series of previous work. Previously (1), it has been shown how cure conditions such as cure temperature and cure time affect the chemistry, morphology, and molecular motion of pMDI (structure similar to commercial resin) bonded to yellow poplar (*Liriodendren tulipifera*). It has also been shown that ^{15}N CP/MAS solid state NMR is a powerful tool for probing chemistry, morphology, and molecular motions in pMDI-wood bondlines (1, 7,8). It remains as the main technique in this study. Microdielectric spectroscopy (DETA) was also employed to investigate the effects of structural isomerism on cure rate.

5.2. Materials and Methods

Materials

99% ^{15}N-labeled aniline was purchased from Cambridge Isotope Laboratories and used as received. It had a deep yellow color indicating some level of impurity, however, further purification was not attempted to prevent loss of the reagent. 95% paraformaldehyde powder, 98% triphosgene and anhydrous 1,2- dichlorobenzene (ODCB) were purchased from Aldrich Chemical and used as received. Chloroform was distilled under N_2 with anhydrous calcium chloride. Montmorillonite K10 (a SiO_4-AlO_6 clay) was purchased from Aldrich and acid-activated before use.

Methods

1. Synthesis of pMDI

The synthesis of pMDI is a two-step process. The first step is the synthesis of polyamine from the acidic clay catalyzed condensation of aniline with paraformaldehyde. The second step involves the phosgenation of the polyamine.

Step 1: Aniline was degassed by N_2 bubbing for 3 minutes before use. The aniline:formaldehyde molar ratio was chosen as 8:1, and the aniline:clay weight ratio was 10:1. First the clay was acid activated. clay (5 g) was mixed with 6N HCl (50 ml) in an erlenmyer. The mixture was stirred for 30 min., then the acid-activated clay was filtered and vacuum dried at 10 mmHg and room temperature overnight. Acid activated clay (2.95 g) was weighed into a high pressure Parr reactor (250 ml), which was equipped with mechanical stirrer. ^{15}N labelled aniline (28.6 ml, 0.317 mole) was transfered into the reactor, followed by of 95% paraformaldehyde (1.25 g, 0.040 mole of formaldehyde). The reactor was flushed with, sealed, and then heated to 200^0 C for 2 hours. The reactor was cooled to room temperature, and the clay was removed by filtration. Distillation of the filtrate at 4 mmHg and 120^0C gave 20.28 g of unreacted aniline and 7.38 g of polymamine (94% yield, assuming the conversion of all formaldehyde to methylenedianiline).

Step 2: By reacting with triphosgene at 175^0C, polyamines were converted to polyisocyanates. The detailed reaction procedure was described previously (1).

The isocyanate content was measured according to ASTM Standard D 5155-91, Test Method C. However, the procedure was scaled down to 10% of the ASTM standard

size. The sample was tested twice yielding isocyanate content of 28.9% and 29.3% (mean = 29.1%).

Molecular weight was determined by using gel permeation chromatography (GPC) at 40^0C. The same GPC procedure was described previously (1). Number average molecular weight (M_n) was determined as 352 g/mole, and weight average molecular weight (M_w) was 413 g/mole. These values have been corrected for urea derivatization.

The diisocyanate isomer ratio was measured using gas chromatography (GC). A Hewlett Packard HP6890 GC System was used with capillary column (Hewlett-Packard, HP-5), the solvent for pMDI was chloroform. GC measurements showed that the diisocyanate fraction was comprised of 63.9% 2,4′- isomer, 26.9% 4,4′- isomer, and 9.1% of 2,2′- isomer.

2. Preparation of Wood Composites

All wood flakes were cut from the radial face of a block of yellow poplar. After being conditioned to equilibrium moisture content of 4.5-5.0% (based on dry weight of wood), two pieces of flakes were bonded with pMDI to make a composite. Details of this procedure were described previously (1).

3. NMR measurements

^{15}N CP/MAS spectra were obtained at 30.4 MHz on a Bruker MSL-300 MHz spectrometer using a 7 mm Probenkopf MAS.07.D8 probe. Small disks were punched out of the composites using a paper hole puncher, randomly inserted into a zirconium oxide rotor with a Kel-f cap, and filled in and around with powered aluminum oxide to facilitate

rapid spinning. The ^{1}H channel was tuned using adamantane while ^{15}N-glycine was used to set the Hartmann-Hahn Condition. Standard phase cycling was used during acquisition. $T_{1\rho H}$ measurements were made using a standard CP acquisition with a variable spin-lock delay (0.5 ms to 12 ms) prior to a fixed contact time (5 ms). The proton 90^{0} pulse was 8 μs in duration. 800 scans were collected for each contact time with a repetition time of 6 s. Samples were spun at 6 KHz and the magic angle was set using the KBr method. Spectra were referenced externally to ^{15}N-glycine at 31 ppm.

4. Dielectric Analysis

Dielectric analysis was performed using a Micromet Eumetric System III Micro-Dielectric Analyzer equipped with a Micromet Instruments MP-2000 Minipress. Measurements were performed using an inter-digitated electrode (IDEX) sensor with a high conductivity signal interface. All scans were performed at frequencies of 1Hz, 100 Hz, and 1KHz. The procedure for making wood composites in section 2 was followed, except that the resin used was unlabeled pMDI. Before bonding two pieces of wood flake, an IDEX sensor was put in the center of the composites. Composites were pressed between thin Teflon sheets using the minipress at $120^{0}C$ and $185^{0}C$ under 500 psi for 20 minutes.

5.3. Results and Discussions

The synthesis of pMDI is a two-step process. The first step is the synthesis of polyamine. The second step involves the phosgenation of the polyamine. The isomer

ratio of pMDI synthesized is determined in the condensation reaction. In the industrial manufacturing process of pMDI, a homogeneous HCl catalyzed condensation is used to produce high 4,4′- isomer content polyamine. A heterogeneous condensation reaction method has been reported to vary the isomeric content of the diamine portion (9,10). It was claimed that this method can vary the 2,4′- isomer content of the diamine portion from about 15 wt.% to about 95 wt.% of the diamine product. In my study, a solid acidic clay was used as the catalyst. The reagent ratio and reaction temperature and time were determined to give a product very similar to commercial pMDI except for isomer ratio. The pMDI resin is composed of 26.9% 4,4′- isomer, 63.9% 2,4′- isomer, and 9.1% of 2,2′- isomer.

Figure 5.1 shows the ^{13}C solution NMR spectra (methylene carbon only) of pMDI. The top spectrum is for the pMDI with higher 4,4′- isomer content (the resin used in chapter 4), and the bottom one is for the pMDI synthesized in this study. The peaks at 34.5 ppm, 37.8 ppm, and 41.0 ppm correspond to methylene carbons of 2,2′-, 2,4′-, and 4,4′- isomers respectively (1). Because of the complications from signals of polyisocyanates, isomer ratio of the resin was not determined using solution NMR. Instead, GC was employed to give a more accurate result. Figure 5.2 shows the ^{15}N spectra for both spectra. Their differences in isomer contents are demonstrated through the NMR spectra.

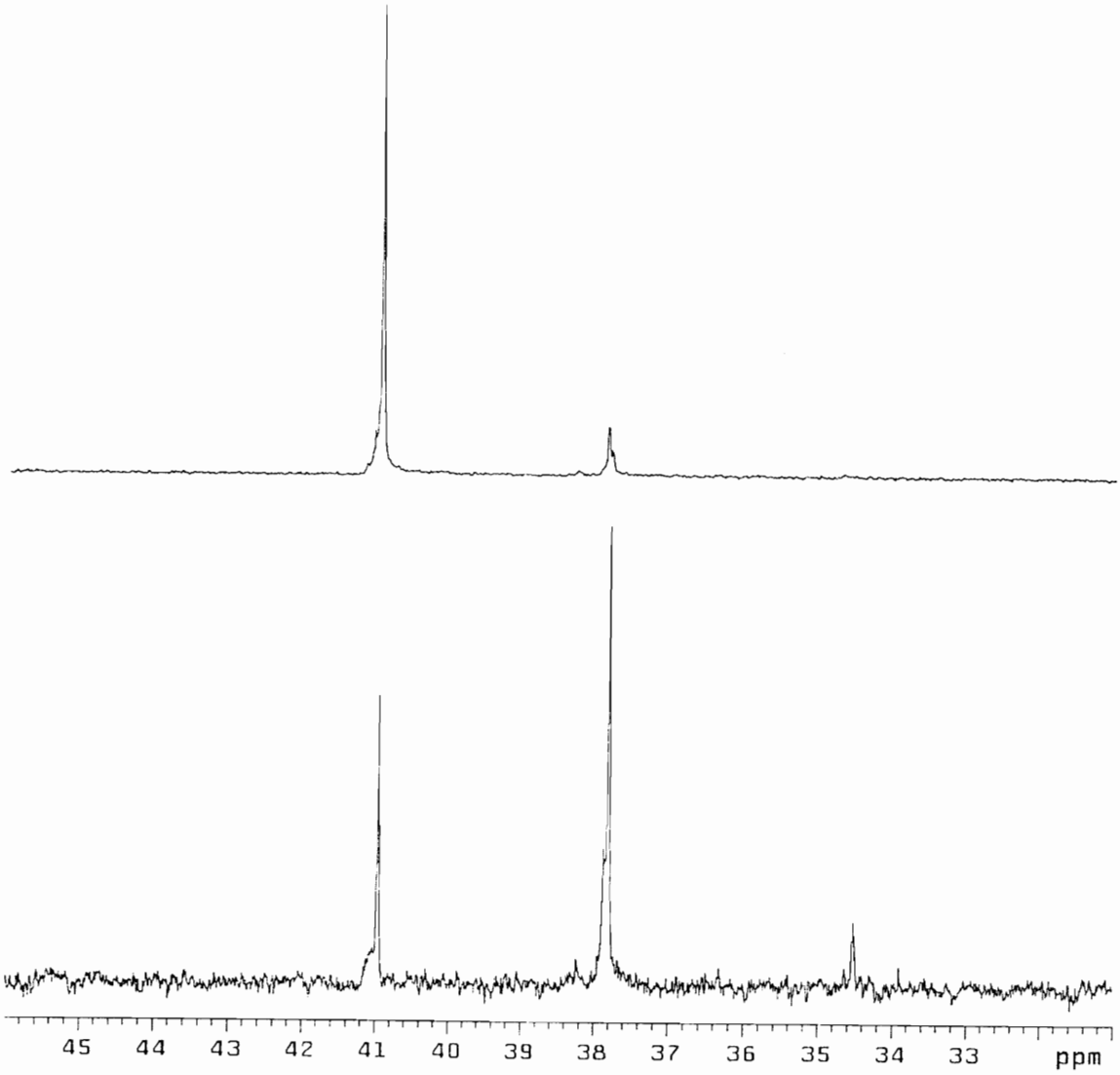

Figure 5.1: Solution state ^{13}C NMR spectra of the ^{15}N-labeled pMDI synthesized for this study. The top one has a higher 4,4′-MDI content. The bottom one has a higher 2,4′-MDI content.

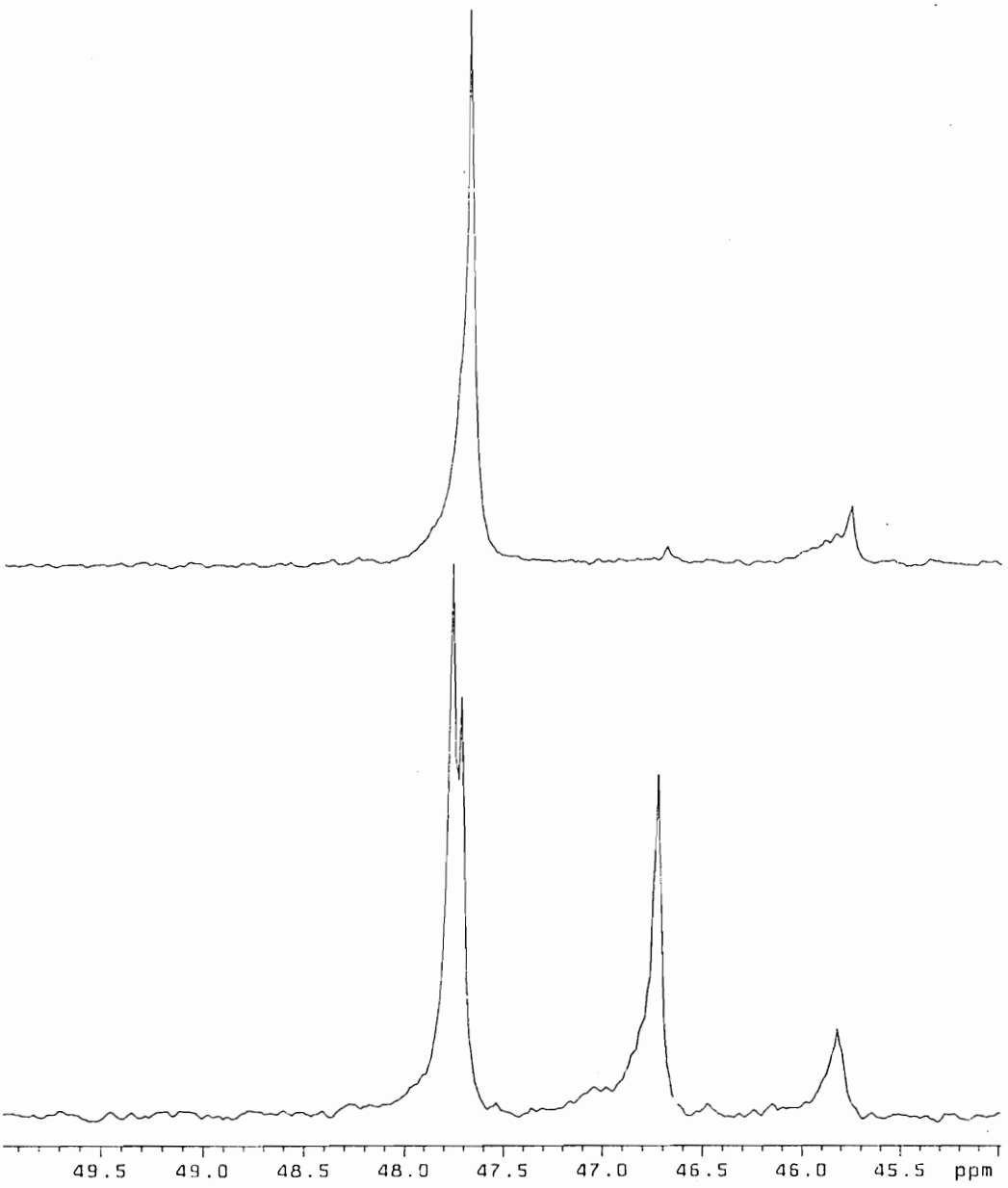

Figure 5.2: Solution state ^{15}N NMR spectra of the ^{15}N-labeled pMDI synthesized for this study. The top one has a higher 4,4′-MDI content. The bottom one has a higher 2,4′-MDI content.

Two series of wood/^{15}N-pMDI (high 2,4′-) composites were cured under two different cure temperatures, 120^{0}C and 185^{0}C. They were chosen as respective approximations of target mat core temperature and platen temperature, which occur during industrial manufacture processes. In each series, samples with 4.5-5.0% wood precure moisture content and 10 wt.% resin were hot pressed under 500 psi pressure for 140sec., 4 min., and 10 min.

Figure 5.3 displays the ^{15}N CP/MAS spectra for the samples cured at 120^{0}C as a function of cure time. Chemical shifts are referenced to glycine at 31 ppm and reported previously (1). The peak at 44 ppm corresponds to residual isocyanate, urea appears at 104 ppm. Biuret amide nitrogen occurs at 111 ppm, and biuret imide nitrogen is located at 138 ppm. Urethane linkage overlaps the urea signal, appearing at 101 ppm.

At 140 sec., there are three major resonances in the spectrum: residual isocyanate (44 ppm), biuret imide (138 ppm) and a broad peak centered at around 104 ppm. A small shoulder on the left side of the 138 ppm peak is also noticed. It has a chemical shift of about 143 ppm, which corresponds to isocyanate dimers (uretidione linkage). The broad central peak contains possibly three peaks at 101 ppm, 104 ppm, and 111 ppm. The maximum at 104 ppm indicates the presence of polyurea. The left shoulder at 111 ppm also supports the presense of biuret network. On the right side of the central band, there is a slight shoulder, which may indicate the formation of urethane.

As cure time increases, residual isocyanate content decreases. More isocyanates were consumed in cure process. The intensity of biuret imide remains approximately

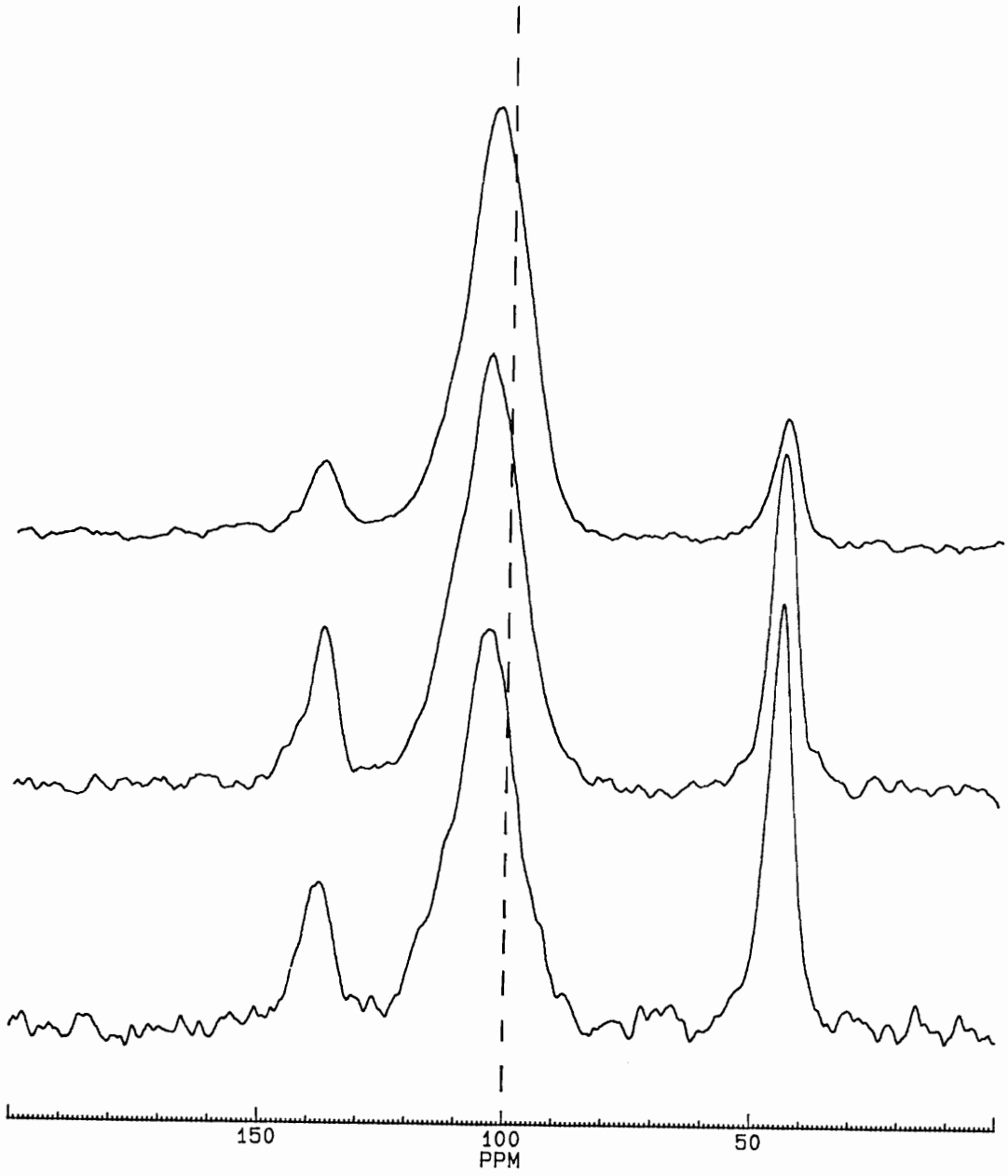

Figure 5.3: ^{15}N CP/MAS NMR spetctra for wood/pMDI (high 2,4'-) composites as a function of cure time. The composites were cured at 120^0C.

constant up to 4 min., then drops slightly. This indicates that biuret may be unstable and decompose as cure time progresses. The maxima of the central band remains at 104 ppm. The two shoulders (101 ppm and 111 ppm) on the central peak become weaker at 4 min. At 10 min., only the biuret amide (111 ppm) shoulder is slightly visible.

Figure 5.4 illustrates the ^{15}N spectra for the series of composites cured at 185^0C. At 140 sec., there are three main peaks (44 ppm, 104 ppm, and 138 ppm). Comparing to the spectrum at 120^0C, it has less residual isocyanate. The isocyanate consumption is faster at 185^0C than at 120^0C. Otherwise, the spectrum is very similar to the one in Figure 5.3.

As cure time increases to 4 min., the intensity of residual isocyanate drops. The central band expands to the left side dramatically. A strong shoulder appears at about 111 ppm, which corresponds to biuret amide. The biuret imide resonance also rises. It indicates that more biurets formed in the bondline. As cure time further increases to 10 min., the central band becomes narrower again. The shoulder at 111 ppm drops considerably. The intensity of biuret imide also declines. This suggests that earlier formed biurets are disappearing with longer cure time. This may likely be due to the thermal instability of biuret linkages which decompose to produce urea and isocyanate. Wendler et al. have reported a similar phenomena (8). They found that the biuret imide intensity drops as the cure time increases at 185^0C. Furthermore, they found that urethane formation becomes evident after 10 minutes of cure time. They attributed this to that the thermally liberated isocyanate may react with wood to form urethane linkage. However,

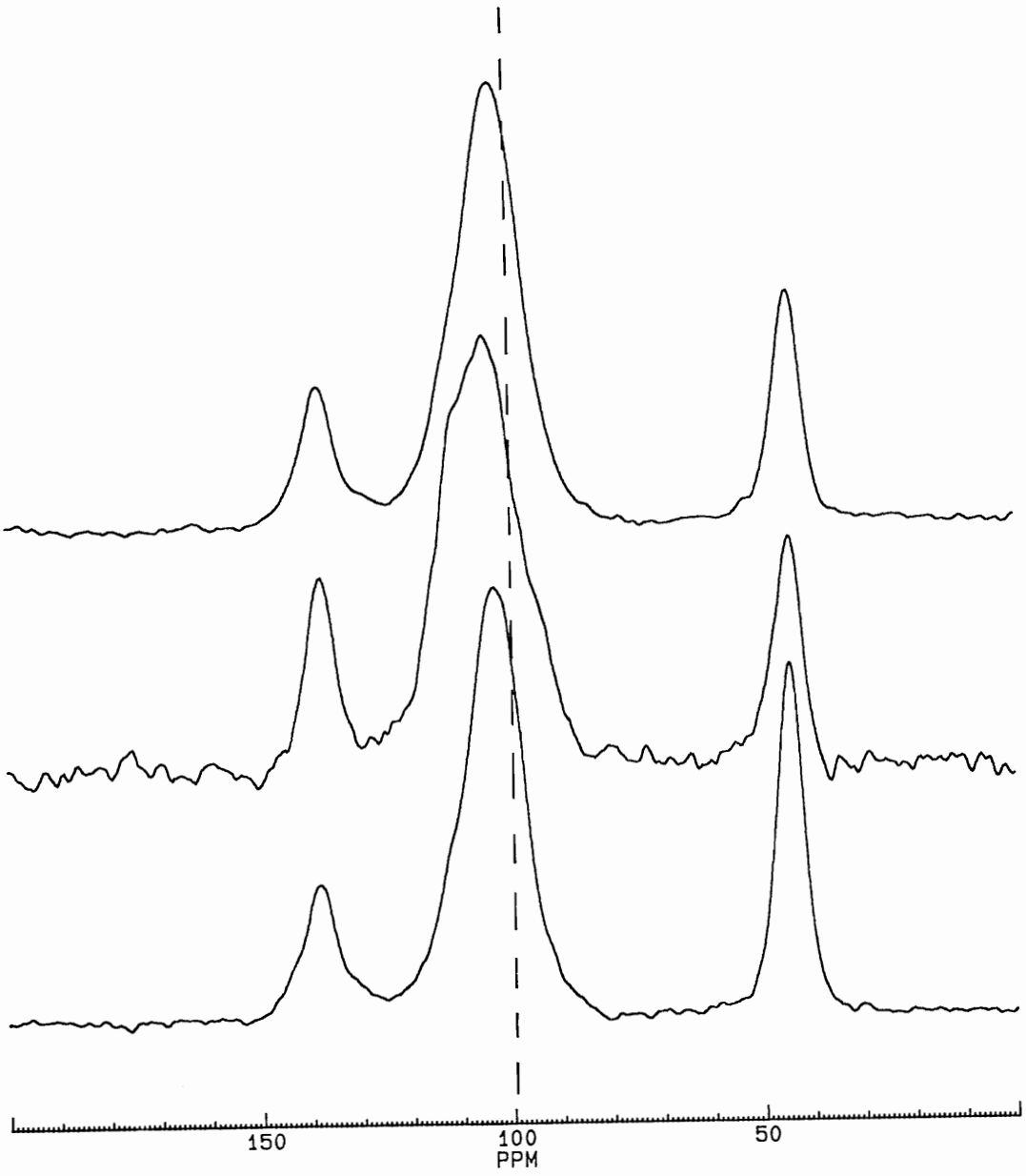

Figure 5.4: ^{15}N CP/MAS NMR spetctra for wood/pMDI (high 2,4′-) composites as a function of cure time. The composites were cured at 185^{0}C.

no clear shouder on the right side of the central band at 10 minutes in figure 5.4.

The two resins show very similar cure chemistry. They both contain biurets, polyurea, and residual isocyanates in the bondline. Urethane formation is also evident in both resins, especially in the high 4,4′- resin. At 120^0C, the high 4,4′- resin shows a signal maxima at 101 ppm after being cured for 140 second and 4 minute. In the case of high 2,4′- resin, it only appears as a slight shoulder. The decomposition of biurets were found in both cases, especially in the high 2,4′- resin. However, all of these above discussions about cure chemistry are only qualitative rather than quantitative. This is because of the relaxation rate effects on signal intesity as well as the complication from signal overlap. Relaxation behavior of the bondline is discussed next. This will offer morphological and dynamic information about the bondline.

The relaxation times, $T_{1\rho H}$, are presented in Table 5.1 and 5.2. Most of values were reproduced two or three times by preparing separate sample composites. At 120^0C, $T_{1\rho H}$ decreases with cure time. However, $T_{1\rho H}$ of each chemical specie declines at different rate. $T_{1\rho H}$ of polyurea drops gradually from 7.4 ms to 5.3 ms. For biuret imide, $T_{1\rho H}$ decreases quickly in first 4 min., then remains almost unchanged. $T_{1\rho H}$ of residual isocyanates only drops slightly through the course. Comparing to the results for the high 4,4′- resin, the two resins show totally opposite trend. $T_{1\rho H}$ of the composites made from the high 4,4′- resin increases with cure time. A variable temperature experiment was carried out, and it was found that increase of $T_{1\rho H}$ correlate with reduced mobility. The same experiment was performed on a composite made from the high 2,4′- resin. The

Table 5.1. Effects of cure time on $T_{1\rho H}$ of pMDI-wood composites cured at 120^{0}C.[a]

Cure Time	Peak (ppm)		
(min:s)	138	104	44
2:20	4.9 (0.2)[c]	7.4 (0.2)	4.5 (0.2)
4:00	3.8 (0.2)	6.7 (0.2)	4.3 (0.2)
10:00	3.8 (0.1)	5.3 (0.1)	4.0 (0.1)

a. Cured at 12 wt.% resin, 500 psi.

b. Values in parenthesis are standard errors of the $T_{1\rho H}$.

Table 5.2. Effects of cure time on $T_{1\rho H}$ of pMDI-wood composites cured at 185^{0}C.[a]

Cure Time	Peak (ppm)		
(min:s)	138	104	44
2:20	3.1 (0.1)[b]	4.3 (0.1)	3.4 (0.2)
4:00	4.4 (0.2)	5.9 (0.1)	4.6 (0.1)
10:00	3.7 (0.1)	4.8 (0.1)	3.6 (0.1)

a. Cured at 12 wt.% resin, 500 psi.

b. Values in parenthesis are standard errors of the $T_{1\rho H}$.

results are shown in Table 5.3. It shows that $T_{1\rho H}$ of residual isocyanate and biuret imide clearly increases with temperature. Therefore, increase of $T_{1\rho H}$ of these species associate with higher mobility. As cure time increases, the reductions of $T_{1\rho H}$ of these two species suggest a more rigid bondline. However, $T_{1\rho H}$ of polyurea remains unchanged as the temperature increases. Polyurea is highly hydrogen bonded, it may take a lot more energy to mobilize these urea molecules.

Table 5.2 displays the $T_{1\rho H}$ values for the series cured at 185^{0}C. Unlike the series cured at 120^{0}C, their $T_{1\rho H}$ increases as cure time increases from 140 sec. to 10 min. It is expected that a sample cured at higher temperature would be more rigid than the one cured at lower temperature. As cure time increases, the cured sample gets more rigid and its $T_{1\rho H}$ increases. However, it is noticed that the sample cured for 4 min. does not follow this trend. It has a higher $T_{1\rho H}$ value than the other two. As mentioned before, this sample is different in its chemical structure from the other two. In its bondline, there is more biurets, which may make it more rigid than the other two.

As discussed above, the series of the cured high 4,4′- resin has a different molecular mobility than the series of the cured high 2,4′- resin (120^{0}C). The cured high 2,4′- resin series may have a higher mobility, and is more flexible than the high 4,4′- resin series. This is somewhat expected. In the pMDI-wood bondline, polyureas resulting from 4,4'-MDI would likely be highly regular and extended straight chains. It promotes crystallinity or sub-three dimensional order. Extended chains impart rigidity to network structures because they are incapable of significant torsional rotations about atomic bonds. The

Table 5.3. $T_{1\rho H}$ Values of a pMDI-Wood Composite[a] in a Variable Temperature Experiment.

Temperature	Peak (ppm)		
(^{0}C)	138	104	44
25	4.2 (0.2)[b]	5.1 (0.1)	3.5 (0.2)
40	5.3 (0.2)	5.1 (0.1)	5.0 (0.1)

a. Cured at 12 wt.% resin, 500 psi, and 120^{0}C for 10 minutes.

b. Values in parenthesis are standard errors of the $T_{1\rho H}$.

increase in 2,4'-MDI content in a urea linkage produces a severe kink. Kinked chains provide a greater degree of extensibility and toughness. Therefore the series of the high 2,4'- resin would be expected to be more flexible than the high 4,4'- resin series. The $T_{1\rho H}$ values also shows that the bondline is a heteregenous system. Each chemical species has their distinctive $T_{1\rho H}$. Polyurea has a much higher $T_{1\rho H}$ than residual isocyanate and biuret imide. Residual isocyanate and biuret imide have similar values, which may indicate they are in the same domain. However, similar $T_{1\rho H}$ does not necessarily mean a homogeneous system. Two different domains could have similar $T_{1\rho H}$ values. The previous variable temperature experiment also supports that the bondline is a heteregenous system. As temperature increase, $T_{1\rho H}$ of polyurea remains unchanged while those of residual isocyanate and biuret imide increases clearly in different fasion.

DEA spectra of curing process are shown in Figure 5.5 and Figure 5.6. Ion viscosity is plotted against cure time. Ion viscosity can be used to follow the rheological

change that take place during the curing of thermosets. Prior to gelation, the ions are free to move and the ion viscosity is low. As the resin cures, and the matrix becomes less mobile, the ion viscosity increases. The dielectric response is plotted in Figure 5.5 and 5.6 to monitor curing of both resins at 120^{0}C and 185^{0}C, respectively. Comparing two resins, it can be found that the high 4,4′- resin cures much faster than the high 2,4′- resin at 120^{0}C. At 185^{0}C, the high 4,4′- resin A is only slightly faster than the high 2,4′- resin. Steric bulk near the ortho isocyanate probably reduces the reactivity of 2,4′-MDI as compared to 4,4′-MDI.

5.4. Conclusions

A pMDI adhesive was synthesized by using a heterogenous clay catalyzed condensation reaction. The pMDI has a higher 2,4′-MDI content than the commercial resins, while keeping other characteristics similar to the commercial one. Wood/pMDI composites were cured as a function of cure times at 120^{0}C and 185^{0}C. The bondline was found to consist of urea and biuret linkages, as well as residual isocyanates. Urethane may also exist in the interphase. However, unlike the pMDI with higher 4,4′- isomer content, this resin shows less clear evidence of the urethane formation. Relaxation studies also show a heterogeneous bondline in the composites. The higher 2,4′- isomer content may increases the molecular mobility of the bondline in the kilohertz molecular motion range. By using dielectric analysis, it was also found that higher 2,4′- isomer content retards the cure process, especially at 120^{0}C.

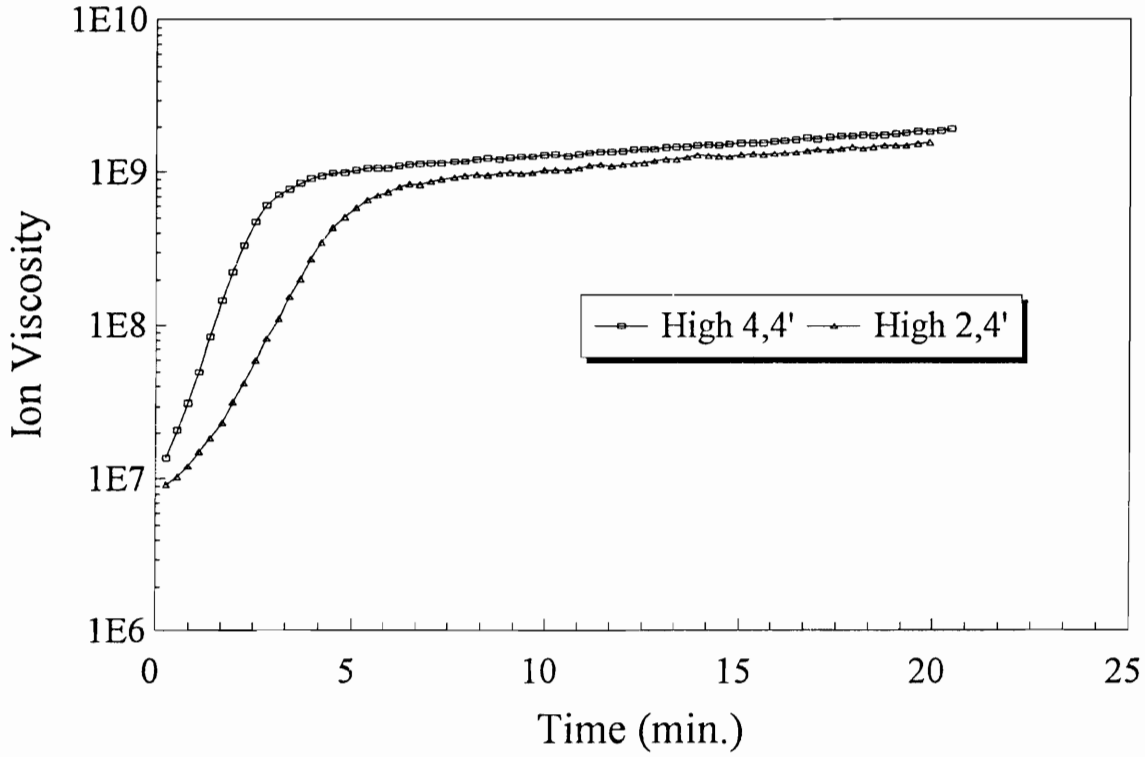

Figure 5.5: DEA spectra for monitoring the cure of two pMDI resins at 120^{0}C.

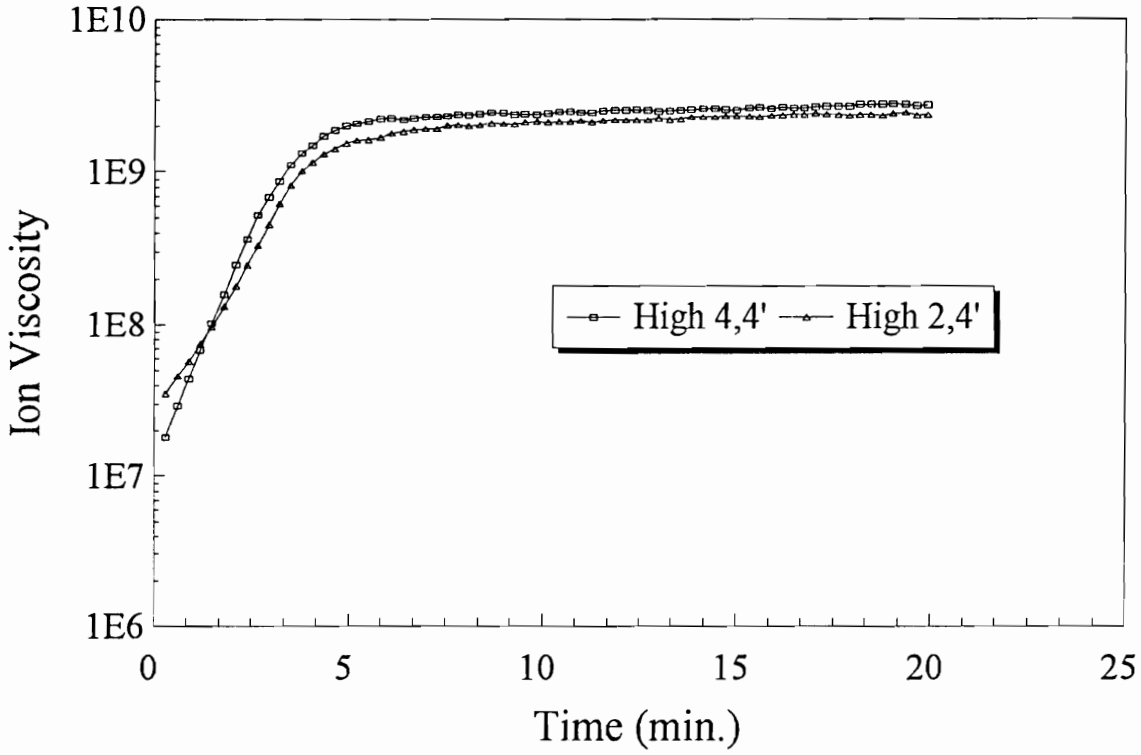

Figure 5.6: DEA spectra for monitoring the cure of two pMDI resins at 185^{0}C.

Refences

1. Personal communication with ICI Polyurethane.
2. Twichett, H. J. 1974. Chem. Soc. Rev. 3 (2): 209.
3. Berkowski, L., C. Reichel, and J. D. Taylor. 1987. Advances in Urethane Science and Technology, Vol. 10, K. C. Frisch and D. Klempner, Ed., Technomic Publish., Lancaster, PA.
4. Buethe, I., C. Reichel, and J. D. Taylor. 1983. Polyurethane: New Paths Prog., Mark., Technol., Proc. SPI Int. Tech./Mark. Conf., 6th, Soc. Plast. Ind., Polyurethane Div., New York, NY.
5. Lockwood, R. J. et al. 1982. Proceedings of the SPI Annu. Tech./Mark. Conf.
6. Domininguez, R. J. G. 1984. U. S. Patent # 4448904.
7. Wendler S. L. and C. E. Frazier. 1996. J. Appl. Poly. Sci. 61: 775.
8. Wendler, S. L. and C. E. Frazier. 1996. Int. J. Adhesion and Adhesives 16 (3): 179.
9. Bentley, F. E. 1978. U. S. Patent # 4071558.
10. Laszlo, P. 1991. Surfactant Sci. Ser. 38: 437-459.

CHAPTER 6

MOLECULAR INTERACTION

6.1. Introduction

Results in previous chapters have shown that the bonding mechanism of pMDI and wood is a combination of covalent bonding and secondary interactions. A complex mixture of urethane, polyurea, polyuret, and residual isocyanates were found in the bondline. However, the morphology of the bondline is still not clear yet.

pMDI has a great tendency to wet and deeply penetrate wood (1-3). It was found that the depth of the penetration of pMDI is larger than UF and PF resins (2,3). This is reasonable, because pMDI has a much lower molecular weight than PF and UF resins. The low molecular weight pMDI is actually composed of monomers and oligomers. This mixture of relatively small molecules could be described as an organic solvent, which can wet the wood surface surface easily and deeply penetrate into wood. Penetration has been shown to be important for the bonding performance (2). The strength properties are directly related to the depth of penetration. The maximum depth of penetration also affects the thickness swell properties of composites panels (2). pMDI was also found to have the ability to cover more wood surface area with less resin (1). This could contribute to the overall better resin efficiency of pMDI.

pMDI has been proven macroscopically to penetrate into wood (1-3). The low molecular weight could allow pMDI to mix molecularly with wood polymers. All

molecular mixing is determined by the Gibbs free energy of mixing, ΔG_M, which can be expressed as:

$$\Delta G_M = \Delta H_M - T\Delta S_M$$

where ΔH_M is the enthalpy of mixing and ΔS_M the entropy of mixing. Wood adhesives, such as PF and UF resins, are truly polymeric. There is an entropic barrier for them to molecular mix with wood polymers. They have to rely on a favorable enthalpy of mixing. Unlike those adhesives, pMDI is composed of monomer and oligomers, the entropic barrier for molecular mixing is absent. However, molecular demixing could occur as the curing starts. However, if pMDI polymerization is faster than an entropy driven demixing during chain growth. Primary forces (urethane linkage) and secondary forces (urea/biuret) might prevent demixing of the growing chains from the wood polymers.

Marcinko et al. (3) have used solid state NMR to demonstrate that pMDI plasticizes aspen (*Populus spp.*) flakes. This indicates that pMDI not only penetrates wood macroscopically, but also mixes with wood polymers on the molecular level. This means a highly reactive and multifunctional mixture of monomers and oligomers are molecularly mixed with wood. One could imagine that subsequent cure may lead to the formation of a network that interpenetrates the wood cell wall. pMDI and wood may form an interpenetrating polymer network (IPN). The IPN morphology may help explain the strong bonding from pMDI. An IPN may reinforce the wood surface, and also improve weather durability. Traditional wood adhesives have based their bonding on secondary interactions, which are subject to disruption by the interaction of mechanical stresses and

water ingression. The bondline for the traditional adhesives is more similar to an interface, whereas, an IPN morphology would give rise to an adhesive interphase. The IPN may preserve these secondary adhesive associations by maintaining interlocking of the interacting species.

Recent work by Vick et al. (4) may offer some support to the IPN theory. They reported that the durability of adhesion of a bisphenol-A epoxy adhesive to Sitka spruce (*Picea sitchensis*) is dramatically enhanced by using a hydroxymethylated resorcinol (HMR) coupling agent. The enhancement of adhesion was attributed to the physicochemical interactions, which includes covalent bonding, hydrogen bonding, and intermolecular dipole-dipole and london forces (4). The HMR consists of mono-, di-, and trihydroxymethyl resorcinol, with a few dimers and higher oligomers. HMR is capable of covalently bonding with epoxy and wood. In addition, HMR may penetrate cell walls, and molecularly mix with wood polymers because of its low molecular weight. It could be that the enforced durability is a result of the formation of an IPN interphase. HMR has a low molecular weight and is reactive. Upon curing, this thermoset resin can form a network associated with wood and epoxy via primary and/or secondary forces.

However, the IPN theory of pMDI-wood bonding is just a hypothesis. This chapter will describe some of the preliminary investigations into this theory. DMTA and ^{13}C solid state NMR were used to investigate the possible plasticization effect of pMDI on wood, as well as the IPN interphase in the bondline.

6.2. Materials and Methods

Materials

Yellow poplar samples were purchased from hardware store. pMDI (Mondur 541) was obtained from Bayer Corporation.

Preparation of Wood Flakes

A block of yellow poplar (*Liriodendron tulipifera*), clear of visible defects with cross sectional dimensions of 1.95 in. by 1.95 in., was immersed in tap water for three days. The block was then sliced with a CAE disk flaker. All flakes were cut from the radial face of the block to a thickness of 0.012-0.015 in. The flakes were vacuum dried at 10 mmHg and room temperature for 24 hours to obtain their dry weight. They were then conditioned in ambient condition. The moisture content was 4.0%. pMDI resin was sprayed onto the flakes in the open atmosphere using an air brush at various percentages of the dry weight of the flakes. A set of flakes with uncured resin were analyzed with ^{13}C CP/MAS NMR and DMA three hours after resin spraying. Another set of flakes were cured in an oven at 120^0C for 60 minutes. Then the cured samples were analyzed with ^{13}C CP/MAS NMR.

^{13} CP/MAS NMR

NMR experiments were carried out on a Bruker MSL-300 at a resonance frequency of 75.47 MHz for ^{13}C nuclei. $T_{1\rho H}$ measurements were made using a standard CP acquisition with a variable spin-lock delay prior to a fixed contact time of 1.5 ms. Spin-lock delay time ranged from 0.1 to 15 ms. The proton 90^0 pulse 4.5 μs in duration. 1200

scans were collected for each delay time with repetition time of 3.75 s. Samples were spun at 5.5 KHz and the magic angle was set using KBr method. Spectra were referenced externally to adamantine at 0 ppm.

DMA

DMA experiments were performed with a Polymer Laboratory Dynamic Mechanical Thermal Analyzer, DMTA, to determine glass transition temperature (Tg) and storage modulus (E'). Typical sample dimensions were 8 x 5 x 0.3 mm. Samples were tested by bending in a single cantilever mode at an oscillation amplitude of 0.4 mm, and a frequency of 1 Hz. Tg was determined by heating the sample from -100^{0}C to 150^{0}C at a heating rate of 2.5^{0}C/min. Dynamic modulus measurements were performed at 25^{0}C.

6.3. Results and Discussions

First, efforts were spent to verify the molecular mixing between pMDI and wood polymers before curing. Figure 6.1 shows a typical ^{13}C NMR spectrum of yellow poplar. Peak assignments have been reported in the literature (5-8). The peak at 105 ppm corresponds to C_1 of cellulose. For both cellulose and hemicellulose, C_2, C_3 and C_5 carbons appear around 72 ppm. The peak at 89 ppm comes from C_4 of crystalline cellulose and the 84 ppm peak from amorphous cellulose. The lignin methoxyl and hydroxyl substituted C_3 and C_4 carbons of lignin appear at 153 ppm, and the lignin methoxyl carbon appears at 56 ppm. The peak at 20 ppm is the acetyl methyl carbon of hemicellulose. The aromatic resonances from pMDI have chemical shifts from 125ppm -

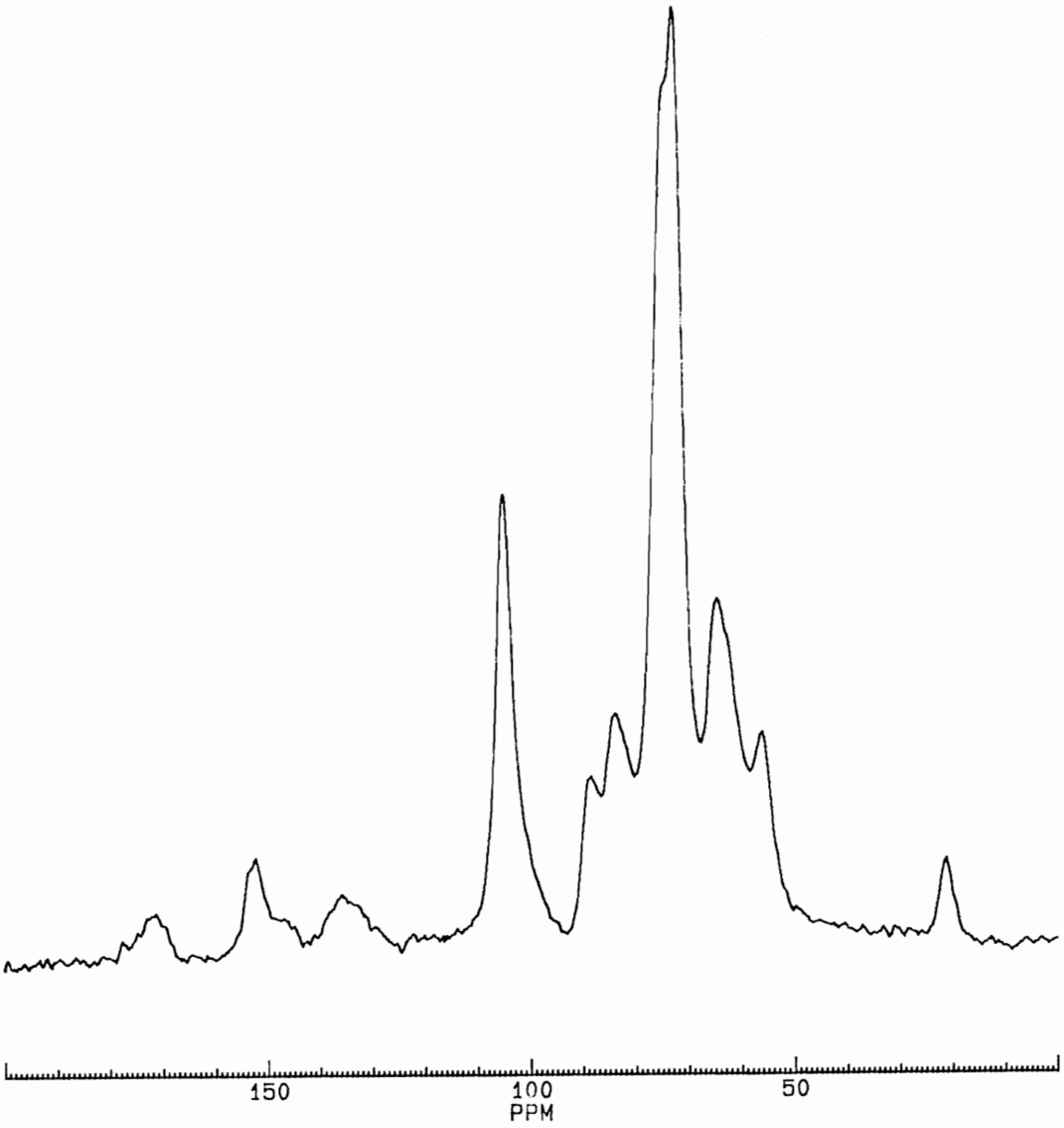

Figure 6.1: A typical ^{13}C CP/MAS NMR spectrum of yellow poplar.

140 ppm and the methylene carbons appear at about 41 ppm. Therefore signal overlap is not a serious concern. However, for cured pMDI-wood flakes, this becomes an important issue. Besides the signals from residual isocyanates, the cured pMDI can also be observed from urea and biuret (115 ppm to 158 ppm).

A set of yellow poplar samples coated with variable quantities of a commercial pMDI were analyzed with ^{13}C CP/MAS NMR. Their $T_{1\rho H}$ values are listed in Table 6.1.

Table 6.1 $T_{1\rho H}$ data of yellow poplar coated with uncured pMDI. Data in parentheses is the standard error for each value.

Wt.% of pMDI	^{13}C Chemical Shift		
on wood flake	153 ppm	105 ppm	21 ppm
0 %	8.9 (0.6)	8.3 (0.2)	8.5 (0.8)
20 %	8.9 (0.4)	8.8 (0.2)	8.2 (0.9)
30 %	7.3 (0.7)	8.2 (0.2)	6.8 (0.3)
50 %	8.5 (0.4)	8.3 (0.5)	7.6 (0.4)

$T_{1\rho H}$ measures the kilohertz frequency molecular motions in the samples. It can be used to elucidate the homogeneity or compatibility of solid polymeric blends as discussed in previous chapters. The results show that all of the wood components have very similar $T_{1\rho H}$. It may suggest that these wood polymers are associated with each other tightly. The table also shows how various amounts of uncured pMDI affect $T_{1\rho H}$ for lignin (153 ppm), cellulose (105 ppm) and for hemicellulose (21 ppm). The samples coated with pMDI resin show little change in $T_{1\rho H}$ values as compared to the uncoated wood samples,

even the sample with 50 wt.% of pMDI coating. The results indicate that pMDI may have minor effects on hemicellulose, but no dramatic effect on kilohertz frequency motions in these yellow poplar samples. It does not support the hypothesis that pMDI plasticizes wood. The significance of these results will be discussed later.

Another set of cured pMDI-wood flakes (120^{0}C for 60 min.) were also analyzed with ^{13}C NMR. Their $T_{1\rho H}$ values are shown in Table 6.2.

Table 6.2. $T_{1\rho H}$ data of cured pMDI-yellow poplar flakes (120^{0}C for 60 min.). Data in parentheses is the standard deviation for each value.

Wt.% pMDI	^{13}C Chemical shift				
on flakes	89 ppm	84 ppm	72 ppm	56 ppm	21 ppm
0 %	7.4 (0.3)	7.2 (0.3)	7.6 (0.2)	6.6 (0.2)	7.0 (0.3)
10 %	7.7 (0.3)	7.2 (0.2)	7.5 (0.2)	6.8 (0.2)	6.2 (0.3)
30 %	7.5 (0.5)	7.7 (0.3)	7.9 (0.1)	6.3 (0.3)	7.4 (0.3)
50 %	7.8 (0.3)	7.2 (0.2)	7.8 (0.1)	7.0 (0.2)	6.2 (0.2)

Because of the signal overlap between wood and cured pMDI, only the signals with chemical shift below 100 ppm were measured. Interestingly, the $T_{1\rho H}$ of yellow poplar (0% resin) have different values from the ones in Table 6.1. These two experiments were done on two different yellow poplar blocks. As we know, wood has high variability, even two blocks from the same tree could show different properties. The different $T_{1\rho H}$ values may arise from this sample difference. Also the sample in Table 6.2 has gone through heat treatment (120^{0}C for 60 minutes). This will certainly affect its $T_{1\rho H}$ values. Comparing

the $T_{1\rho H}$ values between the coated and uncoated samples, there is still no significant difference found. Again, this indicates that cured pMDI has only a slight effect or no effect on kilohertz frequency motions in the wood polymers. If cured pMDI-wood flakes forms a IPN, the polymer network would be expected to be more rigid, therefore a change of its relaxation behavior may be observed. The results in Table 6.2 do not support this theory.

The results in Table 6.1 and Table 6.2 seem to suggest that pMDI does not plasticize wood and no IPN network forms in pMDI-wood bondline. However, Marcinko et al. reported that liquid pMDI had a significant effect on kilohertz frequency molecular motions in aspen flakes. The $T_{1\rho H}$ values decrease for the uncured samples and increase in the cured binder samples. The resin loading was about 25%. The plasticization effect was most evident in the lignin component. These contrasting results could be due to a species effect (yellow poplar vs. aspen). It could also be due to the different NMR acquisition parameters. There is about 12% difference in proton decoupling power in these two experiments, which could artificially place the specimens in different motional regimes. Therefore, $T_{1\rho H}$ in different frequency range may be observed. Therefore, although the results in this study do not support molecular mixing, it can not disprove this theory either.

To further investigate the plasticization effect of pMDI on wood, DMA experiments were carried out. A series of yellow poplar samples with moisture content of 4% were analyzed with DMTA as temperature ramps from -100^{0}C to 150^{0}C. Their dynamic

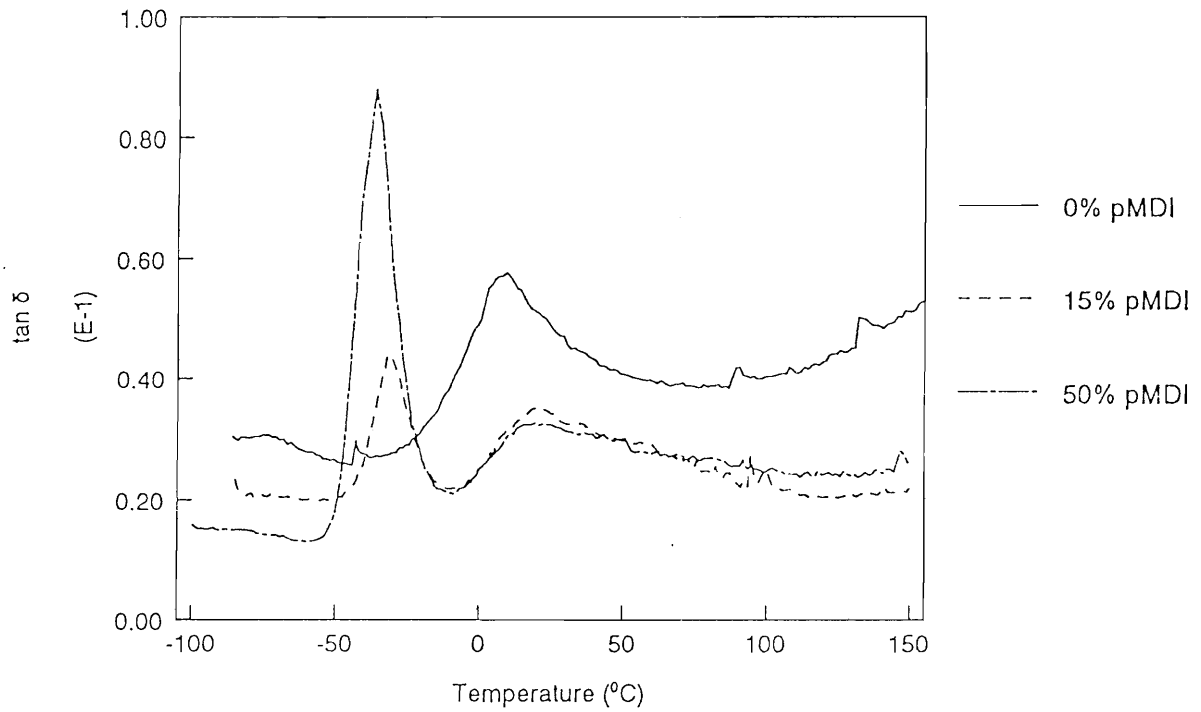

Figure 6.2: DMA spectra for wood with uncured pMDI resin as a function of resin loading.

mechanical spectra are shown in Figure 6.2. For the uncoated sample, there is only one peak at around 10^0C. According to the literature (9), this peak is assigned to the Tg of hemicellulose. For the samples coated with pMDI, there are two peaks, one at about 20^0C or above, the other at about -30^0C. The lower temperature peak corresponds to a transition temperature of pMDI. The higher temperature peak is Tg of hemicellulose. Instead of decreasing with pMDI content, Tg of hemicellulose increases slightly. This phenomena certainly does not support the plasticization theory. The lignin component has been reported to be mostly plasticized by pMDI. Unfortunately, Tg of lignin is out of this experiment range. No observation could be made on it. Interestingly, no pMDI curing was observed in these DMTA spectra. pMDI starts cure even below 100^0C. The reason of this phenomena is not clear.

Another set of yellow poplar samples was measured to determine the effects of pMDI on their storage moduli. After being analyzed with DMTA, the same sample was sprayed with 10% pMDI. Then the storage modulus of that sample was measured. The same sample was again sprayed to 30% and 50% pMDI. Each storage modulus was measured after pMDI application. Three samples were studied. The results are shown in Table 6.3.

The results shows that storage moduli of these samples do decline slightly as more pMDI was coated on them. Drom 0% to 50% of pMDI, the storage modulus drops about 13%. This may indicate that pMDI is plasticizing wood. However, this may not be a

significant change considering the sensitivity of DMTA. No conclusion can be drawn based on this experiment.

Table 6.3. Effects of pMDI on storage moduli (E′) of yellow poplar.

Wt.% of pMDI	log E′			
on wood flakes	Sample 1	Sample 2	sample 3	mean
0 %	9.44	9.44	9.44	9.44
10 %	9.43	9.43	9.42	9.43
30 %	9.40	9.43	9.41	9.41
50 %	9.38	9.38	9.39	9.38

6.4. Conclusions

It has been hypothesized that pMDI plasticizes wood and molecularly mixes with wood polymers. If this is true, upon curing, pMDI-wood bonding will form an IPN network. This hypothesis can be used to explain the strong bonding of pMDI-wood. ^{13}C CP/MAS NMR and DMA have been used to investigate this theory. No clear evidence was found to support this hypothesis. Instead the results are unfavorable for this theory. Studies by Marcinko et al. have shown that pMDI does plasticize wood. However, due to the limitation of these experimental techniques, no clear conclusion can be made at this point. Further study on this issue will be very beneficial because of the potential for this mechanism to enhance bond durability.

References:

1. Johnson, Stephen. Master Thesis. Virginia Tech.
2. Phanopouluos, C., C. Van Den Bosch and J. Vanden Ecker. 1996. Conference Paper, PG-44, ICI Polyurethane.
3. Marcinko, J. J., W. H. Newman and C. Phanopoulos. 1994. Second Pacific Rim Bio-Based Composites Symposium, Vancouver, Canada. Pp. 286-293.
4. Vick, C. B., K. Richter, B. H. River and A. R. Fried, Jr. 1995. Wood and Fiber Sci. 27 (1): 2-12.
5. Atalla, R. H., J. C. Gast, D. W. Sindorf, V. J. Bartuska and G. E. Maciel. 1980. J. Am. Chem. Soc. 102 (9): 3249-3251.
6. Earl, W. L. and D. L. VanderHart. 1980. J. Am. Chem. Soc. 102 (9): 3251-3252.
7. Wiilis, J. M. and F. G. Herring. 1987. Macromolecules 20 (7): 1554-1556.
8. Kolodziejski, W., J. S. Frye and G. E. Maciel. 1982. Anal. Chem. 54: 1419.
9. Kelly, S. S., T. G. Rials and W. G. Glasser. 1987. J. Mater. Sci. 22: 617-624.

CHAPTER 7

FRACTURE TOUGHNESS TEST

7.1. Introduction

In order to design wood adhesives, it is critical to develop reliability criteria for adhesive joints. A great number of test methods are presently in use to evaluate adhesive bond performance. However, there is no single generally accepted test. This is because all of these tests have their shortcomings in various degrees.

Wood adhesives have traditionally been tested in shear and tension (1). Specimens used in these tests include: button specimens, torsion shear specimens, cross-lap specimens, block shear specimens, plywood shear specimens, single-lap specimens, and internal bond test specimens, etc. (2). It has been pointed out that these tests in shear or tension have their intrinsic problems when being applied to wood structures (3-4). Because wood is anisotropic, stress is not distributed equally in all directions. Stress concentration is inherent in the test specimens due to their geometry and the methods of loading employed. The test results depend on the stress distribution specific to the test geometry and peculiar to the anisotropic wood adherend. The coupling of complex stresses often lead to stress concentrations in the wood that lead to wood failure and not adhesive failure. Due to lack of control of wood sample properties, such as flaw sizes, grain angle orientation, etc., a large sample size is needed to make the results statistically meaningful. Adhesive joints are generally strongest in shear, moderate in tension, and

weakest in cleavage (22). Therefore, wood failure is more significant in shear and tension tests than in cleavage tests. All of these above factors overshadow actual adhesive performance. It makes actual adhesive comparisons very complex and possibly misleading.

In the 60's, the fracture mechanics approach to evaluate adhesive strength and durability was developed (5-7). The failure of adhesive joints in service is thought to result from the extension of preexisting crack-like flaws, such as bubbles, dust particles, or unbonded areas. The techniques of fracture mechanics make it possible to measure the strength of structural members in the presence of such flaws. The value of fracture mechanics for testing bond strength is that it is a measure of a response near an imposed crack tip which can be experimentally directed at the interface alone and not the random response of the bulk phases and the interphase. In the 70's, there was an active interest in applying the principles of fracture mechanics to wood-adhesive bonds (8-12). These works have investigated the load to propagate a crack and the crack growth rate under a constant or variable load rate using a uniform double cantilever beam.

In 1979, contoured (tapered) double cantilever beam (CDCB) specimens were reported for testing wood adhesives (1,13). It was demonstrated that fracture testing with the CDCB specimen affords a superior capacity for evaluating several effects in wood bonding such as: wood grain angle (1,13), resin cure time (1), wood surface roughness, surface aging (14), resin constitution (15,16), and wood processing variables (17) etc. For example, when bonding hard maple (*Acer saccharum*) with a phenol resorcinol-

formaldehyde resin, fracture toughness tests were sensitive to small changes in phenol/resorcinol/formaldehyde ratio (15). It was also shown that fracture toughness increased with cure time to a maximum, and then declined to a constant value as network embrittlement set in (15). These studies demonstrate that the sensitivity of the CDCB test is remarkable. However, they used contoured solid wood specimens, which are difficult to be cured in a conventional press due to their contoured shape.

More recently, River et al. (18,19) have modified the CDCB specimen to a composite specimen of wood and aluminum to overcome difficulties in the fabrication of the solid wood beam specimen. In this composite specimen, a thin wood laminate bonded with test adhesive was bonded between a pair of contoured aluminum beams. The test adhesive can be cured in a conventional hot or cold press. This composite specimen also reduces variability from the variable mechanical properties from wood. However, the contoured aluminum beams are expensive to fabricate and must be chemically etched before bonding. After testing, the specimen must be treated to soften the adhesive and remove the wood laminate. The old adhesive must be scraped and wiped off before the aluminum beams can be reused. And the aluminum must be re-etched to renew its bondability. These procedures are time consuming and expensive.

Recently, it was reported that these aluminum beams can be replaced by wood-based materials, especially oriented strand board (OSB) (20,21). Wood-based beams can be easily and inexpensively contoured with conventional woodworking tools. The wood test laminates can bond easily to them without special surface preparation. After testing,

the wood test laminate can be quickly removed by sawing. It was also found that the length dimension of the bonded area could easily be extended which provides more useful data from one test.

This chapter describes the application of this CDCB technique in this laboratory. The CDCB tests were performed on two types of pMDI (high 2,4'- isomer content and high 4,4'- isomer content). The effects of isomer ratio of pMDI on fracture toughness were investigated.

7.2. Fracture Mechanics

Griffith (24) associated the decrease in the stored elastic energy of a large plate, due to the opening of a crack, with the energy required to form the surfaces of the crack. If a load is applied to the plate with a fixed crack, then a critical value of stress will be reached so that the system will decrease its potential energy by increasing its crack length. This critical stress can be found:

$$\sigma_c^2 = \frac{2\delta E}{\pi a} \tag{7.1}$$

where σ_c is critical stress, δ is the surface energy, E is the elastic modulus, a is the crack length. Irwin (24) replaced 2δ by G_c which he interpreted as the energy required to create a crack surface and called it the strain energy release rate (fracture toughness). Rewriting equation 7.1, the fracture toughness can be obtained as:

$$G_c = \frac{\pi a \sigma_c^2}{E} \tag{7.2}$$

The fracture of a material can be described in terms of three modes. Mode I is designated the opening or cleavage mode where a force is applied perpendicular to the crack plane. Mode II is termed the forward shear mode in which the force is applied parallel to the crack plane and parallel to the direction of crack propagation. Mode III is called the transverse shear mode where the applied force is parallel to the crack plane and perpendicular to the direction of crack propagation.

As mentioned before, the cleavage mode is of the most interest for studying the wood adhesive bond. Ripling et al. (5) have designed contoured double cantilever beam specimens for cleavage tests. The fracture toughness under mode I is given by the following relation:

$$G_{Ic} = \frac{P_c^{\,2}}{2b}\frac{dC}{da} \tag{7.3}$$

where P_c is the critical load at crack initiation, b is the width of beam, C is the compliance of the specimen, a is the crack length. According to elastic beam theory, the compliance of a cantilever beam can be determined by

$$\frac{dC}{da} = \frac{8}{Eb}\left[\frac{3a^2}{h^3} + \frac{1}{h^2}\right] = \frac{8m}{Eb} \tag{7.4}$$

where h is beam height. If the term inside the brackets (m) is constant for any crack length, dC/da will be constant. Therefore only the crack initiation load P_c is needed to calculate G_{ic}. Therefore, the difficult task of measuring crack lengths at each crack tip position can be avoided.

7.3. Materials and Methods

7.3.1. Preparation of OSB Beams

According to the literature (20), OSB was chosen to make the contoured beams. OSB boards with a thickness of 3/4 inch were purchased from local lumber yards. They were cut to a size of 254 mm by 330 mm on a table saw and cut to the predetermined geometry with a bandsaw. The dimensions of this OSB specimen are shown in Figure 7.1. Two holes were drilled 13 mm from the end of the specimen and 25 mm on either side of the centerline. These two holes were used for attaching the specimen to the test machine.

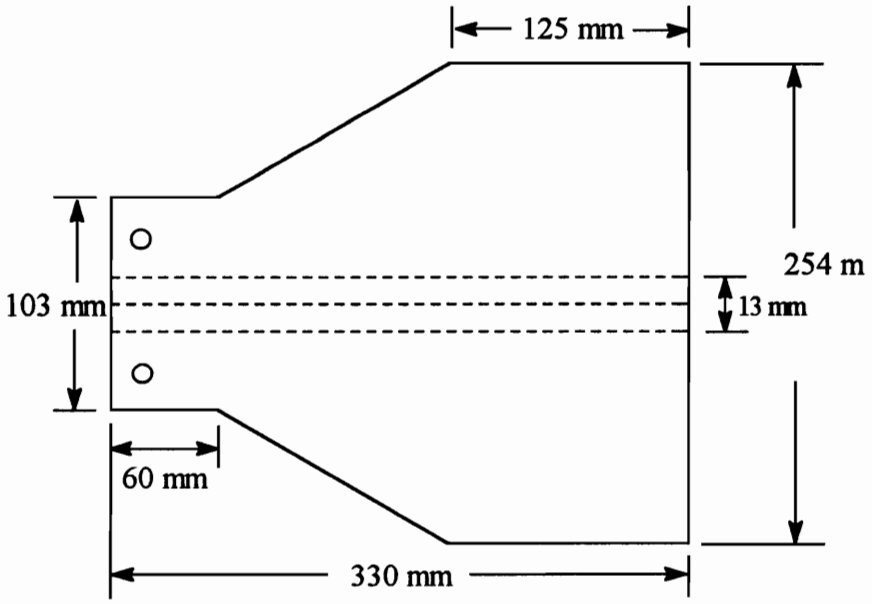

Figure 7.1 Solid OSB specimen

Ten sets of OSB specimens were made and calibrated. At first, a 10 mm crack was sawn along the centerline of the OSB beam with a thin bandsaw blade, starting from the end at which the load is applied. The crack length 10 mm was measured from the loading point, i.e. the center of those two holes. The specimen was then attached to the setup for a Material Test System (MTS) machine. A tensile load (P) was applied through a constant crosshead displacement rate of 0.5 mm/min. Upon reaching 200 N, the load was decreased at 1.5 mm/min. to zero. The load-displacement (P-Δ) relationship during loading was recorded on a Hewlett Packard HP-7004B X-Y recorder. After unloading, the specimen was removed from the MTS machine and the crack was extended for 10 mm by sawing. This load-displacement measurement and crack-extension procedure was repeated until the simulated crack reached 200 mm from the loading point. After testing, compliance (C) at each crack length was calculated by using $C = \Delta / P$, and dC/da was calculated for all the specimens.

After the OSB calibration, a 13 mm of strip of material (Figure 7.2) was removed from the center of the OSB beams to make space for the 13 mm thick laminate strip. These wood laminates used for calibration were bonded by a polyvinyl acetate emulsion adhesive. The PVA resin was chosen to insure a good toughness so that the calibration can be performed without crack extension. Each pair of OSB beams was bonded to a laminate strip with a 5 minute epoxy adhesive which was cured at room temperature under pressure for 30 minutes. These composites specimens were calibrated according to the above procedure, except sawing the simulated crack in the bondline of a test laminate

instead of OSB. Their calibration results were compared to the ones for solid OSB specimens.

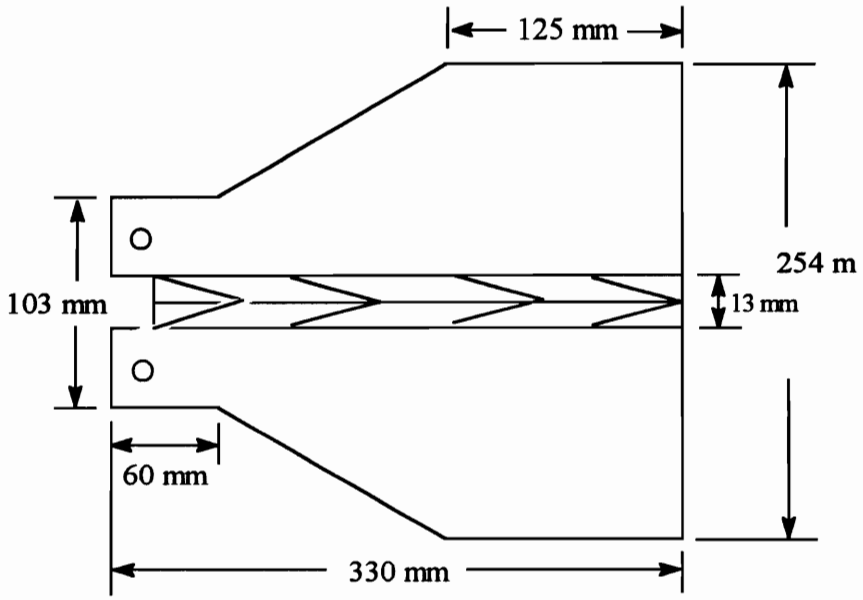

Figure 7.2 Composite specimen

7.3.2 Preparation of Test specimens

Yellow poplar lumbers was planed to 6.5 mm thick, and cut to samples of 127 mm by 305 mm using a table saw. These boards were carefully selected for grain direction to maintain a maximum grain angle of 10^0. These specimens were then conditioned to approximately 11.5% equilibrium moisture content (EMC) in a humidity chamber controlled at 20^0C and 60% relative humidity for one week. After conditioning, a pair of specimens were bonded with pMDI. Before bonding, the surfaces of the specimens were lightly sanded with 220 grit sandpaper, and a small piece of Teflon film was placed across the top edge of one of the laminates to create an initial crack. Two types of pMDI,

Mondur 441 and Mondur 541 from Bayer Corporation, were used with 10 wt% Lignoflex filler (from Robertson). Mondur 441 has a 28-30% of 2,4′- isomer content in the MDI fraction. Mondur 541 has only 6-8% of 2,4′- isomer content. The cure conditions of these laminates were 150^{0}C and 60 psi for 20 minutes. Then the laminates were immediately pulled out of press, and cut into 3/4 in wide pieces. They were conditioned in the humidity chamber (20^{0}C and 65% relative humidity) for another week, and then bonded with OSB beams by using a 5-minute epoxy. The laminate was oriented with the "V" of the fiber angles pointing away from the loaded end of the specimen (Fig. 7.2). This fiber alignment will force the crack to propagate in or near the laminate bondline during testing, rather than towards the laminate-beam interface. Another two days of conditioning was performed for the composites beams before fracture toughness test.

7.3.3. Fracture Toughness Test

The fracture toughness tests were performed with the MTS machine. A load was applied to the specimen with a crosshead speed of 0.5 mm/min. The load continues until the bonding fails. The load and displacement values were recorded on the X-Y recorder.

Three yellow poplar boards were used. One board was cut to make two sets of wood laminates, A and B. Another board was cut to make sets of C and D, and the third one with sets of E and F. A, C, and E were bonded with Mondur 441. B, D, and F were bonded with Mondur 541. There were four specimens in each set. One of those was used for calibration, and the other three were used for fracture toughness tests.

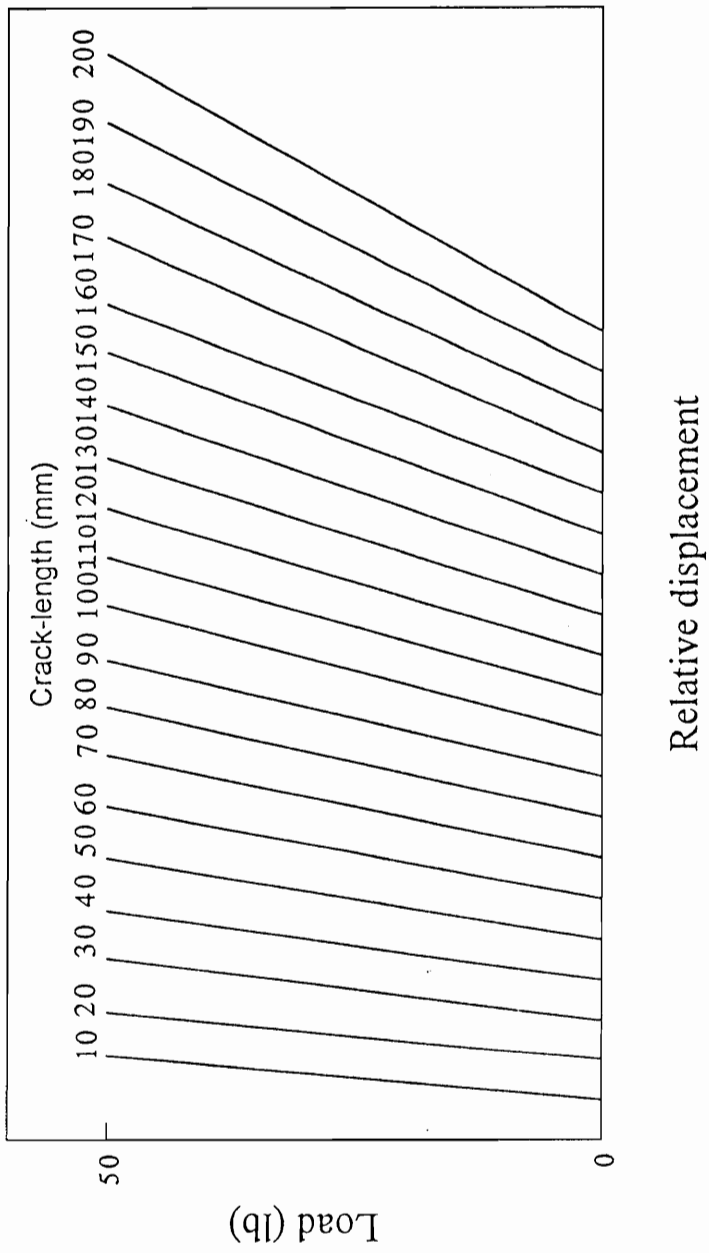

Figure 7.3: A typical load-displacement measurement during calibration.

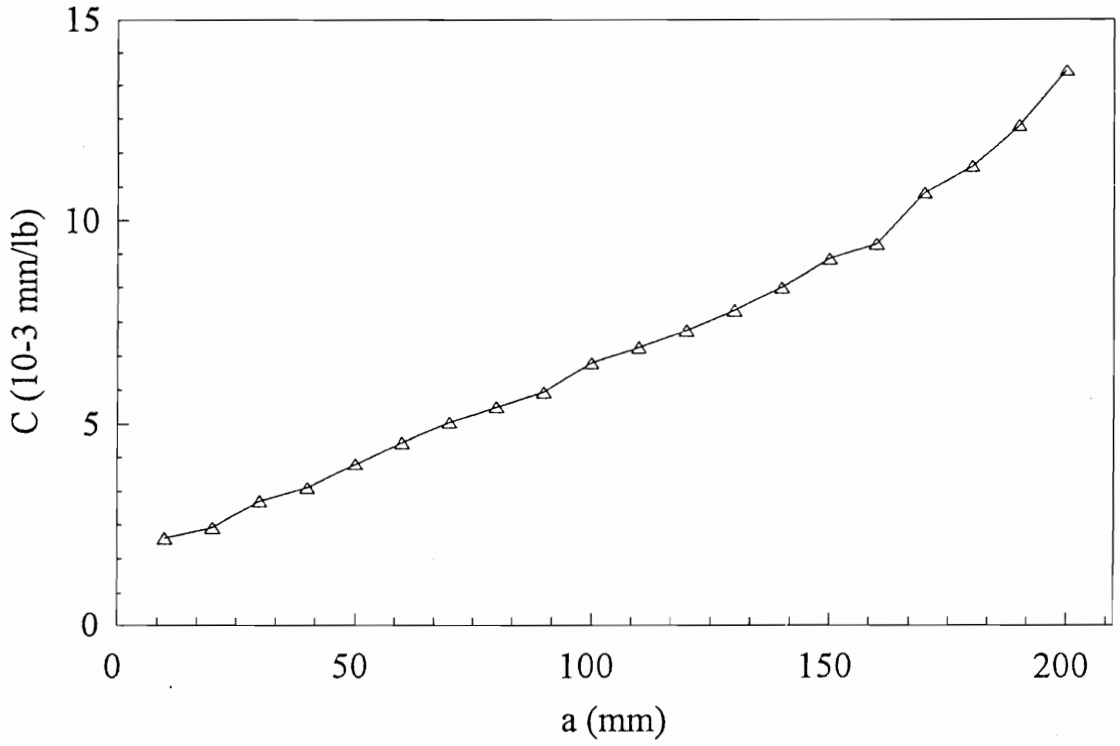

Figure 7.4: A typical compliance vs. crack length plot for calibration.

7.4. Results and Discussion

Ten sets of OSB beams were made according to the specifications in Figure 7.2. Calibrations were done on both solid OSB beams and composite specimens. A typical load-displacement measurement during calibration is shown in Figure 7.3. For each crack length, compliance of the beam was calculated using $C = \Delta / P$. Then a plot of compliance vs. crack-length was used to determine dC/da. A typical C~a plot is shown in Figure 7.4. The compliance and crack-length relationship is fairly linear within the range of 50 mm to 150 mm for both solid OSB and composite specimens. Outside of this range, the relationship is nonlinear. Therefore, this design of the OSB beam gives a linear range of 50 mm to 150 mm, which is fairly good for testing pMDI. dC/da was calculated in this linear range for all ten OSB specimens (solid and composites). The results are shown in Table 7.1.

Table 7.1 shows that all of the solid specimens have very consistent dC/da values. They have an average value of 5.0 x 10^{-5} lb^{-1} with a standard deviation of 0.3 x 10^{-5} lb^{-1}. Most of the composite specimens are consistent, except for two specimens (4 and 6). These two data points are probably due to the variability of the yellow poplar laminates. However, they were discarded to insure a confident fracture toughness result. Without these two specimens, the average dC/da for composite specimens is 4.6 x 10^{-5} lb^{-1}, the standard deviation is 0.2 x 10^{-5} lb^{-1}.

Two types of pMDI (Mondur 441 and Mondur 541) were studied in the toughness test. These two resins were very similar except for their isomer ratios. They both have

Table 7.1. Calibration results

Specimen	dC/da (10^{-5} lb^{-1}) Solid Specimens	dC/da (10^{-5} lb^{-1}) Composite Specimens
1	4.9	4.1
2	5.0	4.8
3	5.4	4.5
4	4.9	3.4
5	5.3	4.4
6	4.8	3.0
7	5.7	4.7
8	5.2	4.9
9	4.4	4.5
10	4.8	4.6

about 45% monomers. In the monomer portion, Mondur 541 has about 6-8% 2,4'-MDI, and Mondur 441 has about 28-30% 2,4'-MDI. By testing these two adhesives, effects of isomer ratio on fracture toughness of bonding were investigated.

Hard Maple was first chosen due to its high modulus and uniform texture. Neat pMDI was also used. However, the results were not satisfactory. Bonding was very weak, and samples failed catastrophically in most of the cases. It has been well known that pMDI does not bond solid wood very well. pMDI has a low molecular weight, and tends to penetrate into the wood substrate deeply. Therefore a starved bondline is often

formed. In order to keep more resin in the bondline, a Lignoflex filler was mixed with pMDI (10 wt.%). The pMDI with 10% filler showed better performance, but it still was not very satisfactory. The fracture surfaces of the broken wood laminates were examined. Very little filler was found in the bondline, instead they were pushed out of the laminates during pressing (by the excessive bubbling that occurs when pMDI reacts with water to produce polyurea and carbon dioxide). If not much filler left in the bondline, it means that filler is not holding much resin there either. Since hard maple has high density, filler is not easily held during pressing. To solve this problem, a lower density species, yellow poplar, was chosen, and fairly good results were obtained.

Three yellow poplar boards were used. Each board was cut to two sets of wood laminates (A and B, C and D, E and F). A, C, and E were bonded with high 2,4′- resin. B, D, and F were bonded with high 4,4′- resin. There were four specimens in each set. One of those was used for calibration, and the other three were used for fracture toughness tests. The calibration results are shown in Table 7.2, and compared to the previous results.

Table 7.2. dC/da (10^{-5} lb^{-1}) for test specimens

	A	B	C	D	E	F
Individual	4.9	4.8	4.5	4.4	3.9	3.8
Average[a]	4.9		4.5		3.9	
Previous[b]			4.6			

a. Average values for the set A and B, C and D, E and F.
b. The average value from the previous calibration results (Table 7.1)

Table 7.2 shows different dC/da values for test specimens. dC/da for set A, B, C, and D, are similar to the previous results. But sets of E and F have a much smaller value. Set A and B were tested first, then set C and D, E and F. Therefore the drop of dC/da may be due to the wear of OSB beams. After the above improvement, pMDI bonded wood laminates showed a strong fracture toughness. It took a high load to break the bonding. Because of the geometry of the OSB beams, the beams start to deform under these strong load. The deformation got worse in set E and F. Therefore, for set A,B,C, and D, the previous value 4.6 was used for calculation of fracture toughness, while the average value of dC/da for set E and F was used for these two sets of data.

In addition the crack-initiation energy G_{ic}, the crack-arrest energy G_{ig}, the energy stored in the beams when the cracks stops growing, was also measured. It can be calculated by using the following equation.

$$G_{Ic} = \frac{P_c^2}{2b}\frac{dC}{da} \tag{7.5}$$

where P_a is the crack-arrest load.

The brittle index I was also calculated from the values of G_{Ic} and G_{Ia}. It is the ratio of energy lost during crack growth to energy required to initiate crack growth:

$$I = \frac{G_{Ic} - G_{Ia}}{G_{Ic}} \tag{7.6}$$

The fracture toughness results are shown in Table 7.3 and 7.4.

The G_{Ic} values showed a good fracture toughness of the pMDI-wood bonding. They are either comparable to or better than the values of UF (18), PF (1,14,17), and

phenol-resorcinol-formaldehyde (16). It can also be found that there is very little difference between the G_{Ic} and G_{Ia}. This resulted a small I value, which indicates a stable crack growth. The bond does not fail catastrophically. The I values of pMDI are smaller than UF (18) and phenol-resorcinol-formaldyhyde (16). Therefore, pMDI has a good fracture performance.

Table 7.3: Individual Fracture toughness values

Resin	G_{ic} (J/m^2)	G_{ia} (J/m^2)	I
High 2,4′-	151.6	144.8	0.045
	150.3	144.4	0.039
	179.5	172.1	0.041
	158.3	153.4	0.031
	129.0	122.8	0.048
	171.0	157.9	0.077
	173.7	167.2	0.037
	164.9	154.5	0.063
High 4,4′-	155.6	148.0	0.049
	160.9	148.0	0.080
	141.5	135.9	0.040
	178.9	170.2	0.049
	151.0	144.6	0.042
	169.6	161.3	0.049

Table 7.4. Average fracture toughness values

Resin	G_{Ic} (J/m^2)	G_{Ia} (J/m^2)	I
Mondur 441[a]	159.8 (16.2[b])	152.1 (15.3)	0.048 (0.015)
Mondur 541[c]	159.6 (13.4)	152.8 (11.9)	0.052 (0.015)

a. Mondur has a high 2,4′- isomer content.
b. Values in parentheses are standard deviations.
c. Mondur 541 has a high 4,4′- isomer content.

There was no significant change in fracture behavior occurred between the two types of resins. In the previous chapter, the effects of isomer ration on the bondline were discussed on molecular level. It was found that higher 2,4′-MDI content probably will make the bondline tougher. From the toughness test here, the results do not support the this suggestion. However, the previous discussions were based on the $T_{1\rho H}$ results from solid state NMR. The $T_{1\rho H}$ results correspond to KHz molecular motion, while the fracture toughness test detects the Hz range of motion. Two different frequency ranges of the molecular motion are compared. Therefore, it is not surprising that these two results do not show the same trend. So this test is not sensitive to the molecular differences that were discovered with NMR. Also it needs to be noticed that the high 2,4′- pMDI (Mondur 441) used in this study has a much lower 2,4′- isomer content than the one used in NMR study (2,4′- isomer content was 63.9%). This may further reduced the sensitivity of this test.

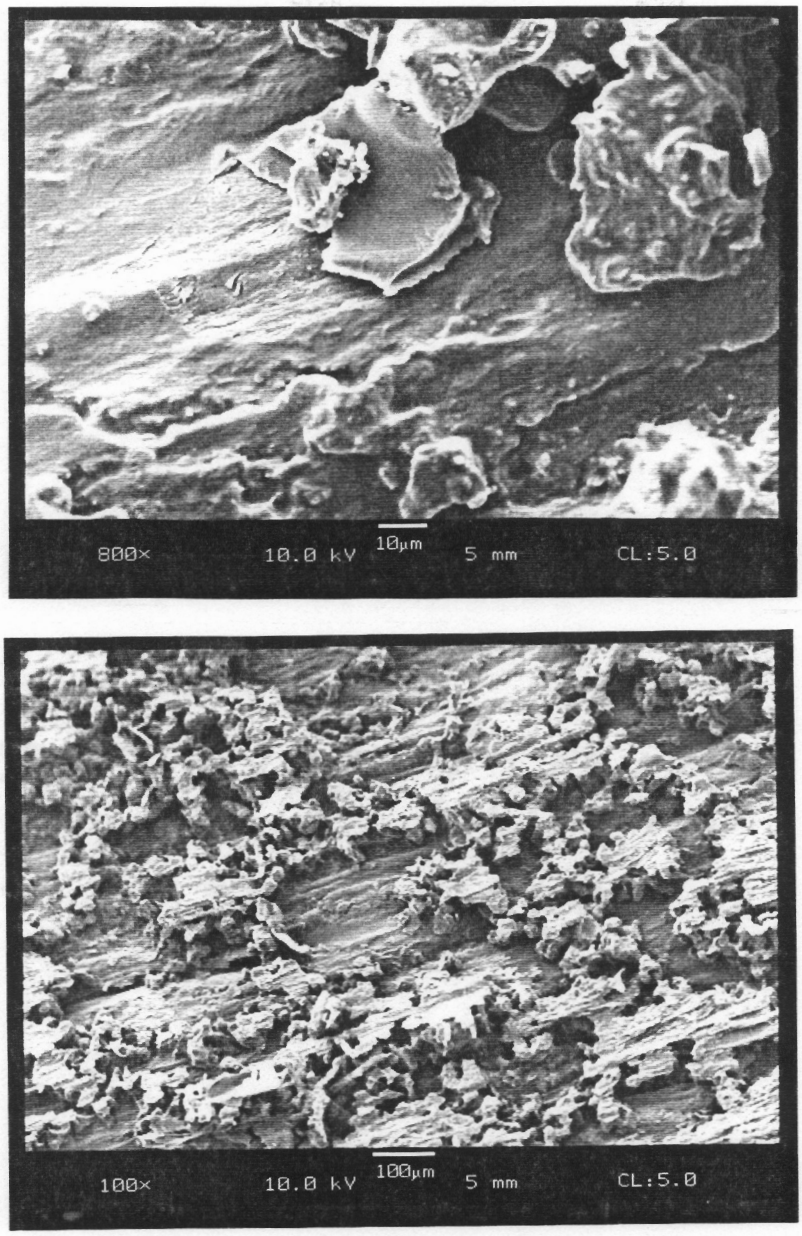

Figure 7.5. SEM picture of pMDI-wood frature surface.

The fracture surfaces of failed specimens were examined under scanning electronic microscope (SEM). The SEM pictures are shown in Figure 7.5. The surfaces are very similar for all of the samples. In most cases, a continuous waxy film was seen on the sufaces. This indicates that the bond failed cohesively. In some areas, adhesive failure was also detected. This proves that the test method measures mostly the inherent pMDI-wood bond properties. Little variability was introduced from bulk properties of wood samples.

7.5 Conclusions

A fracture toughness test method, contoured double cantilever beams, has been developed. The fracure toughness test was used to evaluate the effects of isomer ratio on pMDI bonding performance. There was no significant difference found between the two types of resins (different isomer ratio). The frature toughness values of both resins show a good bonding strength, which is comparable to PF and UF resins.

References:

1. Ebewele, R., B. River and J. Koutsky. 1979. Wood and Fiber 11 (3): 197-213.
2. Marra, A. A. 1992. Technology of Wood Bonding: Principles in Practice. Van Nostrand Reinhold, New York, NY.
3. Strickler, M. D., and R. F. Pellerin. 1973. For. Prod. J. 23 (10): 34-36
4. Johnson, J. A.. 1973. Wood Sci. 6(2): 151-158.
5. Ripling, E. J., S. Mostovoy, and R. L. Patrick. 1964. Mater. Res. Stand. 4 (3): 129.
6. Mostovoy, S., P. B. Crosley, and E. J. Ripling. 1967. J. Mater. 2 (3): 661.
7. Ripling, E.J., S. Mostovoy and H. T. Corten. 1971. J. Adhesion 3: 107-123.
8. White, M. S. 1975. Ph.D. dissertation. Virginia Tech.
9. Ruedy, T. C. 1977. M. S. thesis, Virginia Tech.
10. White, M. S. and D. W. Green. 1977. Wood Science 10 (1): 6-14.
11. Takatani, M. and H. Sasaki. 1980. Japanese Wood Research Society 66: 30-51.
12. White, M. S. 1980. Wood Science 12 (3): 149.
13. Mijovic, J. S. and J. A. Koutsky. 1979. Wood Science 11 (3): 164-168.
14. Ebewele, R. O., B. H. River and J. A. Koutsky. 1980. Wood and Fiber 12 (1): 40-65.
15. Ebewele, R. O., B. H. River and J. A. Koutsky. 1982. J. Adhesion 14: 189-217
16. Ebewele, R. O., B. H. River and J. A. Koutsky. 1986. J. Appl. Polym. Sci. 31: 2275-2302.

17. Ebewele, R. O., B. H. River and J. A. Koutsky. 1986. J. Appl. Polym. Sci. 32: 2979-2988.

18. River, B. H., C. T. Scott and J. A. Koutsky. 1989. Forest Prod. J. 39 (11/12): 23-28.

19. Scott, C. T., B. H. River and J. A. Koutsky. 1992. J. Testing and Evaluation 20 (4): 259-264.

20. River, B. H. and E. A. Okkonen. 1993. J. Testing and Evaluation 21 (1): 21-28.

21. Ebewele, R. O., B. H. River and G. E. Myers. 1993. J. Appl. Polym. Sci. 49: 229-245.

22. Stanger, A. G. and R. F. Blomquist. 1965. For. Prod. J. 15 (12): 468-474.

24. Griffith, A. A. 1920. Philisophical Transactions, Royal Society, London 221 (Series A): 163-183.

VITA

The author was born in Shanghai, China on October 17, 1967. He grew up in Shanghai, with his grandmother, Mrs. Baoyu Xiao. During his high school years, he moved to live with his parents, Yongpei Ni and Xueli Cheng. In July 1985, he graduated from Changzhou No.1 Senior High School in Jiangsu.

In July 1989, he received a B.S. degree in Applied Physics from Shanghai Jiao Tong University (China). Then he was employed as an assistant engineer in a physical and chemical laboratory for Changzhou Diesel Engine Inc. for half year. Shortly after that, he entered John Carroll University in Cleveland, Ohio. In August 1992, he received a M.S. degree in Physics. He enrolled at Virginia Polytechnic Institute and State University in September 1992, and earned his Ph.D. degree in Wood Science and Forest Products in December 1996.